1-1-2008

Application of Surface Thermal Lens Technology Combined With Polarization to the Study of Polymers

Daeha Joung

Application of Surface Thermal Lens Technology Combined With Polarization to the Study of Polymers

by

Daeha Joung

Thesis

Submitted to the Department of Physics and Astronomy

Eastern Michigan University

in partial fulfillment of the requirements

for the degree of

MASTER OF SCIENCE

in

Physics

Thesis Committee:

Marshall Thomsen, PhD, Advisor

Alexandria Oakes, PhD, Department Head

Donald Snyder, PhD

Diane Jacobs, PhD

June 2008

Ypsilanti, Michigan

CONTENTS

ABSTRACT

A new approach was attempted to investigate the characteristics of polymers by using photothermal technology. The Surface Thermal Lens (STL) technique was employed to study polymers because of its higher spatial resolution and greater sensitivity than the classical photothermal detection techniques (PDT). Zeonex [Cyclo-Olefin-Polymer] and acrylic [Poly–Methyl- Meth-Acrylate] were used as the samples. Polarization was applied to the STL technique. The signals of Zeonex were different from those of acrylic when the STL probe beam was polarized. Two different polarizer orientations for the probe beam, crossed and parallel, were used to observe the STL signal response to the samples. No time dependence in the STL signals of both Zeonex and acrylic was observed when the probe beam was unpolarized, but time dependence of the signals was observed when the probe beam was polarized. Zeonex showed the most significant signal changes under the crossed-polarizer conditions, and acrylic showed the most significant changes under the parallel-polarizer conditions, indicating a difference in the response of the chain-like molecules to the heating beam. Therefore, STL techniques using polarized light may provide new insight into structural changes in polymers.

LIST OF TABLES

LIST OF FIGURES

ACKNOWLEDGEMENT

The funding for this research was provided by the Department of Physics and Astronomy and Department of Chemistry at Eastern Michigan University.

I would like to thank my thesis advisor, Dr. Marshall Thomsen, for his persistent guidance and enthusiasm throughout the research process. His constructive comments, suggestions, and insight gave me clarity and direction. I am also grateful to Dr. Alexandria Oakes, Head of the Physics and Astronomy Department, for her constant support during the course of my graduate study as well as for offering me the opportunity to serve as a graduate assistant. I would also like to extend my gratitude to Dr. Donald Snyder for providing the necessary understanding and ideas on the chemical background of polymers. I would also like to thank Dr. Diane Jacobs for her encouragement and support in completing this thesis as well as my graduate study.

To all other family members and friends who gave generously of their support, thank you.

Most of all, I am truly indebted to my mother, whose love, patience, and encouragement inspired me to begin this journey. Without her faith and support, I would not have been able to finish this thesis. I dedicate my thesis to my mother.

Chapter 1: INTRODUCTION

Lasers have been used in many applications, including bar code reading [1], electronic highway tollgate vehicle collection [2], and material surface studies [3]. These applications have proved the efficiency of lasers. In addition, lasers have been used to study the micro-scale of surface morphologies [4]. The applications of lasers in science and engineering are numerous.

Polymers have become one of the most widely used materials in various industries including medical, pharmaceutical [5], paint [6], and display manufacturing. Polymers are appropriate material for such applications because of their unique physical and chemical properties [7-9]. In surface science, there is numerous research methods used to understand polymers. Much research has been performed in departments of material science, polymer science, physics, electrical engineering, chemistry, and biology.

Recent studies [10, 11] show that the laser can be used to study the characteristics of polymers. However, early use of the laser to investigate the micro-scale morphologies indicated that the heat produced by the laser might affect the interpretation of the results. The Surface Thermal Lens (STL) technique [13] was developed to minimize laser heating of the sample during measurements and has been applied to plastic materials [10]. The signals from other techniques are so weak that they are difficult to detect even with a high-powered beam [13]. However, the STL technique easily allows detection of the signal with the use of a high power pump beam. The STL technique is sensitive enough to detect even very small surface deformations and resilient enough to provide a strong signal without needing the precise beam

alignment required by other techniques [14]. Thus, one important advantage of the STL technique is the combination of the sensitivity of the photothermal deformation method and the simplicity of the traditional thermal lensing detection scheme.

The STL technique was applied to polymers in this study in order to investigate whether the technique could determine the characteristics of polymers such as thermal, optical, or mechanical properties. Additionally, the changes to the surface condition over time could also be determined since the technique involves the repeated laser heating of the sample.

This investigation focused on the STL technique using polarized light to understand the unique properties of polymers, their chain-like structure [15-17]. The different chain-like molecular structures of polymers is expected to be accentuated through the use of polarized light. The effect of polarization on the STL signals technique was studied with Zeonex and acrylic.

Both Zeonex and acrylic are thermoplastic but show different structures, properties, and chemical compositions [18]. Thus, different STL signal responses were expected. Zeonex is a high performance Cyclo-Olefin-Polymer (COP), which is produced by ring opening olefin metathesis polymerization of various cyclic monomers, followed by hydrogenation. On the other hand, many studies have been done on acrylic, which is also known as Poly–Methyl- Meth-Acrylate (PMMA).

This study is primarily focused on comparison of STL signals from polymers using polarized and non-polarized probe beams. The study can provide a new insight into changes in structures of polymers.

Chapter 2: LITERATURE REVIEW

1. Polymer science

Polymers-“poly” means “many” and “~ mer” means “parts”- are substances that consist of a large number of structural units that are linked to form a chain-like structure [19]. Polymers in the natural world have been around for hundreds of millions of years. Today, the polymer industry has grown to be larger than the aluminum, copper, and steel industries combined [20].

1.1. History of polymers

Polymers have different types and applications. The discovery of polymers can be described by the types of polymers that have been found in the natural world or that have been modified for specific applications.

The ancient Mayan civilization in Central America is believed to be among the first to use polymers [17]. For example, balls were made from local rubber trees for children to play with. Beginning in the 1800s, polymers were modified to create various materials. For instance, Charles Goodyear, in 1839, developed vulcanization by mixing natural rubber with sulfur and heating it to 270 degrees Fahrenheit [17, 19]. The resulting rubber, specifically vulcanized rubber, is a polymeric substance that is highly durable. Today, vulcanized rubber is commonly used in automobile tires. In 1907, the first synthetic plastic, Bakelite, was made by Leo Bakeland [19]. Bakelite’s firmness and resistance to high heat made it ideal as an electrical insulator.

Until the 1920s, polymers were believed to be made up of small molecules.

However, in 1922, H. Staudinger had proved the existence of large or long-chain molecules, referred to as “macromolecules,” which he described as polymers [17]. The recognition of macromolecules was the first step in the development of modern polymer theory.

Since the 1920s, synthetic polymers have formed the basis for a burgeoning polymer industry [17, 19]. The details of the history (from 1920s to 1970s) of modern polymer industries and its applications are listed in Appendix I-1.

After 1976, the polymer/ plastic industry outstripped steel, producing the nation’s most widely used material by volume [20]. Now, polymers are more widely used than steel, aluminum, and copper combined.

1.2. Polymer science

Polymers already have a range of applications in agriculture [21, 22] and agribusiness [23], medicine [24, 25], high-tech industry [26], and sports. Of particular interest to me are the current applications in adhesives [27, 28], coatings, foams, and packaging materials [29] to textile and industrial fibers [30] and structural plastics. Polymers are also used for most composites, electronic devices, biomedical devices [31, 32], and optical devices and are the precursors for many newly developed high-tech ceramics [33].

1.2.1. Classification

Thermoplastic

Polymers are often commonly referred to as plastic. However, this is misleading. Plastics refer to one type of polymers known as thermoplastics [19, 34-35]. The simple definition is that these are polymers that melt when heated and re-solidify when cooled. Thermoplastics are polymers that require heat to make them possible to process. After cooling, such materials retain their shape. This process is called reversible [36]. Thermoplastics include Zeonex and acrylic, discussed later in this paper. I discuss the applications of several thermoplastics in Appendix I-2.

Thermoset

Thermoset polymers possess a cross-linked structure [19, 34-35]. Such a structure may be formed by heating or via chemical reaction. They tend to possess excellent thermal stability and rigidity. However, this polymer can not be recycled. The non-recycled process is called irreversible [36]. The applications are shown in Appendix I-3.

Elastomers

Elastomers, or rubbers, are polymers that may have their dimensions changed when stressed [19, 34-35]. However, after the stress is removed, the polymer returns to its original dimensions. The process is reversible. The applications are shown in Appendix I-4.

High-performance polymers

Polymers that can cope with stringent high-temperature engineering environments are termed High-Performance-Polymers (HPPs) [37]. Therefore more recent work has focused on these polymers. The applications are shown in Appendix I-5.

Copolymer

Copolymers are composed of chains containing two or more different types of monomers [38, 39]. The applications are shown in Appendix I-6.

Mixtures of polymeric materials

Mixtures of polymeric materials consist of at least two polymers or copolymers [40, 41]. For instance, Acrylonitrile – Butadiene- Styrene (ABS) blends currently dominate the market. The applications are for piping, electrical, and automotive engineering.

Specialty polymers

Specialty polymers have recently been developed, such as Liquid-Crystalline-Polymers (LCPs) [42]. The main application of LCPs is in Liquid-Crystal-Displays (LCDs) for computers and watches. Another specialty polymer is a conventional polymer [43] or conducting polymer, which has highly conjugated structures that show unusual conducting properties, such as poly (p-phenylene), polypyrrole, poly (p-phenylene sulfide), and Intrinsically-Conducting-Polymers (ICPs).

Thermoplastic Elastomers

Thermoplastic Elastomers (TPEs) are also a type of copolymer [44]. The main advantage of these materials is that when they are heated above the melting temperature of the hard phase, they melt because the physical cross-links are disrupted. This allows TPEs to be easily processed.

Biomedical polymers

Biomedical polymers are used in cardiac, dental, and orthopedic applications and in drug delivery [34].

1.2.2. Polymerizations

The chemical reaction, in which high molecular mass molecules are formed from monomers, is known as polymerization [45, 46]. Polymerization is a process of bonding monomers, or "single units," together through a variety of reaction mechanisms to form longer chains named polymers. There are two basic types of polymerization, step growth and chain growth [19].

Step growth polymerization

Step growth polymers are defined as polymers formed by the stepwise reaction between functional groups of monomers. Most step growth polymers are also classified as condensation polymers, but not all step growth polymers release condensates. Among the common step growth polymers are polyesters, nylons, polycarbonates, polyurethanes, and polyaramids.

Chain growth polymerization

Chain growth polymerization involves two chemical entities in a three-step process that includes initiation, propagation, and termination [19]. The first entity, known simply as a monomer, can be regarded as one link in a polymer chain. The other chemical reactant is a catalyst. The catalyst can be free-radical peroxide added in relatively low concentrations. A free-radical is a chemical component that contains a free electron that forms a covalent bond with an electron on another molecule [47]. The mechanism is described as free-radical chain polymerization.

Emulsion polymerization

Emulsion polymerization is a type of free-radical polymerization [47]. The most common type of emulsion polymerization is an oil-in-water emulsion, in which droplets of monomer (the oil) are emulsified (with surfactants) in a continuous phase of water. The most common polymer of this type is latex.

Copolymerization

A copolymer is a polymer resulting from more than two monomeric species [47]. Copolymerization refers to methods used to chemically produce a copolymer and includes Acrylonitrile-Butadiene-Styrene (ABS) plastic, Styrene-Butadiene (SBR), and Ethylene-Vinyl-Acetate (EVA).

Ionic chain polymerization

Ionic chain polymerization can be either cationic or anionic polymerization [19].

This difference stems from the nature of the carrier ions on the growing polymeric chains.

Ring-opening polymerization

Ring-opening polymerization [34] is also a form of addition chain growth polymerization, in which the terminal end of a polymer acts as a reactive center, where further cyclic monomers join to form a larger polymer chain through ionic propagation. The treatment of some cyclic compounds with catalysts brings about cleavage of the ring followed by polymerization to yield High-Molecular-Weight-Polymers (HMWP).

Bulk polymerization

Bulk polymerization gives the highest-purity polymers [23]. The processes can be used for many free-radical polymerizations and some step growth (condensation) polymerizations. Poly-Methyl-Mmeth-Acrylate (PMMA) polymers are usually polymerized by free-radical bulk polymerization. PMMA is often referred to as acrylic.

Ring opening olefin metathesis polymerization

Ring opening olefin metathesis polymerization is a kind of new ring opening polymerization, in which cyclic olefins (Zeonex) are polymerized with a metathesis catalyst [48].

1.2.3. Zeonex and acrylic

In this experiment, Zeonex 48R and acrylic HS3125 were used as samples. Zeonex is a new technology polymer, while acrylic is widely known as PMMA. Both

Zeonex and acrylic are thermoplastic. Zeonex was developed in 1990 using a new technology. Zeonex is a high performance Cyclo-Olefin-Polymer (COP) that is produced by ring opening olefin metathesis polymerization of various cyclic monomers, followed by hydrogenation [49, 50]. Studies of Zeonex have recently begun. On the other hand, many studies have been done on acrylic. Table I compares the physical, chemical, and mechanical properties of Zeonex and acrylic [48-53].

Table I.
Comparison of Zeonex and acrylic.

Properties	Zeonex	Acrylic
Polymer type	Cyclo-Olefin-Polymer (COP)	Poly–Methyl- Meth-Acrylate (PMMA)
Manufacturer	Zeon corporation (Zeonex E48R)	Lucite international (HS3125 acrylic)
Specific gravity or density $(\frac{g}{cm^3})$	1.01	1.18
Water absorption (%)	< 0.01	0.3
Light transmittance (%)	92	90
Refractive index (n_D)	1.531	1.49
Glass transition Temp. (T_g) (^{0}C)	139	90 ~ 110
Thermal expansion coefficient $(\frac{1}{^0C})$	6×10^{-5}	$(5\sim9) \times 10^{-5}$
Tensile strength (MPa)	71	65.5
Flexural strength (MPa)	104	99
Dielectric constant	2.3	2.6
Rockwell hardness	20	93
Modulus of elasticity in tension (MPa)	2200-2500	2400-3300
Pencil Hardness	H	3H
Thermal conductivity W/m.K	0.16	0.15 - 0.25
Photo elastic constant (cm^2/dyne)	6.5×10^{-13}	6.0×10^{-13}

The following diagram shows the structure of Zeonex [50] and of acrylic [19].

(i). Zeonex (ii). acrylic

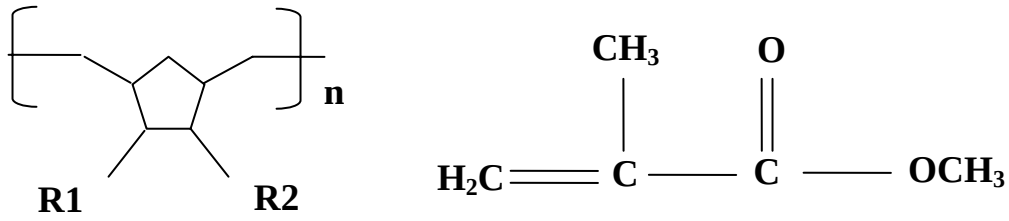

Figure 1. Chemical structures of (i) Zeonex (COP) and (ii) acrylic (PMMA)

The polymerization of Zeonex as shown in Figure 1 is ring opening olefin metathesis polymerization [50]. In the structure of Zeonex, “R1” and “R2” refer to organic groups that contain some number of carbon atoms. These groups may or may not be different from each other. As mentioned in the previous section, the polymerization of acrylic is a free-radical bulk polarization [19].

Table II shows the applications, advantages, and limitations of Zeonex and acrylic [48-53].

Table II.
Applications, advantages, and limitations of Zeonex and acrylic [48-53].

Characteristics	Zeonex (COP)	acrylic (PMMA)
Advantages	Excellent transparency, high heat resistance, low water absorbency, low birefringence, good chemical resistance, excellent moisture barrier, and excellent dimensional stability compared to other transparent polymers.	Outstanding transparency, excellent UV resistance, high color brightness and stability, surface hardness, half the weight of glass, good dimensional stability, and good insulating properties
Limitations	Glass transition is 135°C, and sensitive to stress cracking.	Poor impact resistance, limited heat resistance (80°C), limited chemical resistance, and poor wear and abrasion resistance.
Applications	Optical applications for lenses and prisms, liquid crystal display components, and medical and food containers.	Optical glass, medical technologies and implants, artistic and aesthetic uses, and laserdiscs and DVDs.

The advantage of using two samples, Zeonex and acrylic, in this experiment is that both of them are thermoplastic polymers. When a laser beam irradiates the sample, the sample will expand locally. However, after relaxation time or recovery time, the sample will return to its original state. This means that the experiment can be reproduced or repeated to bring about similar results. In addition, the optical, mechanical and thermal properties of both polymers are not too different, and both polymers were bulk polymers. The only significant difference is their structure. Therefore, the resulting STL signal may be compared for insight into the influence of these structural differences.

1.3. Recent researches in Polymer Physics

The Russian and Soviet schools of physics have been particularly active in the development of polymer physics [54]. As the name suggests, polymer physics is the study of polymers within the field of physics that focuses on their unique properties, their chemical reactions, and their fluctuations [55, 56]. Although polymer physics is associated with the study of condensed matter physics, it has become a part of statistical physics. Currently, polymer physics deals with issues in macromolecular science and engineering, including a variety of topics. Recent research of the polymer physics includes:

- Structure and thermodynamics of polymers in the bulk states [56].
- Block copolymer film statistical mechanics and dynamics [57].
- Particle dynamics in polymer thin film on nanometer scale using optical media [58].
- Polyelectrolyte and biological structure of polymers [59].
- Dynamics of polymer nanoparticles and polymer chains [60].
- High energy density capacitors using nanoparticle polymers [61].
- Dynamics and structure in polymer melts, surfaces, thin films and adhesion [62].
- Mechanical and elastic properties, fracture and adhesion of polymers [63].
- Magnetic nanostructures of polymers [64].

2. Surface science methods

Surface science is an important research area because the surface of materials, or layers, plays a critical role in processes such as catalysis, adhesion, wear, and corrosion, with applications in the polymer industries, metallurgy, thin films, and surface coatings and microelectronics. Many basic theoretical concepts have already been developed. Surface science has undergone great development, and still continues to do so. There are many different kinds of methods in surface science based on the equipment used. These are divided into electron spectroscopy, x-ray absorption fine structure**,** ion spectroscopes, microscopy, and diffraction methods [65]. Characteristics and application are shown below.

2.1. Electron spectroscopies

Electron spectroscopy is an analytical technique used to study the electronic structure and its dynamics in atoms and molecules. The technique includes Photoelectron Spectroscopy, and Auger Electron Spectroscopy (AES). The Photoelectron Spectroscopies (PES) include X-ray Photoelectron Spectroscopy (XPS) and Ultraviolet Photoemission Spectroscopy (UPS). In XPS the sample is illuminated with X-rays, which excite photoelectrons from the sample surface [66]. XPS can provide chemical bonding information and is a new tool for examining nanostructures [67]. While XPS is not sensitive to hydrogen or helium, it can detect all other elements. K. Siegbahn was awarded the Nobel Prize for Physics in 1981 for his work on XPS [68]. UPS is used for studying valence and conduction bands. In AES a beam of electrons is used to excite Auger electrons from the surface [66]. AES is usually used for the

characterization of thin films, multilayer stacks and for determining the composition of the top few layers of a surface.

2.2. X-ray Absorption Fine Structure

Extended X-ray Absorption Fine Structure (EXAFS) is another surface structure determination method [66]. EXAFS can determine the adsorption site and bond length of atoms and molecules on the surface. The adsorbate can include organic and biological species. EXAFS has the advantage that it does not require long-range order.

2.3. Ion spectroscopes

Secondary Ion Mass Spectrometry (SIMS) is the most popular of the ion-based techniques. In SIMS, a beam of ions is used to remove surface atoms, the ionized fraction of which is analyzed in a mass spectrometer [65, 66].

Energy Ion Spectroscopy (EISS) involves accelerating ions and causing them to impinge on a sample. The technique is divided into three regimes that depend on the energy of the ions: Low Energy Ion Spectroscopy (LEIS), Medium Energy Ion Spectroscopy (MEIS), and High Energy Ion Spectroscopy (HEIS).

Ion Scattering Spectroscopy (ISS) uses the same techniques as EISS to probe surfaces themselves [65, 66]. With a sufficiently well understood inter-atomic potential, an appreciation of the mechanisms of atomic collision and charge exchange. A study of the energy spectrum and angular distribution of the scattered ions can provide a wealth of information on the structure and composition of the near surface of a bombarded target.

2.4. Microscopies

Scanning Probe Microscopy (SPM) measures the strength of the interaction between an extremely fine tip and the surface of a material. The relative position of the tip to the surface produces an image of interaction strength as a function of position. SPM configurations include the Scanning Tunneling Microscope (STM), the Atomic Force Microscope (AFM), and the Magnetic Force Microscope (MFM). The principle behind the STM is that the very sharp tip of the microscope is placed so close to the probed surface that the wave functions of the closest tip atom and the surface atoms overlap [65, 65]. The STM was developed in the early 1980s by Gerd Binnig and Heinrich Rohrer, who were awarded the Nobel Prize in Physics in 1986 for this invention. The AFM works by sensing the deflection of a tiny cantilever. The AFM is a very high-resolution type of scanning probe microscope. The AFM is one of the foremost tools for imaging, measuring, and manipulating matter at the nanoscale. The MFM senses the spatial distribution of magnetism by measuring the magnetic interaction between a sample and a tip [65, 66].

Field Emission Microscopy (FEM) is an analytical technique used in materials science to investigate molecular surface structures and their electronic properties. The technique is applicable for studying adsorption-desorption kinetics and surface diffusion [66].

The electron microscope, including the Transmission Electron Microscope (TEM), the Reflection Electron Microscope (REM), the Scanning Electron Microscope (SEM), and the Scanning Transmission Electron Microscope (STEM) uses electrons as a way to illuminate and create an image of a specimen. The disadvantage of the method is the

expense of the equipment. The TEM uses a high voltage electron beam emitted by a cathode and focused by electrostatic and electromagnetic lenses. In the TEM, the image is formed by electrons passing through the sample [65]. In the REM, high energy electrons are incident at glancing angles to the sample, and reflected electrons are used to form an REM image of the sample surface. A magnified image of the surface is projected on the observation screen of the microscope. In the SEM, a high energy electron beam is scanned across the surface. SEM images have a characteristic three-dimensional appearance and are useful for judging the surface structure of the sample [65].

2.5. Diffraction methods

Reflection High Energy Electron Diffraction (RHEED) is a surface-sensitive technique. Surface specificity at high energies is provided by using both grazing incidence of the primary beam and grazing detection angles of the diffracted beams [65].

X-ray diffraction (XRD) is one of the most useful diffraction techniques for bulk material. “An advantageous effect of the weak scattering of x-rays by material is the weak multiple scattering effects, which make the single scattering approximation, justified well” [65].

In transmission electron diffraction (TED), the diffraction pattern of the electrons passed through the sample is recorded. A disadvantage of the TED is that the sample must be very thin [65].

In Helium Atom Scattering (HAS), a He atom beam is directed toward the sample surface, and then the diffracted atoms provide information on the surface structure

of the material [65].

Another diffraction method is Low Energy Electron Diffraction (LEED). LEED provides mostly information about the 2D atomic structure of the sample surface [65].

3. Photothermal techniques

3.1. Principle of Photothermal techniques

Photothermal techniques are based on the conversion of absorbed optical energy into thermal energy [69]. The absorbed optical energy is converted into thermal energy in a wide range of materials including solids, liquids, and gases. Photothermal signals contain information about the properties of the sample-thermodynamic and energy transfer that may be used to analyze the thermal structure of the materials [69-77].

Photothermal techniques employ a modulated source of light, such as a laser, to generate modulated heating in a sample. This heating makes a number of physical changes to the sample. Figure 2 shows a schematic illustration of the phenomena resulting from the exposure of a sample surface to a localized periodically modulated light source.

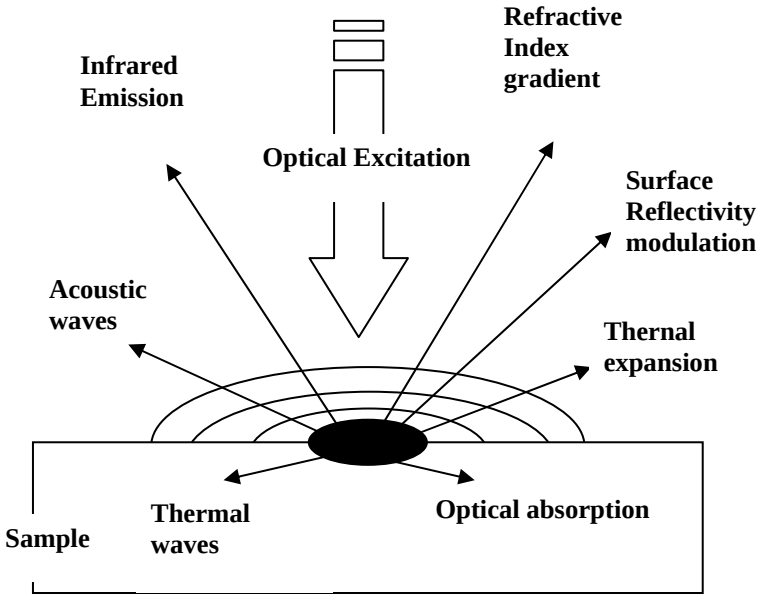

Figure 2. A schematic diagram of the changes sample by optical excitation (re-drawn from [78]).

.

These effects have been used to measure acoustic velocities, thermal diffusion coefficients, temperature rises, bulk sample heat flow rates, specific heats, thermal expansion coefficients, optical absorption, and thermal conductivities [79] in a wide spectrum of materials, such as semiconductors [80], glasses [81, 82], biological specimens [83-85], ceramics [86], and polymers [87, 88]. The technique does not have any limitation regarding optically thin, bulk, or multilayer samples [89].

In addition, understanding photothermal studies requires knowledge about thermal waves, which are generated when a laser beam is partially absorbed by a sample. Thermal waves are analyzed to investigate the characteristics or properties of the sample used in an experiment [90, 91]. As mentioned above, the heat causes various responses to occur in the sample and its surrounding media [92]. In most photothermal experiments, a modulated light beam is used to produce a time-dependent heat source by

a mechanical chopper or an acousto-optic modulator. However, modulation can be broadly described as any arbitrary function of time, in which case, it could be a mixture of modulations with various frequencies. The time-dependent heat source leads to time-dependent temperature fields in the material and its surrounding media because of the conduction process in the material. Such changing temperature fields are referred to as thermal waves [90]. Thus, understanding thermal waves serves as the basis for understanding photothermal studies.

3.2. Photothermal techniques

3.2.1. Photoacoustic spectrometry

The changes in pressure that occur during periodic and pulsed sample heating can be observed through a microphone or other pressure transducer to monitor the acoustic wave [93]. Photoacoustic spectroscopy is used to analyze this pressure wave.

3.2.2. Photothermal radiometry

Given that thermal infrared emission is related to the temperature of the sample, changes in temperature can be indirectly measured by using methods that monitor infrared emission [94]. The method of thermal emission or photothermal radiometry of infrared radiation can be utilized to observe changes in temperature due to optical absorption. Although the method is not very sensitive, it can be applied to non-destructive analysis and testing of materials.

3.2.3. Photothermal deflection

Photothermal Deflection Spectroscopy is a type of spectroscopy that assesses the change in refractive index that occurs when a surface is heated with a laser [95]. This method is known as the mirage effect since a probe laser is used to detect changes in the refractive index of the air or gas adjacent to the surface of the sample. The probe laser beam is diffracted proportional to the temperature of the surface and the optical absorption can be determined from this scattering. Even though the set up for this method is very simple, it can produce very sensitive measurements of surface absorption.

3.2.4. Photothermal deformation

The Photothermal Deformation Technique is one of the most sensitive techniques for detecting thermal waves [96]. The technique has been used to analyze solid surfaces [97]. The modulated pump beam is used to heat the sample while a second, and weaker, probe beam is reflected from the deformation produced by the heating. The probe beam is deflected from its original path because of the surface deformation. The slope of the surface deformation is monitored by the probe beam. This technique is applied to optical films for studying thermal and mechanical properties [98].

3.2.5. Thermal lens

The thermal lens technique is a sensitive tool used to analyze thermo-optical properties of optical glasses, polymers, and liquids. In this technique, the pump beam and the probe beam are arranged collinearly [92]. The thermal heating causes a localized change in the refractive index of the sample. In turn, this change produces a thermal

lens, which is then detected through the focusing and defocusing of the pump beam and the probe beam. The technique's sensitivity is less than that of the photothermal deflection method but it is simpler.

3.2.6. Photothermal reflectance

Photothermal reflectance is comparable to the photothermal deformation technique [95, 99-104]. However, in this technique, the probe beam is irradiated at the center of the heated area. Thus, angular deflection of the probe beam does not occur. By measuring the amount of reflected radiation, this technique is used to detect the change in the refractive index of the sample spot. The temperature change produces a change in the refractive index. In turn, such change causes a difference in the amount of the reflected radiation. This technique is used to determine the thermal conductivity of dielectric thin film coatings with a metallic overcoat [105].

In addition, the photothermal technique can be used to monitor excitation and relaxation processes in the sample. The magnitude of the signal is measured as a function of time or excitation irradiance. The time dependent data are used to further understand the physical properties of the sample. The excitation irradiance dependent data can be used to calculate multiphoton absorption cross-sections and parameters relating to optical saturation.

4. Surface Thermal Lens

4.1. Concepts of Surface Thermal Lens (STL) technique

Absorption is one of the important optical properties of a sample; it can determine the ability of a material to resist laser damage, and it can be a factor in determining the application of a material. One technique to measure absorption of a sample is Surface Thermal Lensing (STL) [14, 105-114]. Figure 3 illustrates the principle of the STL technique.

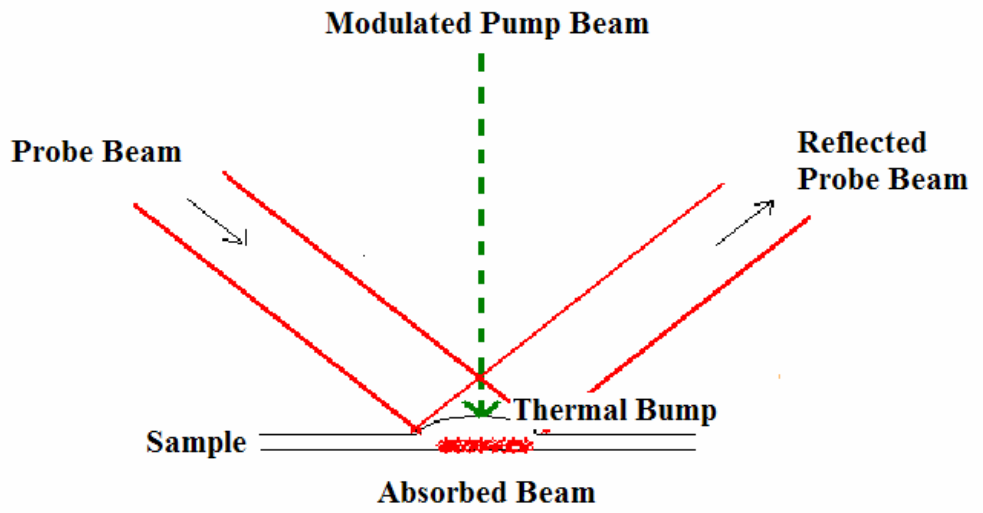

Figure 3. Principle of the STL technique.

When a small portion of the modulated pump beam irradiates the sample, it produces local heating and deformation of the surface, a thermal bump, due to thermal expansion. The thermal bump behaves as a curved reflection mirror and is mathematically similar to a lens. So, the technique is called Surface Thermal Lens (STL). The presence of the bump is detected by a weaker probe beam scattered off the

surface. The deformed area on the sample surface acts as a lens that diffracts the probe beam. Since the probe beam is broader, the components of reflected probe beam experience changes in direction that are proportional to the local slope of the surface deformation. The shape of the surface deformation is thus recorded in the diffraction pattern of the reflected probe beam, which can be analyzed by a photodetector. These steps allow us to observe the thermal expansion, telling us how the sample reacts to the thermal energy. The STL technique is a very promising one for photothermal characterization of optical films, especially weakly absorbing film, including nominally transparent thermoplastics.

One advantage STL has compared to the well known photothermal deflection technique (PTD) is its higher spatial resolution [14]. In the PTD set-up, the probe beam size is much smaller than that of the lateral dimension of the deformed area. The STL technique uses a probe beam diameter that is greater than the lateral dimension of the deformation, so STL has the same high sensitivity but avoids the critical alignment requirements of PTD. STL obtains the full field information of the surface deformation. This can be an important advantage over PTD, where the probe beam samples only a small spot of the deformed area.

4.2. Factors that affect the Surface Thermal Lens

Although various models describing Surface Thermal Lensing (STL) signals have been developed, in actuality, no modeled geometry matches the geometry most commonly used and that used in this thesis. Thus, the following discussion will focus on factors that affect the STL signal in order to qualitatively understand their importance

in STL studies. Much of this information is discussed in more detail by Hussain [115].

When the pump beam irradiates the sample, the amplitude of vibrating atoms in the sample will be increased. As a result, the separation between the atoms in the sample will increase. If the material does not go through a phase change, the expansion can be easily related to the temperature change. The coefficient of thermal expansion α is:

$$\alpha = \frac{1}{L_0}\frac{\partial L}{\partial T} \quad \left(\frac{1}{^0C}\right) \tag{2.1}$$

where L_0 represents the original length, L is the new length, and T is the temperature. Therefore, if the linear coefficient of thermal expansion is known, the expanded length L can be calculated for each degree of changing temperature. A linear relationship exists between the size of the thermal bump and the coefficient of thermal expansion. As such, a larger expansion coefficient would cause a greater expansion per degree rise in temperature, resulting in a larger thermal bump [116].

Elasticity is defined as the ability of a material to return to its original shape. It is partly determined by the material's elastic modulus. Here the elastic modulus is known as Young's modulus. Sometimes, it is also expressed as the tensile modulus. The elastic modulus (E) is defined as the ratio of stress to strain:

$$E = \frac{\sigma}{\varepsilon} \quad (Pa) \tag{2.2}$$

where σ represents the applied stress, and ε is the strain produced. The strain can be found by taking the ratio of expanded length over the original length. In STL, the greater the modulus, the smaller the strain produced by a certain amount of stress. Therefore, a higher modulus will produce smaller thermal bump [117].

The thermal diffusivity also influences the size of the thermal bump. Thermal diffusivity describes the ability of a material to conduct thermal energy compared to its ability to store thermal energy. Thermal diffusivity is represented as:

$$D = \frac{k}{\rho \cdot c} \quad \left(\frac{m^2}{s} \right) \tag{2.3}$$

where k, ρ, and c are the thermal conductivity, the density, and the specific heat of the material, respectively. Thermal conductivity is defined as the rate of heat (Q) transmitted through a unit thickness (L) in a direction normal to a surface of unit area (A) due to a unit temperature gradient (ΔT) under steady state conditions and when the heat transfer is dependent only on the temperature gradient. The thermal conductivity, k, can be found through:

$$k = \frac{Q \cdot L}{A \cdot \Delta T} \quad \left(\frac{W}{m \cdot K} \right) \tag{2.4}$$

For low thermal diffusivity, the height of the thermal bump increases to a higher value than that for high thermal diffusivity. Such a phenomenon is apparent given that

lower thermal conduction results in greater thermal energy storage. For high thermal diffusivity, the thermal bump may be wider and less high. Overall, when the thermal diffusivity is increased, the STL signal is decreased due to flattening and broadening of the thermal bump.

Optical absorptivity of a material can be defined as the fraction of the incident radiation absorbed [116]. The STL signal is largely contingent upon how much energy is absorbed by a sample in each pulse. A greater absorptivity results in a greater fraction of energy being absorbed by the sample spot, thereby increasing the size of the thermal bump and its curvature. However, in STL, the relationship between the absorptivity and STL signal is not always linear. This issue will be discussed in the results.

Beam characteristics in the STL signal

As discussed in the previous section, a pump beam and a probe beam irradiate the sample at the same time in an STL experiment. Each beam can be a factor in the STL signal.

The size of the beams is important because the spot size of the probe beam should allow reflections to occur from the thermal lens generated by the pump beam as well as from the surface surrounding the thermal lens. If the diameter is too large, most of the reflections of the probe beam will not occur from the surface thermal lens. On the other hand, if the diameter of the probe beam is too small, it would generate a deflection signal instead of a diffraction signal because the probe beam will scatter off only a small portion of the thermal bump. In addition, the size of the probe beam has to be larger than the size of pump beam, since the pump beam generates the thermal lens.

The probe beam is used to understand any changes in the sample due to the pump beam. Therefore, it is also important to choose a probe beam intensity that is neither too low nor too high. If the intensity of the probe beam is too weak, it would make it impossible to detect a signal through the lock-in-amplifier. If the intensity of the probe beam is too high, a significant absorption would occur on the sample spot, generating a thermal bump of its own. This bump will, in turn, overlap with the bump produced by the pump beam, making it difficult to interpret the data. There is no need to chop the probe beam since the STL signal is modulated by modulating the thermal bump through chopping the pump beam.

Polymers have long chain-like molecules that may treat different polarizations of light asymmetrically. Polymer molecules can be altered or reconfigured by repeated flexing, as in the production of a modulated surface thermal lens. Information about the reconfigurations may be gained from the use of a polarized probe beam.

The intensity of the pump beam influences how much energy is absorbed by the sample spot; a greater intensity of the pump beam results in a greater amount of energy absorbed at a given optical absorptivity. Such increased amount of absorbed energy enhances the size of the thermal bump, which is shown by an increase in the signal amplitude with intensity.

A lower chopping frequency of the pump beam produces a longer exposure time and a decreasing modulus. This effect tends to produce a bigger thermal bump since more energy is absorbed per pulse at lower chopping frequencies than at higher chopping frequencies. Therefore, the expected STL signal is inversely related to the chopping frequency of the pump beam [115].

Relaxation time in polymers

Thermoplastic polymer samples were used in this experiment. The applied stress or pump beam is a factor in determining the phase lag between input and output signals [118] in a polymer. In an elastic material such as rubber, the phase lag between the stress and strain cannot be found, since when the stress is removed, the expanded area can return instantaneously to the original state. In a thermoset (see section 1.2.1), when the stress is applied to the material, it never returns to the original state, while, in a thermoplastic, it always tries to return to its original state. The main property of the thermoplastic is recycling. When the stress is removed from the material, the material can be returned the original state after the relaxation time. The relaxation time, τ, to reach the original state, is obtained by

$$\tau = \frac{\eta}{E} \quad (s) \tag{2.5}$$

where η is the viscosity, and E is the elastic modulus ($E = \frac{\sigma}{\varepsilon}$). Therefore, as the stress or pump beam is applied to a polymer, a periodic strain, with a phase shift, is observed with respect to the phase of the stress due to relaxation time. The thermal bump cannot be relaxed completely, or returned to the original state, when the chopped time of the pump beam is less than the relaxation time.

The relationship between time lag and phase lag

The mechanical expansion of the thermoplastic does not occur immediately; there is a time lag because of the viscoelastic behavior of the spot. The spot does not reach mechanical equilibrium at any time due to the constant rise in temperature. The instant the pump beam is chopped, the height at which the bump would be in mechanical equilibrium begins to fall, the rate of which depends on the rate of fall in temperature. However, the actual mechanical bump height does not begin to decrease instantly but keeps building up due to the time lag. Eventually the bump cools enough so contraction must take place.

The relationship between the phase lag and the time is represented in the diagram and equation below:

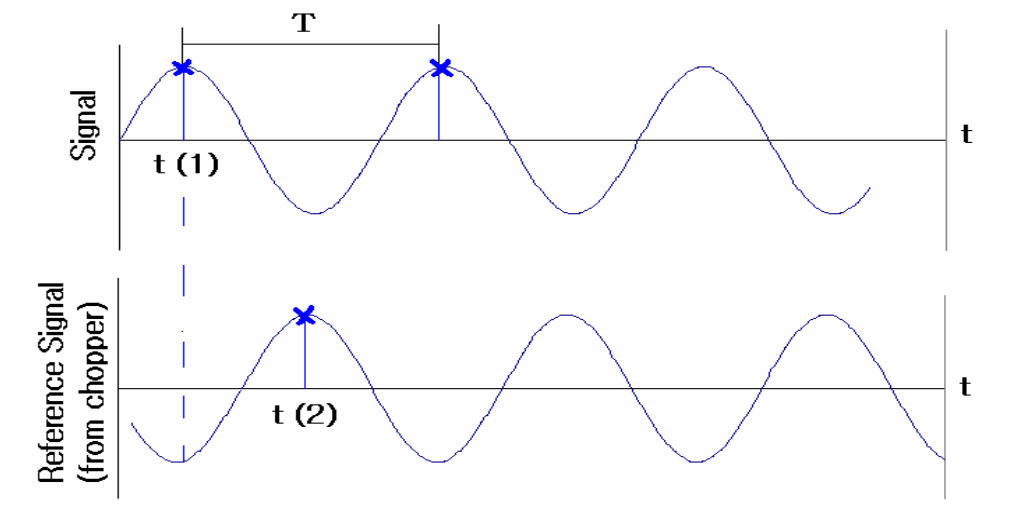

Figure 4. A diagram of the relationship between phase lag and time.

$$\Delta\phi = -\frac{\Delta t}{T} \times 360^0 = -\frac{t_2 - t_1}{T} \times 360^0 \quad \text{(deg)} \tag{2.6}$$

in which $\Delta\phi$ is measured in degrees, T is the time period of both the signal and the reference signal. The minus sign is included because Δt refers to how much the STL signal lags behind the pump beam. It indicates that the negative value of the phase lag may increase linearly with the chopping frequency. In this thesis, most of the discussion is focused on the amplitude of the signal, so the relaxation time and phase study is left for future study.

4.3. Research by using Surface Thermal lens (STL) technique

In order to develop a theoretical model, Kuo worked [90, 108-109] with the assumption that the height of the thermal bump has a Gaussian profile and the phase of the bump is spatially uniform. These assumptions are acceptable if the length of the thermal diffusion is much smaller than the radius of the heating beam and if no viscoelastic response occurs in the sample. Under these conditions, the size of the thermal bump hardly exceeds the size of the heating beam [108-109].

Other assumptions are linked to the geometry of the set-up. In quantitatively analyzing the data with Kuo's model, the probe beam is assumed to be irradiated close to the normal of the sample. In addition, the pump beam is assumed to have sinusoidal variations in its intensity. These assumptions do not accurately fit the geometry of the experimental set-up in this study given that the probe beam is irradiated significantly off the normal to the surface. Moreover, the pump beam used to produce the thermal bump is chopped, which then generates waves or a train of pulses rather than sinusoidal waves.

Therefore, some adjustments in the model would need to occur to fit the geometry of the experimental set-up of this study.

The study of STL is still developing. The topics of the research include:

- A study of the contamination effects on the optical components [106].
- A study of the laser induced surface deformation of the thin film [107].
- A study of the thermal-mechanical properties of the polymer thin film [76, 77].
- A measurement of weak absorptance of thin film coating [110].
- An investigation of the optical, thermal, mechanical properties of the bulk polymer [115].
- An investigation of transient absorption by two double pulse excited photothermal lenses based on STL [119].

Recently, Bincheng Li and his research group have been researching the STL technique [120, 121]. They found a nonlinear absorption coefficient of multilayer bulk materials with this technique. The research was performed by combining Laser Calorimetry (LC) and the Surface Thermal Lens technique (STL). LC can directly measure the absolute absorptance of the optical component. However, in LC, long irradiation time is required to create a measurable temperature change, and cooling time is necessary for observing data. The STL method is more sensitive than the LC method. The STL method can measure absorption loss of the optical component in short irradiation time (in milliseconds) or with single-pulse irradiation. The STL method has

been used in high-resolution absorption studies of optical coatings [122, 123]. However, the STL method can measure only the relative value of the absorption loss. In addition, the STL method is difficult to calibrate since the measured STL signal is a complicated function of the optical, thermal, and thermoelastic properties of the investigated sample. Therefore both LC and STL can be usefully combined. The combined technique can accurately measure the absolute linear and nonlinear absorption coefficients of optical coatings with a short irradiation time, and monitor instantly and *in situ* any irradiation-induced changes of the optical and thermal properties of the optical components.

Chapter 3: EXPERIMENTAL PROCEDURE

1. Schematic diagram of Surface Thermal Lensing (STL) set up

A schematic diagram of our STL set up is shown in Figure 5. A similar arrangement has been used by several researchers [76-77, 115].

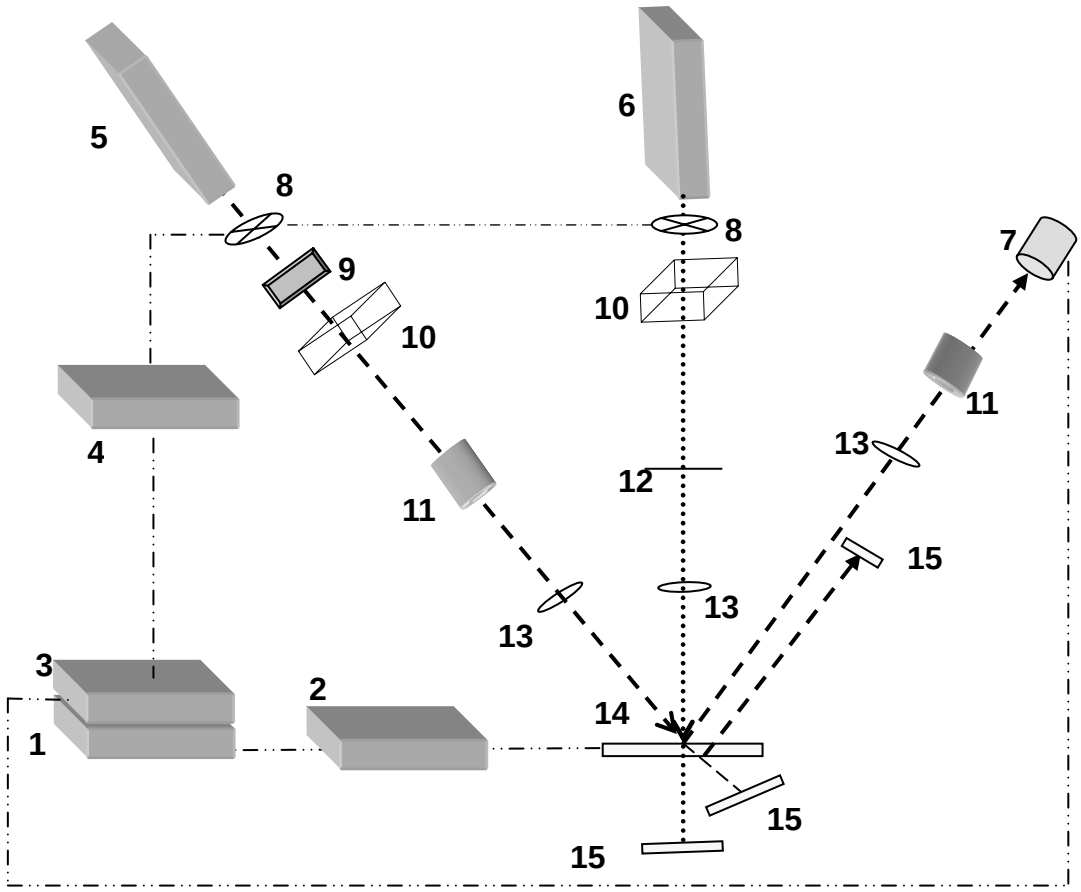

1. Soft ware 2. Sample positioner 3. Signal Amplifier 4. Chopping controllers
5. Probe Beam 6. Pump Beam 7. Photo Detector 8. Optical Choppers
9. Attenuator 10. Beam Steerers 11. Polarizers 12. Diaphragm 13. Lenses 14. Sample
15. Beam Blocker

Figure 5. A schematic diagram of the experiment set up.

A He-Ne laser **(5)** was used as the probe beam and a solid state laser **(6)** as a pump beam to produce the thermal bump. After the pump beam was chopped by an optical chopper **(8),** the beam was focused by a lens **(13)** to adjust the size of the beam on the sample **(14).** The pump beam was oriented perpendicular to the sample spot. Also, the incident probe beam was focused by a lens. The size of probe beam should be larger than that of the modulated pump beam in the STL configuration. The angle of the incident probe beam was about 18^0 from the normal to the sample.

When the modulated pump beam irradiated the sample, the probe beam was reflected from the sample **(14).** Polarizers **(11)** were used to determine the effect of the polarized probe beams on the STL signal. The reflected probe beam was detected by a photo-detector **(7).**

The detector was usually located at or near the peak of the diffraction pattern, and it monitored the signal over time. Figure 6 shows a schematic representation of the diffraction patterns produced when the probe beam was reflected off a thermal bump.

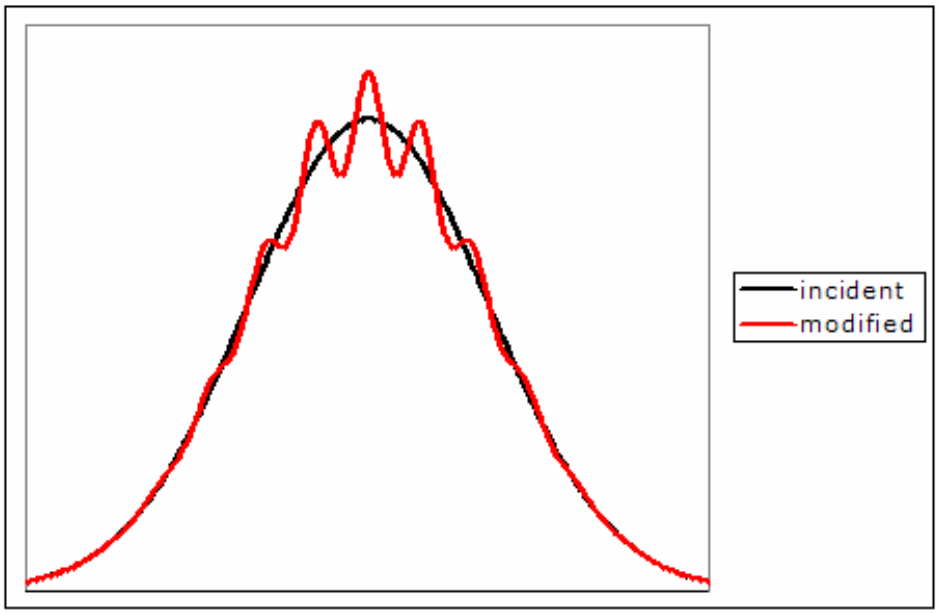

Figure 6. A schematic representation of the diffraction pattern produced when the probe beam was reflected off a thermal bump measured [124].

The central peak in the diffraction pattern is in fact a peak and hence will be larger intensity than when the thermal bump is not present.

The detected reflected probe beam as selected and amplified by a lock-in amplifier **(3)** is called the STL signal. The computer **(1)** is connected to the lock-in amplifier. It accumulates data from the signal such as phase and amplitude. Details of the elements in Figure 5 are as follows:

(1). Software

A PTM YC software program was used on a DELL XPS P120c computer to record and analyze the data collected from the experiment. The software used Visual Basic 6.0, and the PTM YC program communicated with a motion controller **(2)** and the lock-in amplifier **(3).** The PTM YC software had two functions: i) to record the STL

signal as a function of time and ii) to scan the horizontal and vertical axis of the detector position.

(2). Beam (or Sample) movement

A 4-axis motion controller (MM3000) with four 850F-HS motors was used to position devices with precision from a remote location outside of the enclosure. The MM3000 was connected to a pinhole detector to scan the STL signal and to the sample holder to change spot positions. The controller produced repetitive, reproducible movements with approximately 0.05 micron accuracy.

(3). Signal Amplifier

The lock-in amplifier, an SR830 DSP Stanford Research Systems, simultaneously displayed the magnitude and phase of a modulated signal. The lock-in amplifier had two inputs, the signal from the detector **(7)** and the reference frequency from the optical chopper **(4).** It also has one output to the computer **(1).**

(4). Chopping controllers

The chopping controller, an SR 540 Stanford Research Systems, was connected to two optical choppers and produced chopping frequencies in the range from 4 Hz up to 3.7 kHz. The frequency was displayed on the screen of the chopping controller and that of the lock-in amplifier. I was able to adjust the frequency with the controller. The stability of the chopping controller was 250 ppm/^{0}C and the drift of frequency was less than 5 %.

(5). Probe Beam

A probe beam, the He-Ne Laser M1145 JDS Uniphase, was used in this investigation. The wave length was 632.2 nm, and the maximum output power was 35 mW. The beam passed through a line attenuator **(9),** which then adjusted the power of the beam. The size of the beam was determined by the lens. The size of focused beam was approximately 100 μm on the sample, as measured by a CCD profiler (see Appendix II-1).

(6). Pump Beam

The pump beam, a Millennia II Spectra-Physics, was a diode-pumped CW visible solid state laser and consisted of a laser head, a power supply, and a remote control. The pump beam provided power ranging from 0.2 ~ 2.0 W of green 532 nm output. However, in this experiment, an effective range of 0.2 W to 1.0 W was used. The beam diameter at the output port is less than 1 mm. The size of the focused beam was approximately 50 μm on the sample (see Appendix II-2).

(7). Photo Detector

The photo detector, a PD 3000 IB Precision Applied Science, can be used to detect light signals with wavelengths ranging from 190 nm to 1700 nm. The detector position was controlled by two linear actuators connected to the motion controller. The diffraction pattern could thus be easily scanned.

(8). Optical Choppers

In this research, two optical choppers (SR 540 Stanford Research System) were used. One chopper was placed in front of the probe beam and the other in front of the pump beam. The chopper produced a modulated beam by rotating a slotted wheel in front of the beam. Both choppers cut in half the average power of the beam. The chopper that was placed in front of the probe beam was a 30/25 slot chopper and produced frequencies ranging from 400 Hz to 3.7 KHz. The other chopper that was placed in front of the pump beam was a 6/5 slot chopper and produced frequencies ranging from 4 Hz to 400 Hz.

(9). Attenuator

The variable attenuator, an M 935-5 OPT Newport, was able to control the power of the probe beam. However, in this experiment, the power of the probe beam was not altered. The chopped probe beam passed through the attenuator that was fixed at 5 mm aperture.

(10). Beam Steerers

The beam steerer was constructed with two axis micro-motion control stages and two adjustable optical mirrors. The direction (two axes) of both beams was shifted by controlling the beam steerers. The beam steerer allows movement in 2 dimensions (x and y) without changing the angle of the beam, and it allows for some independent angular adjustment. Thus, the beam was adjusted so that it was parallel to the table and hitting the sample at right angles, and then positioned to be able to move the beam side to

side or up and down without changing its angle.

(11). Polarizers

Two linear polarizers were used in this research. One was placed between the probe laser and the sample, to produce an incident polarized probe beam, while another one was placed between the sample and the detector, to polarize the reflected probe beam.

(12). Diaphragm

The diaphragm was an adjustable apparatus that removed multiple reflections from the beam steerer of the pump beam.

(13). Lenses (bi-convex lenses)

Three lenses were used in this research to control spot size on the sample and to focus the reflected probe beam onto the pinhole.

(14). Samples

Two different types of samples were used in this investigation: (i) Zeonex® E48R, Cyclo-Olefin-Polymer (COP), (the thickness of the Zeonex was 3.0 mm and the diameter was 24 mm.), and (ii) acrylic HS3125, Poly-Methyl-Meth-Acrylate (PMMA), Lucite International Inc. (the thickness of the acrylic was 3.0 mm and the diameter was 24 mm.) Both polymers were bulk polymers.

(15). Beam Blockers

One blocker placed behind the sample was used for safety purposes to absorb the remaining pump beam. Two other blockers were used to absorb unwanted portions of the probe beam.

(16). Actuator (not shown in the Figure 5)

Three actuators, an 850 F Newport, were connected to the motion controller (2). Two actuators were attached to the photo detectors for two dimensional moving, and one to the sample holder for one dimensional moving. Each actuator had its own channel on the motion controller.

(17). Optical Filter (not shown in the Figure 5)

A blue optical filter was used to reduce the power of the pump beam while the pump beam was being adjusted, to prevent damage to our eyes.

(18). Optical Power Detector (not shown in the Figure 5)

The optical power detector, 883-SL OD3 Newport, was placed behind the sample for detecting the transmitted probe beam. Detectable power levels ranged from 1 pW to 2 W, and the capable measuring wavelength was from 200 ~ 1800 nm. Its function, at times, was to measure the transmitted probe beam intensity as a way of monitoring the stability of the probe beam; at other times it was used to measure the intensity of the reflected probe beam to study how the polarizers were working.

(19). CCD Camera (not shown in the Figure 5)

The CCD camera, a Monochrome Progressive Scan CCD camera 6400 COHU, was used for aligning the spot position with both the probe and pump beams.

(20). Optical table (not shown in the Figure 5)

All equipment was set up on an optical table, an RS3000 Newport. The table allowed us to install the equipment securely and reposition it easily. To reduce dust that could affect the level of noise, the table was enclosed in a plexiglas box. For safety, the plexiglas was then covered with a shroud of thick blue cloth to block stray beams during experiments.

2. Optimization of STL signal and Pump beam warm up

Before the experiment was started, the STL signal was optimized. First, I completely realigned the beams to make the spots coincide. I performed this realignment occasionally, when the STL signal from the lock-in amplifier became noisy. First the probe beam was switched on, and then the pump beam spot was lined up with the probe beam spot. Because of the hazardous nature of the high power pump beam, I mounted a filter immediately in front of the pump beam. A CCD camera was used to directly view the beam spots on the sample so that the beams could be aligned visually. In particular, the narrow pump beam was positioned in the center of the broader probe beam. Figure 7 is a diagram of the beam alignment.

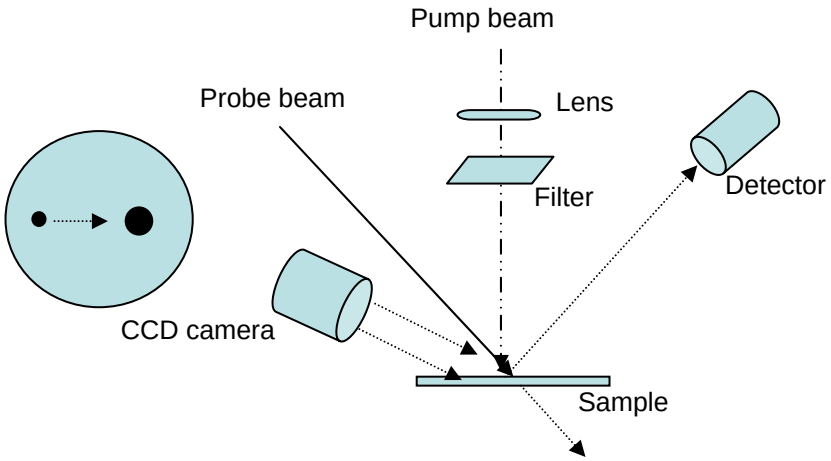

Figure 7. A diagram of the alignment of the beams.

After the beams were realigned, the detector position was optimized. The optimization was done nearly every run, since slight shifts in the detector could have a significant effect on the signal. First, with the pump beam shuttered, the detector was optimized with respect to the reflected probe beam. The optimization was achieved by chopping the probe beam and moving the detector position until the peak in the lock in amplitude was identified. However, the signal obtained from the chopped probe beam was not the STL signal since the pump beam was not hitting the sample at this time. After maximizing the detector signal in this way, the probe chopper was turned off. For some runs, the pump beam was next un-shuttered and the optimization was refined to maximize the STL signal. The above process was performed by moving the detector position until the peak in the lock-in amplitude was identified.

Before the solid state laser pump beam irradiated the sample, the beam was warmed up to stabilize it. The warm-up procedures took place for 40 minutes at the beginning of each day that the data were collected. The procedure was as follows: first, the laser power supply was warmed up for approximately 40 minutes. Then, the current

of the laser power supply was increased to 70% of its maximum value. After an additional ten minutes of waiting, the laser was switched to the power control mode. The sample was never exposed to the pump beam during warm-up.

3. Phase offset of chopped pump beam

The power meter was connected to the lock-in amplifier and worked as a detector. Before the pump beam hit the sample, the power meter measured the amplitude and phase of the signal from the pump beam. Figure 8 shows a diagram of the procedure for finding the phase offset of the chopped pump beam.

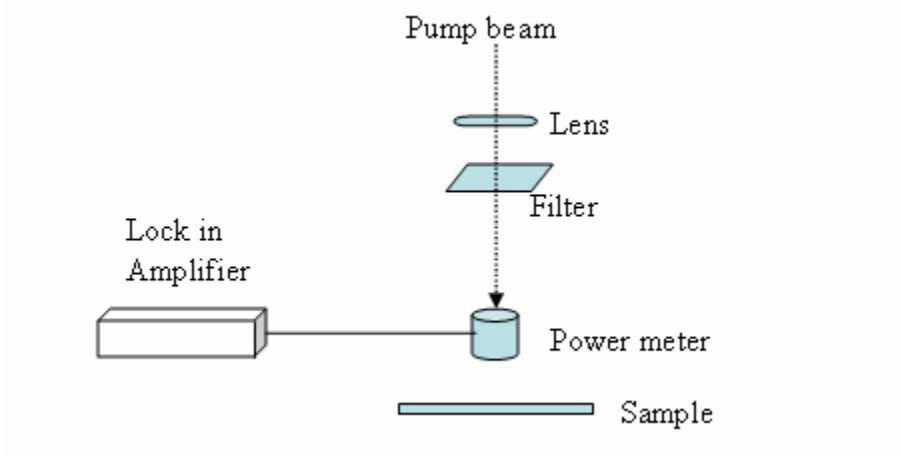

Figure 8. A diagram of "finding phase offset of chopped pump beam."

At this point, only the phase was read from the lock-in amplifier. The chopped pump beam was directly detected; it was expected there would be no phase lag registered by the lock-in amplifier. However, the reality is that the phase lag depended on the relative position of the laser and the chopper wheel. Even though the chopping frequency of the pump beam was varied, the phase was always 135^0. Therefore the

offset phase of the chopped pump beam is 135^0. Thus all the phase readings from the lock in amplifier should be shifted by 135^0.

4. Recording Data

All the data were saved in a file with the author's symbol "dh", month, day, and year (i. e., dh040906 represents data taken on April 9, 2006). The data also included letter codes, when multiple testing was conducted on the same day such as dh040906-1-A. For each graph, the corresponding data file name was noted in the title.

5. Experimental Procedures

After completing the above warm-up and alignment procedure as needed, three types of experiments were performed:

1. Surface Thermal Lens (STL) studies of bulk polymers using unpolarized light.
2. Surface Thermal Lens (STL) studies of bulk polymers using polarized light.
3. Scanning across the diffraction pattern.

5.1. Surface Thermal Lens (STL) studies of bulk polymers using unpolarized light

The purpose of the experiment was to understand the effects on the STL signal of variations in the power and in the chopping frequencies of the pump beam. This experiment used the Zeonex sample.

5.1.1. Measuring the pump beam power dependence of the STL signal

The purpose of this experiment was to understand the changes in STL signal due

to varying the pump beam power. The pump beam's output power was varied from 0.2 W to 1.2 W in steps of 0.1 W, with data being accumulated for 5 minutes at each setting. The chopping frequency of the pump beam was set to 37 Hz. The reflected probe beam from the sample was then detected. In this experiment, two sample spot positions were compared, with all other conditions remaining constant.

5.1.2. Measuring the chopping frequency dependence of the STL signal

This experiment aimed at understanding the changes in STL signal due to varying chopping frequencies of the pump beam. The experiment focused on STL signal changes created by varying the chopping frequency of the pump beam. Eleven frequencies ranging from 37 Hz to 407 Hz were studied. The frequency of 37 Hz was chosen as a reference frequency. Alternate 5 minute runs at 37 Hz, and at a new frequency, were performed as a way of correcting for time dependence in the signal. This process will be discussed further in the results section below. The power of the pump beam was maintained at 1 W. The experiment was carried out on two different sample positions.

5.2. Surface Thermal Lens (STL) studies of bulk polymers using polarized light

This experiment involved a modification of the above-mentioned procedures. The purpose of this experiment was to study the characteristics of bulk polymers, specifically Zeonex and acrylic, using polarized light. This experiment focused on comparing the use of polarized and non-polarized light on the sample. Before the experiment started, the polarizers were tested to confirm the direction of polarization.

One rotary polarizer was rotated, while the other polarizer was fixed. Figure 9 shows a diagram of the set-up.

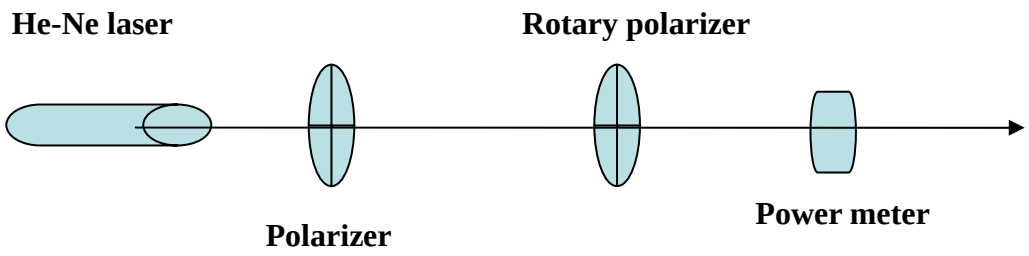

Figure 9. A diagram of polarizers line up.

Data for the power meter reading versus angle of the rotary polarizer were generated.

.

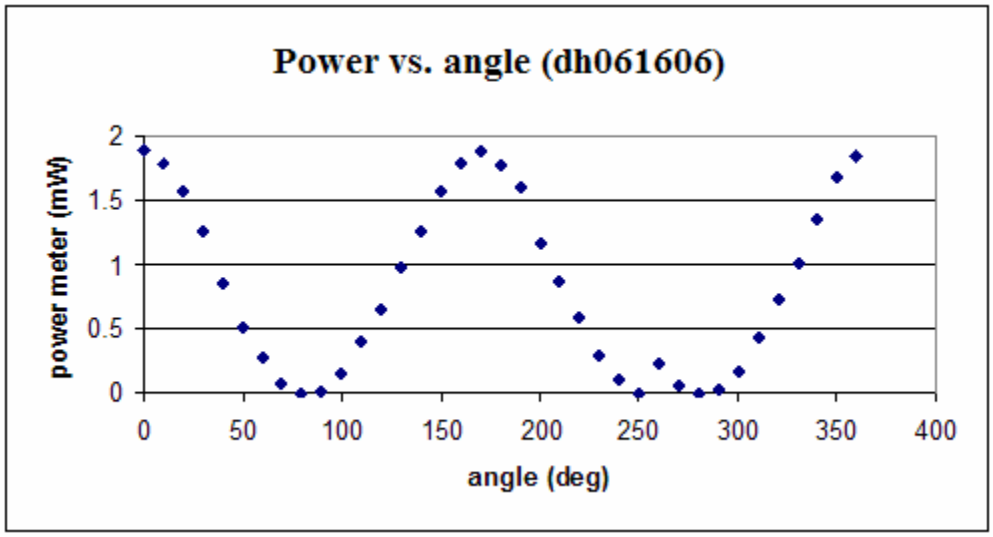

Figure 10. Relationship between the power of the polarized light and the angle of rotary polarizer.

Theoretically, the power of the beam should be proportional to $\cos^2\theta$. The graph of power versus $\cos^2\theta$ was plotted to verify the relationship.

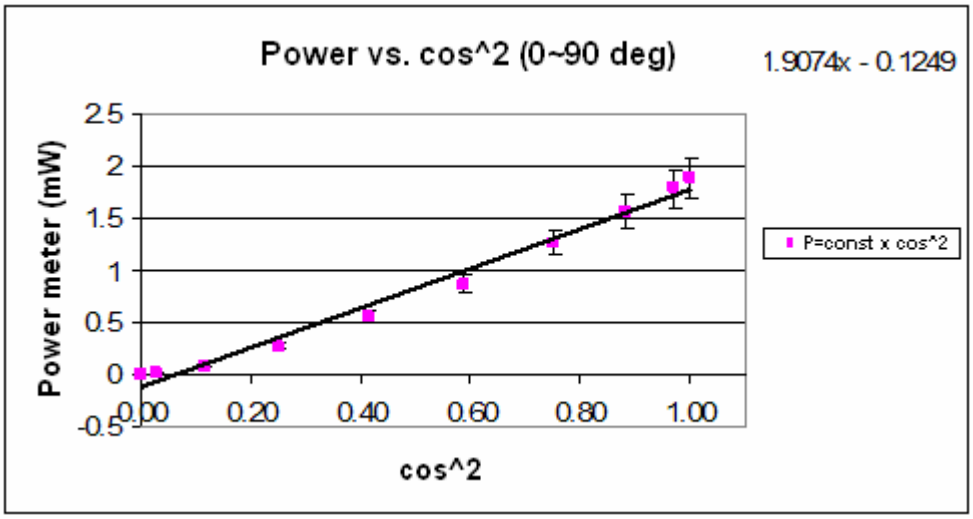

Figure 11. The power of the polarized light versus $\cos^2\theta$.

As can be seen in the above graph, the function was nearly linear and indicates that the results followed the theory as expected. The best fit line on the linear plot was created by the researcher. The linear relationship was expected; however, there was a 10% error as determined from the average deviation of an individual point from the theoretical line. The error may have been derived from adjusting the angle of the polarizer manually. Because the polarizer was not mounted on an optical table, it may have shifted slightly during the experiment. However, the error was deemed as insignificant. Thus, we continued to use these polarizers.

5.2.1. Surface Thermal Lens (STL) studies of Zeonex using polarized light

The purpose of this experiment was to study the characteristics of Zeonex polymers using polarized light. The probe beam was horizontally polarized prior to striking the sample. In addition, the reflected beam was vertically polarized prior to the

detector. Thus, the polarizers were crossed and hence this set-up detected the extent to which the surface rotated the polarization of the reflected beam. The pump beam power and chopping frequency were set at 1 W and 37 Hz. We irradiated the sample for 1 hour with a break time of at least 2 hours between separate runs, to allow for surface recovery. For the comparison between polarized and non-polarized probe beams, non-polarized beams were also used with the same procedure. Figure 12 shows the experimental set-up.

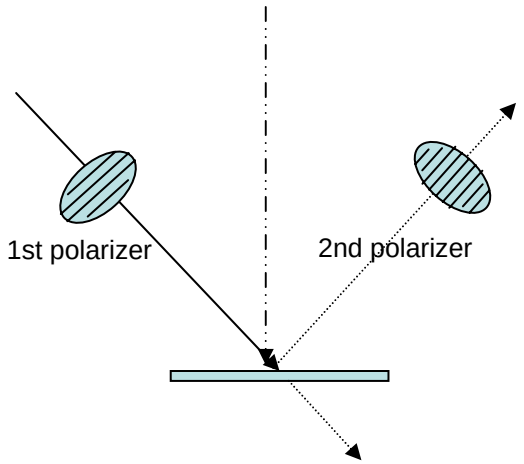

Figure 12. A diagram of the polarized probe beam set-up.

5.2.1.1. Studying the oscillation of the STL signal through variations in power and chopping frequency of the pump beam with Zeonex

The results of the preceding experiment showed time dependence in the STL signal with unusual oscillatory behavior. To study nature of the oscillation in more detail, the following experiments were performed.

The entire running time was 1 hour and 30 minutes. For the first 30 minutes the power was 1 W, for the next 30 minutes it was 0.5 W, and for the last 30 minutes it was

1 W. The chopping frequency of the pump beam was set to 37 Hz. Another experiment focused on varying the chopping frequency of the pump beam in 30-minute intervals (e. g., alternating 37 Hz, 107 Hz, and 37 Hz). The pump beam power was set to 1 W. The modified experiment was conducted with at least 4 hours of relaxation time between runs.

5.2.2. Surface Thermal Lens (STL) studies of acrylic using polarized light

The purpose of this experiment was to study the characteristics of an acrylic polymer using polarized light. The experimental procedure was the same as one used with Zeonex (section 5.2.1), except the angle of the polarizers was changed. The probe beam was horizontally polarized prior to striking the sample. In addition, the reflected beam was also horizontally polarized prior to the detector. This configuration was chosen initially because crossed polarizers did not produce a sufficiently strong signal to detect.

5.3. Scanning across the diffraction pattern of the acrylic

In these experiments, two polarizers were again mounted. Also, both polarizers were set horizontally to make them parallel to each other.

Using the line profile feature that is in the PTM YC software, the STL signal was scanned by the detector, whose position was adjusted along the horizontal axis. The scanning distance was 60 microns. The data were recorded 20 times, while moving forward then resetting the position after each measurement. The 20 scans were broken into 4 groups of 5 and averaged to get 4 plots with reduced noise but with sufficient detail

to observe time dependence in the diffraction pattern. Prior to STL measurement with polarized light, the detector was scanned horizontally with non-polarized light. The detector was, again, scanned horizontally with polarized light. After one hour of the STL measurement, the detector was scanned horizontally as before.

Chapter 4: RESULTS AND DISCUSSION

These experiments utilized polarized and non-polarized light in Surface Thermal Lens (STL) studies with polymers. The samples used in this investigation were Zeonex and acrylic. The experiments were expected to show new insight into polymer structural behavior under the influence of repeated flexing.

1. Surface Thermal Lens (STL) studies of bulk polymers using unpolarized light.

The results of this first round of experiments were useful for the investigation because the initial signals were used as the basis signals to be compared with those of the various experimental conditions and samples. The significant difference in these experiments compared to those of other researchers [76, 115] was the use of a different sample (earlier work involved PMMA thin films and an amorphous bis-phenol A polycarbonate). In these experiments, Zeonex was used as a sample. Although modifications were made in these experiments, similar results were expected because all of the studies utilized polymers. Moreover, the results found from these experiments with unpolarized light have been used as the basis for understanding the results from later experiments that used a polarized probe beam.

1.1. STL signal changes with varying pump beam power

The purpose of this experiment was to understand the changes in the STL signal due to varying the pump beam power. Although the pump beam power was varied, the chopping frequency was maintained at 37 Hz. Previous studies [76] maintained a

chopping frequency of 200 Hz. However, the difference in chopping frequency is not significant since it did not affect the pattern of the signal.

Two sample spot positions were used for the beam target under the same experimental conditions; however, the same pattern of STL signal was obtained as shown in Figure 13.

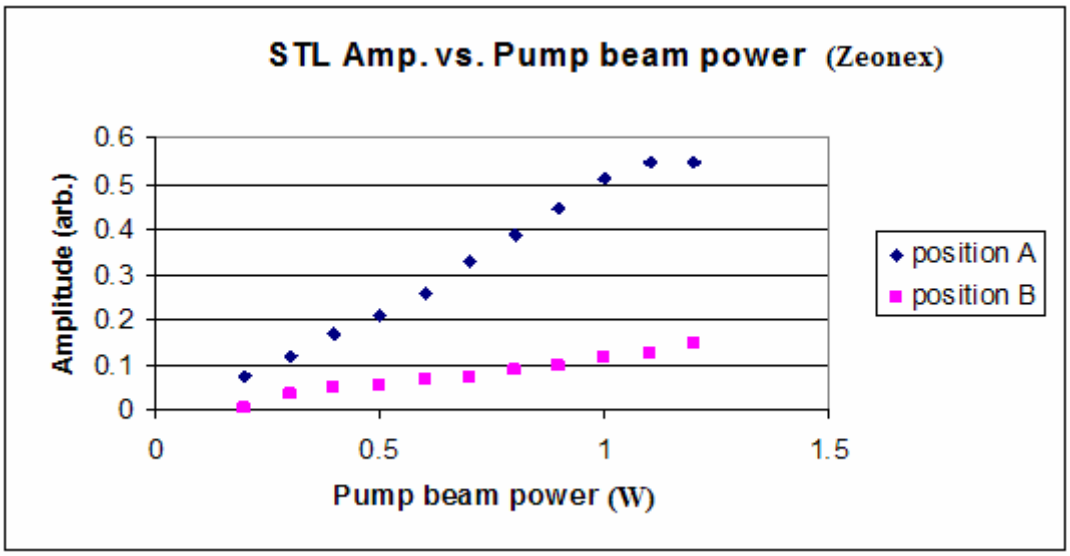

Figure 13. STL amplitude versus pump beam power with two sample spot positions.

As shown in Figure 13, when pump beam power increased, the amplitude of the STL signal also increased because the strength of the amplitude of the signal is proportional to the size of the thermal bump. The STL amplitude has been found to be proportional to the intensity and size of thermal bump. This pattern is the same as one found by Chen [76]. The different slopes probably indicate different properties such as different absorptivities, thermal conductivity, elasticity, and so on, at the two sample positions. Also the relationship may be nonlinear for spot position “A” above 1 W, although it is

difficult to tell. However, what this suggests is that below 1 W, the response is linear in the pump power and hence very likely to be linear in absorptivity also.

1.2. STL signal under various chopping frequencies of the pump beam

This experiment aimed at understanding the changes in STL signal with respect to the chopping frequency of the pump beam. The amplitude and phase of the STL signal were analyzed. The pump beam power was maintained at 1W, and eleven frequencies ranging from 37Hz to 407Hz were used. However, as the experiment proceeded it was observed that the signal was unstable even when the chopping frequency was held constant. Figure 14 shows the results from the trial runs.

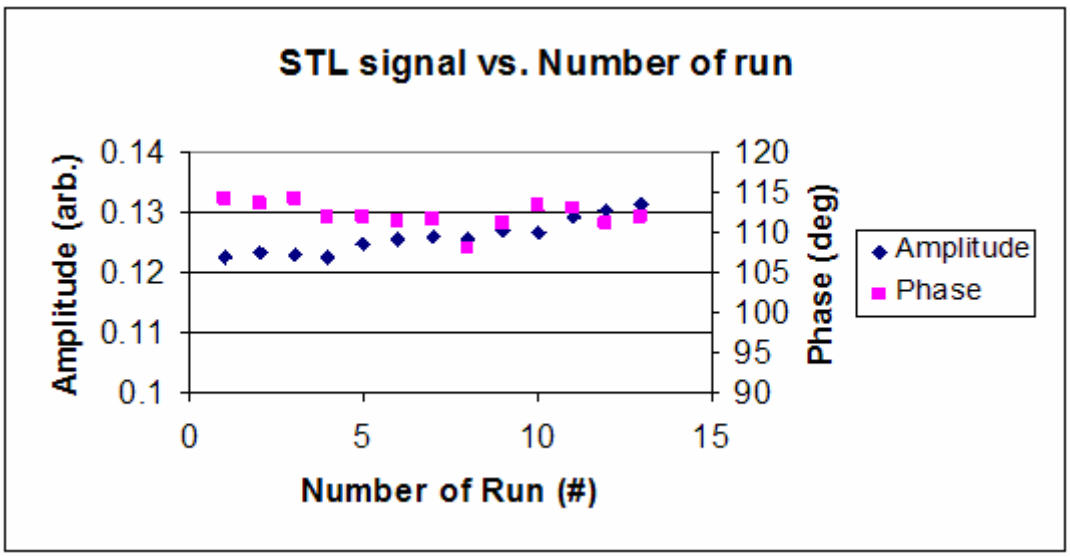

Figure 14. STL signal versus number of run with 37 Hz.

Figure 14 illustrates data collected multiple times at the same chopping frequency, 37 Hz, to test for time dependence in the signal, and shows a presence of time

dependence with the same experimental conditions. Hence, the STL amplitude at other frequencies was normalized with data taken immediately before and after at the reference chopping frequency of 37 Hz.

The normalized STL amplitude was calculated by dividing the STL amplitude at any frequency by the average amplitude at 37 Hz taken immediately before and immediately after the data taken at a particular frequency. For instance, referring to data from Table III,

$$\bar{R}(@\,47Hz) = \frac{0.942}{\frac{1}{2}(1.000 + 1.020)} = 0.933,$$ ($\bar{R}(@\,47Hz)$ is normalized amplitude at 47 Hz.)

Thus, $\bar{R}$ represents the ratio of the amplitude at a given chopping frequency to the amplitude at a frequency of 37 Hz acquired at nearly the same time.

In this sample calculation, 0.942 was the amplitude of signal at 47 Hz. 1.000 was the amplitude at measured at 37 Hz just prior to the 47 Hz measurement, and. 1.020 was the amplitude measured at 37 Hz just after the 47 Hz measurement. Table III shows the normalization of the amplitude of the signal.

Table III.
A sample calculation of data for normalization.

Frequency (Hz)	**Amplitude (arb.)**	$\bar{R}$ **(arb.)**
37	1.000	1.000
47	0.942	0.933
37	1.020	
67	0.874	0.852
37	1.032	
Etc...		

Figure 15 shows the normalized amplitude versus chopping frequency at two different sample spots.

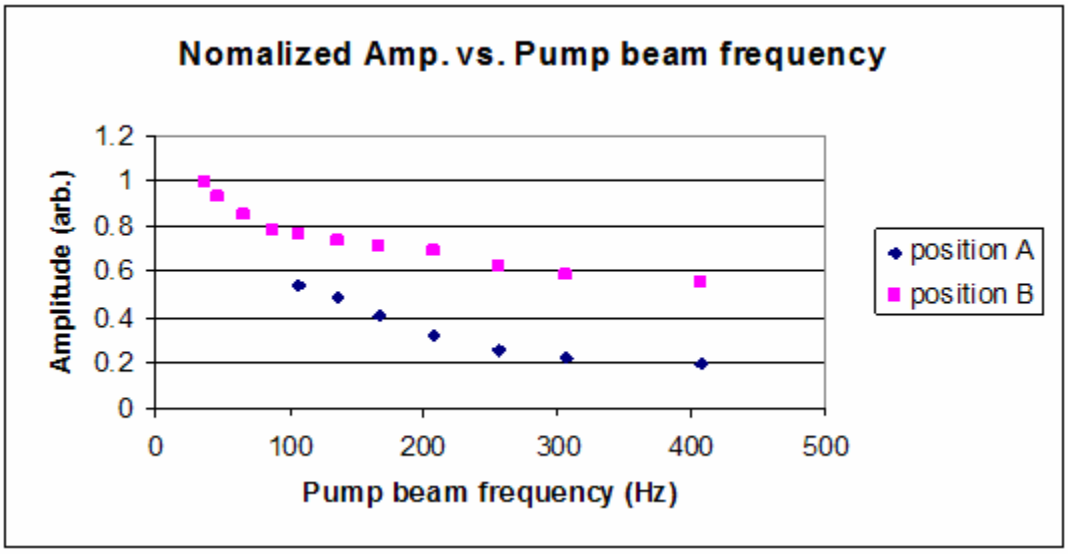

Figure 15. Normalized STL amplitude versus chopping frequency of the pump beam.

Both data sets showed the same decrease in signal with increasing chopping frequency. The amplitude versus 1/f slope can be seen in Figure 15. The value of 1/f determines the thermal bump expansion time interval. Figure 16 shows normalized amplitude versus 1/f.

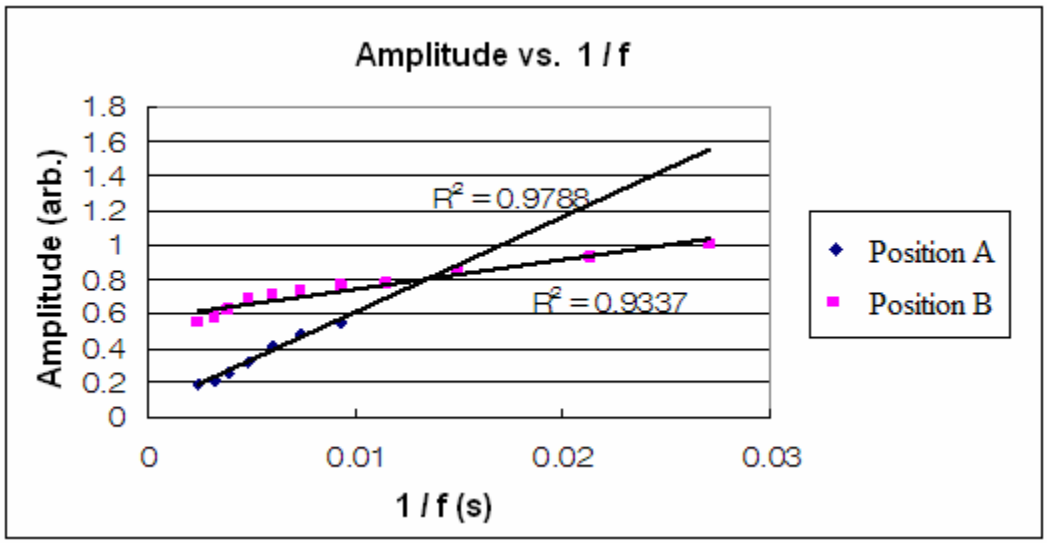

Figure 16. Normalized amplitude signal versus 1/f.

As shown in Figure 16, a plot of the normalized amplitude of the signal versus 1/f is approximately linear, which means the amplitude is proportional to 1/f and t. If the chopping frequency is increased, the thermal bump expansion time interval decreases, which causes the amplitude to decrease. Figure 16 was qualitatively similar at the two positions. Low chopping frequency produced larger STL amplitude as expected.

However, the result shows a different trend with the Zeonex sample than with the polycarbonate sample studied by Hussain [115]. In the experiment with polycarbonate by Hussain, the amplitude versus frequency plot (Figure 15) sometimes showed a peak, rather than always being monotonically decreasing as in the trend with the Zeonex

sample shown in Figure 17. Thus, different polymers have different STL responses.

The phase of the STL signal is used in studying different properties such as thermal conductivity, optical absoptivity, elasticity, and thermal expansion of the sample. Figure 17 below illustrates phase versus varying chopping frequency. In this experiment, normalization of the phase was not required because the phase of the signal was stable.

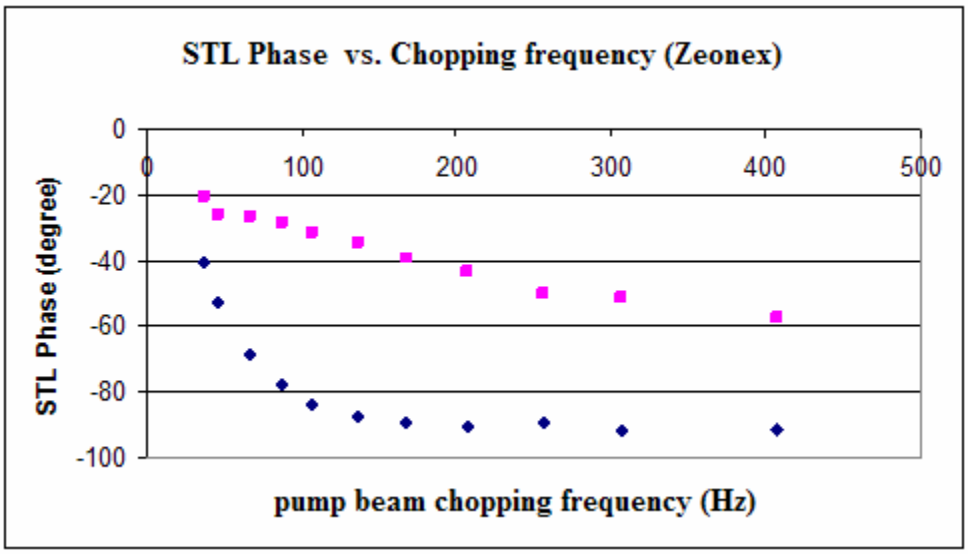

Figure 17. STL phase versus chopping frequency of the pump beam.

Figure 17 also shows the same trend for the two different positions. High frequency decreases the phase of the STL signal. Phase, as shown in Figure 17, is a way of measuring how long it takes for the thermal bump to reach the maximum height and provides information about the thermal properties of the sample. The phases shown have been corrected for the 135^{o} phase offset, as discussed in the previous chapter. The values of the phase were negative as expected, meaning that the response lagged behind the stimulus. A larger phase means more of a time lag before the STL signals peaks. If the phase is zero, there is no time lag.

2. Surface Thermal Lens (STL) studies of bulk polymers using polarized light

Photothermal changes were investigated using a polarized probe beam with Zeonex and acrylic as the samples. Polarized light was used to observe the difference in the signals between the polarized and unpolarized probe beams. Because the polymer molecules might be sensitive to the polarization of incident light, use of a polarized probe beam was expected to provide structural information about the polymer chains.

2.1. Surface Thermal Lens (STL) studies of Zeonex (COP) polymer using polarized light

When polarized light is reflected by a surface, the surface may rotate its polarization vector. If there is no rotation of the vector upon reflection, then there should be no light that makes it through the second polarizer when they are crossed. Reflecting the light off another object in between the two polarizers allows for the possibility that the polarization will get rotated and thus some light will make it through the second polarizer. The fact that a signal was observed with crossed-polarizers suggests that the surface was rotating the polarization vector. This is likely due to the polymer's chain-like structure. Hence, in this experiment, the polarization orientation of two polarizers was crossed.

The following figures show a simple comparison of results using a non-polarized probe beam (Figures 18 and 19) and a probe beam with crossed-polarizers (Figures 20 and 21). In each experiment, the STL amplitude and the STL phase were observed. As seen in Figures 18 and 19, both STL amplitude and phase are stable under non-polarized light. However, with the crossed-polarizers, the STL amplitude showed a

trend of oscillation, and the STL phase showed decay with smaller oscillations in the phase than in the amplitude. The other experimental conditions in both cases were the same; the pump beam power was set at 1 W, while the chopping frequency was set at 37 Hz.

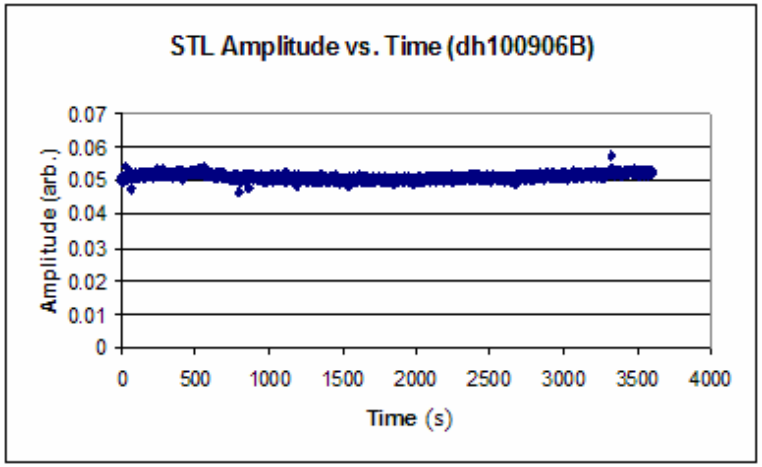

Figure 18. STL amplitude versus time with no polarizer.

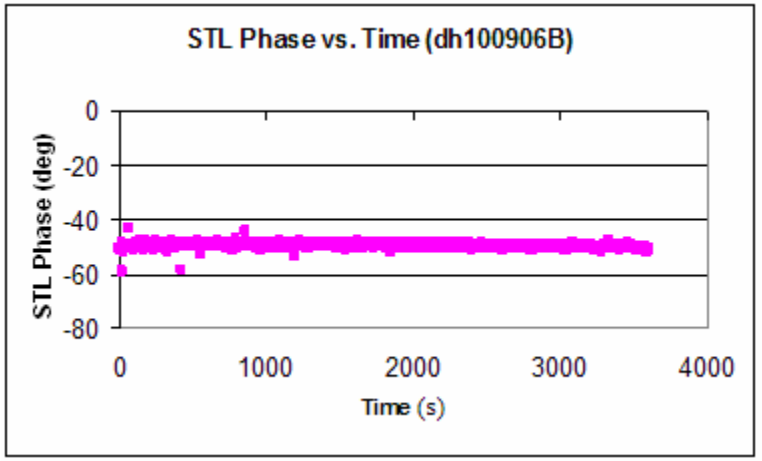

Figure 19. STL phase versus time with no polarizer.

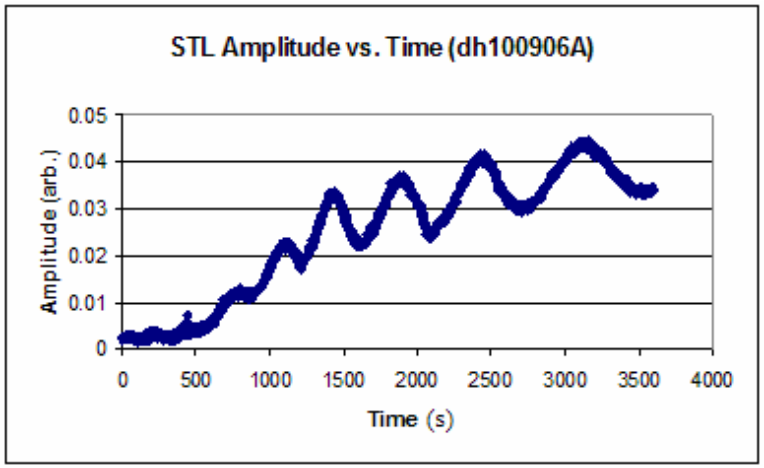

Figure 20. STL amplitude versus time with crossed-polarizers.

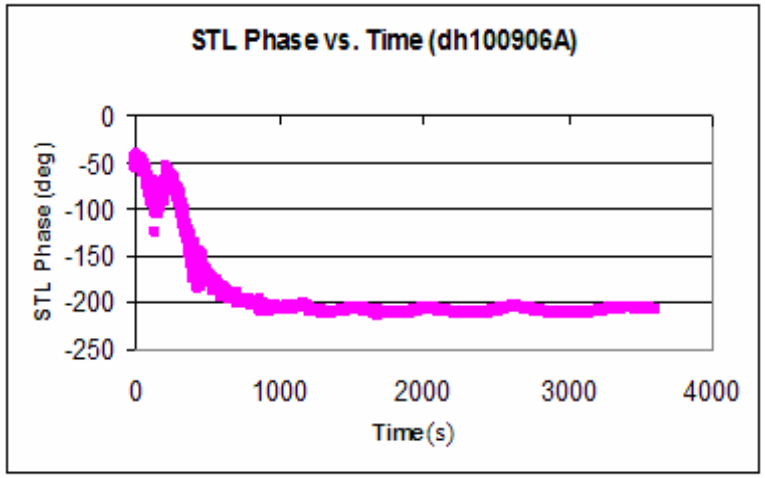

Figure 21. STL phase versus time with crossed-polarizers.

In Figures 20 and 21, the first 500 seconds (approximately 9 minutes) show some kind of noise created from unexpected conditions in the experimental setting. Although noise was present, these data were included to show experiments conducted on the same day. Most of the additional data show the absence of such noise (see Appendix III-1). As shown in Figure 21, except for the noise in the first 9 minutes of the experiment, there are no significant changes in the STL phase. But if the scale was expanded, the STL phase also fluctuated. Figure 22, which has been generated from Figure 21, shows the expanded scale of the STL phase.

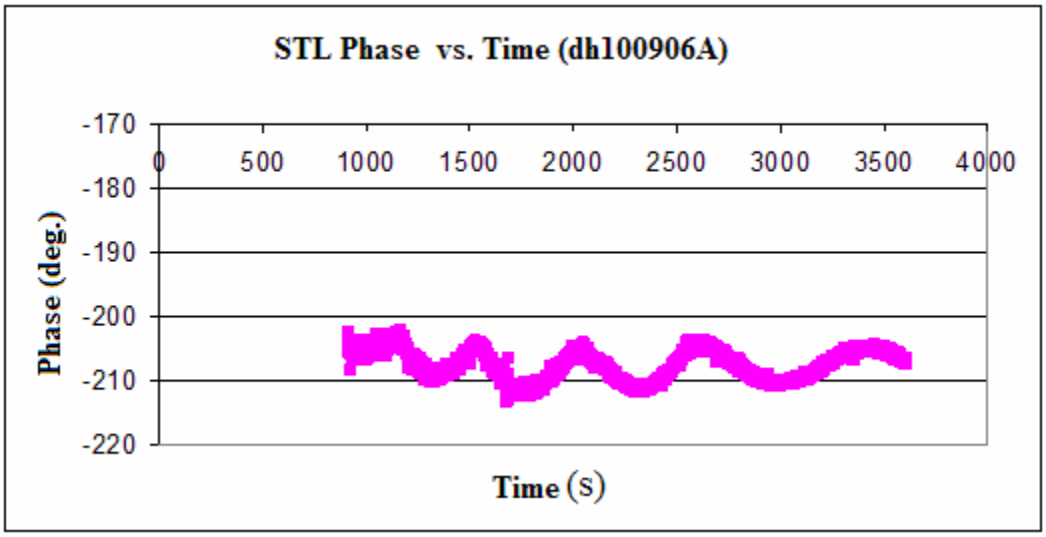

Figure 22. Expanded STL phase versus time with crossed-polarizers.

In using polarizers in crossed-orientation, the height of oscillation was found to be significantly higher than when the orientation of the polarizers was parallel. The oscillation of the STL amplitude using polarized light suggests that a phenomenon is occurring that treats one polarization different from another. Since the polymer molecules have chain-like structure, the difference may be due to whether the polymer

molecules are in a tangled mess (no asymmetry) or whether they are lined up with each other (asymmetry introduced). It may be that the repeated flexing (at a rate of 37 Hz) causes some alignment of the polymer chains.

In order to observe the characteristics of oscillation of the amplitude of the signal, time-dependent experiments were conducted. As such, behavior of the oscillations was observed over a long period of time.

Figure 23 showed the results from the first hour of the experiment, while Figure 24 shows the results of the next hour of the experiment. As with previous runs, the pump beam power was set at 1 W with a chopping frequency of 37 Hz.

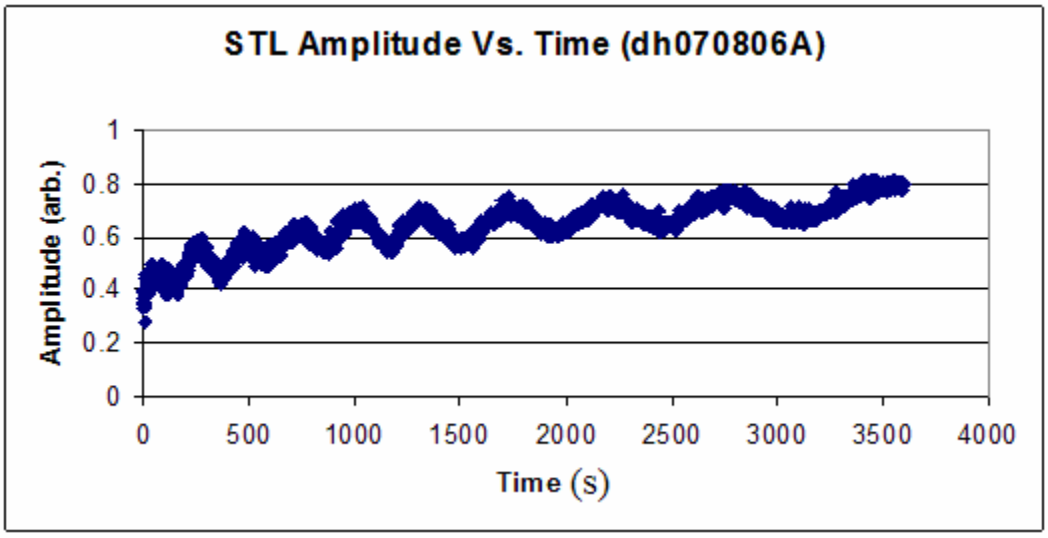

Figure 23. STL amplitude versus time in the first hour of a crossed-polarizers run.

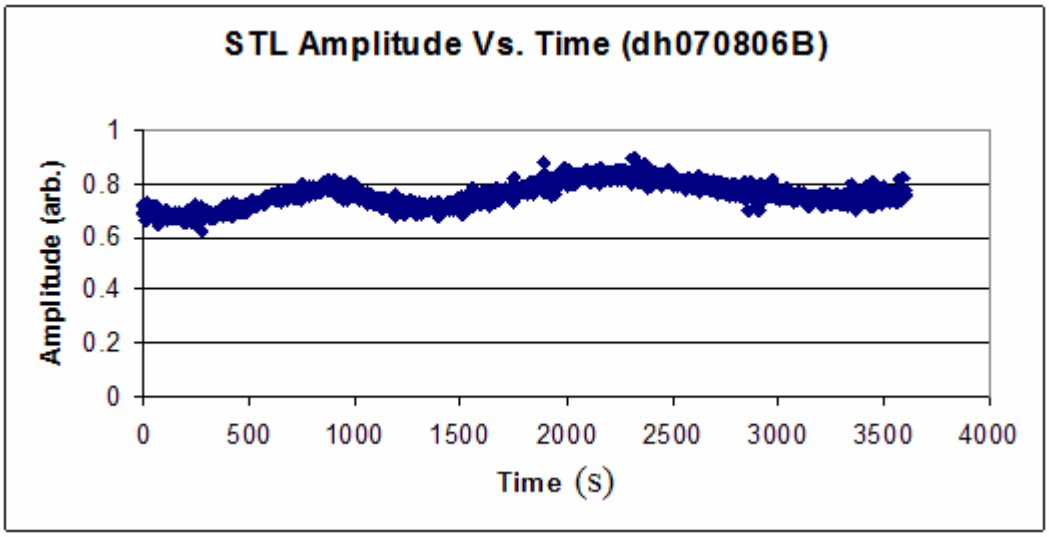

Figure 24. STL amplitude versus time in the second hour of a crossed-polarizer run.

Figure 23 shows that the STL amplitude is fluctuating. However, by the second hour of the experiment, the STL amplitude became steadier, as shown in Figure 24.

2.1. Investigating the period versus time relationship from the oscillation

One way of characterizing the oscillations is to calculate the period $\tilde{T}$ as a function of time t. $\tilde{T}$ is the time between adjacent STL amplitude peaks as determined from the oscillation plots. To illustrate this point, the STL signal from a portion of a run is shown in Figure 25 (see Figure 27 for the full run).

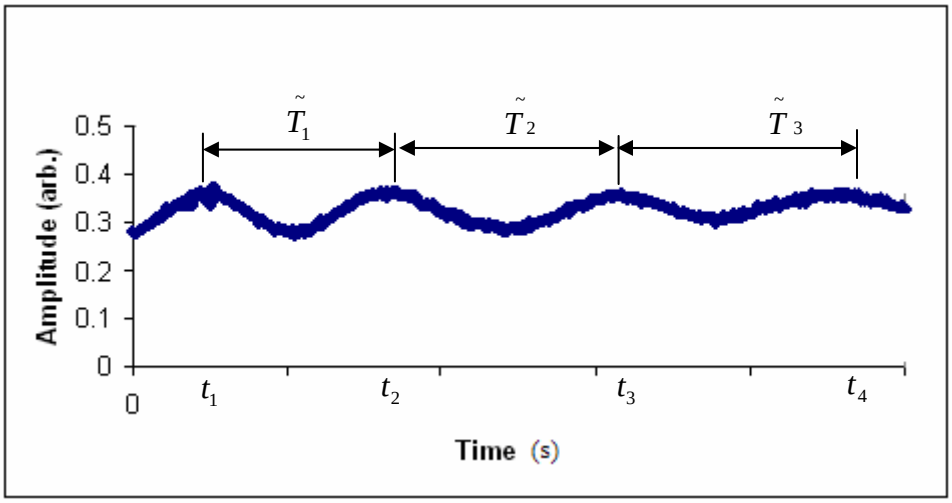

Figure 25. An example plot of STL amplitude oscillation period determination for run dh071106A.

The period, $\tilde{T}$, is found by $\tilde{T}_1 = (t_2 - t_1)$ and the corresponding time at which that period was observed is calculated through $\tilde{t}_1 = \frac{(t_2 + t_1)}{2}$. After finding $\tilde{T}$ and its corresponding $\tilde{t}$, the $\tilde{T}$ versus $\tilde{t}$ graph was plotted as shown in Figure 26.

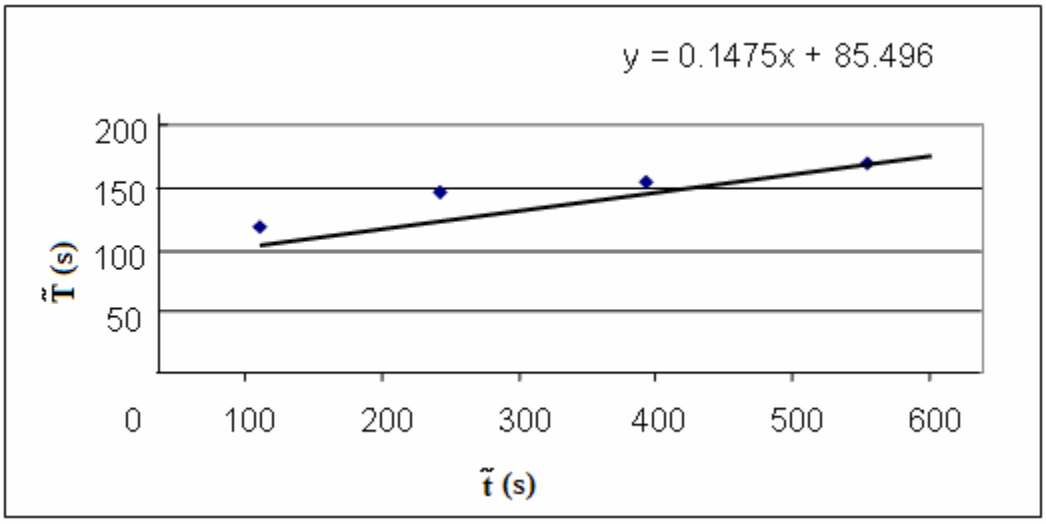

Figure 26. An example plot of period versus time for run dh071106A.

Figure 27 shows the plot of the amplitude of the STL signal over an hour with chopping frequency of 37 Hz and pump beam of 1 W with crossed-polarizers for the probe beam. Based on the previous methods, Figure 28 was generated from Figure 27.

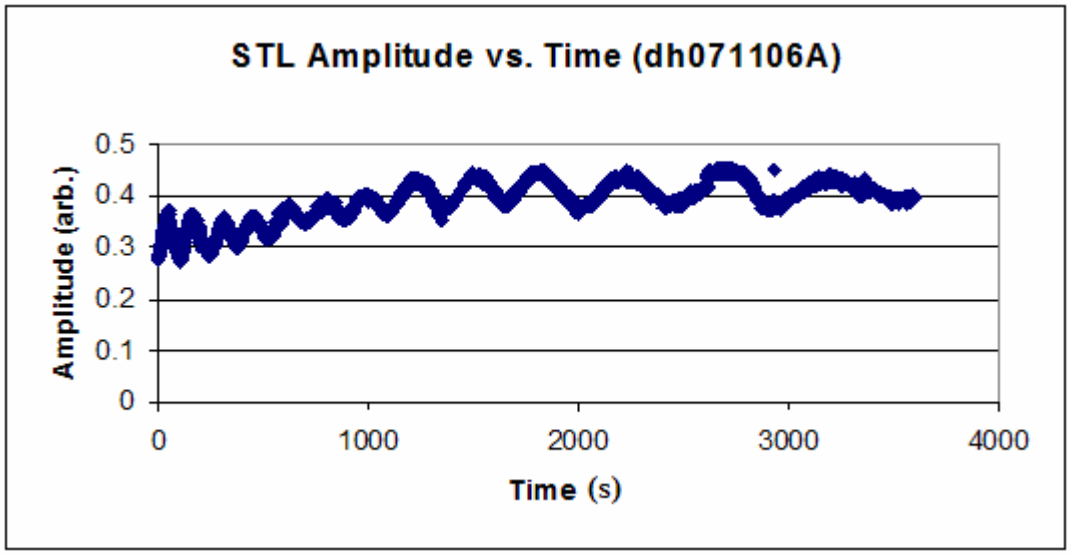

Figure 27. STL Amplitude versus time with 37 Hz, 1 W for 1 hour using crossed-polarizers.

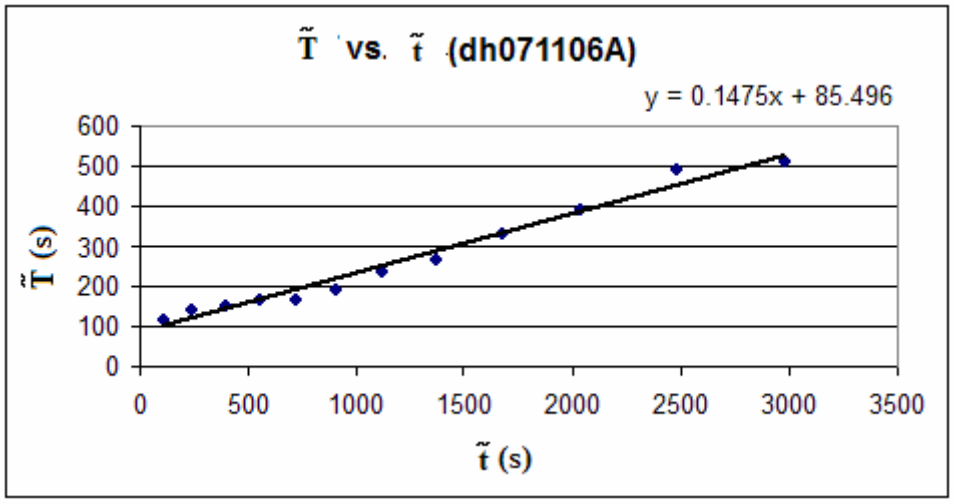

Figure 28. Period $\tilde{T}$ versus time $\tilde{t}$.

Figure 28 shows a linear relationship between the period and the time.

To try to gain insight into the period versus time relationship and to see if the oscillations were reproducible, some modified experiments were done at different powers or chopping frequencies, but other parameters were not changed during the experiment. The first set of experiments aimed at observing the power dependence in the oscillations. The period versus time relationship was linear, but no other pattern in the power dependence was observed. Similar results were found when the pump beam chopping frequency was varied (see Appendix III- 2, 3) in the second set of experiments. From the comparison with the data taken from the variations in power and variation in chopping frequency, no trend was found. The graphs showed the STL amplitude to be primarily a function of time. No pattern in the power dependence was noticed. When the run time is longer, the period of the oscillation will be longer. There was also little significant change in the phase of the signal. Further study is needed to understand the significance of these findings.

2.1.1. Studying the oscillation of the STL signal under while varying the power and chopping frequency of the pump beam with Zeonex

The most direct way to see if the power and frequency of the pump beam affect the experiment is to change it right in the midst of a run. The power and frequency of the pump beam were varied in order to study whether power of the pump beam affected the oscillations in the STL signal. In Figures 29 and 30, the power of the pump beam was varied (at 1 W, 0.5 W, and 1 W for half an hour per power setting at 37 Hz) while in Figures 31 and 32, the chopping frequency of the pump beam was varied (37 Hz, 107 Hz, and 37 Hz for a half an hour per frequency setting at 1 W of pump beam power).

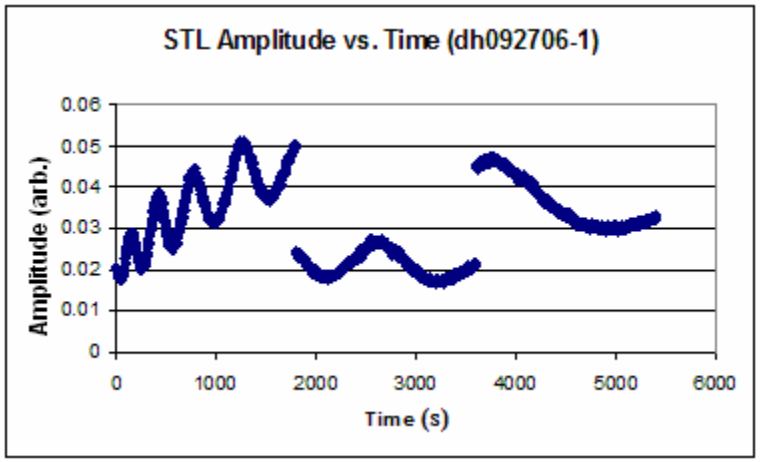

Figure 29. STL amplitude versus time with 37 Hz, varied pump beam power (1 W, 0.5 W, and 1 W) for 1 hour and 30 minutes.

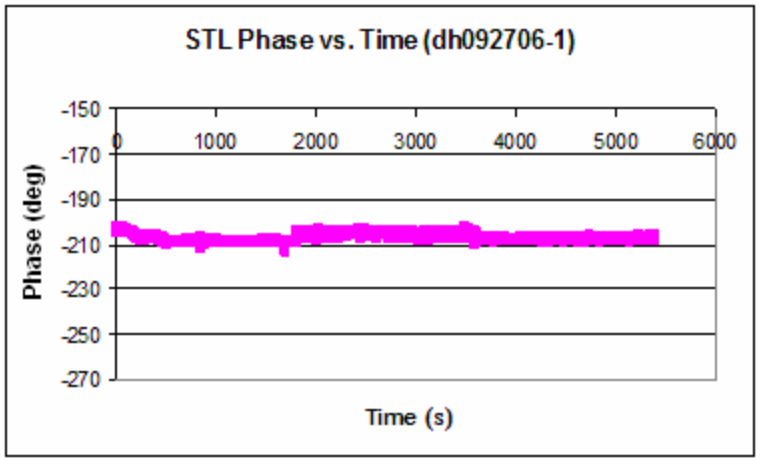

Figure 30. STL phase versus time with 37 Hz, varied pump beam power (1 W, 0.5 W, and 1 W) for 1 hour and 30 minutes.

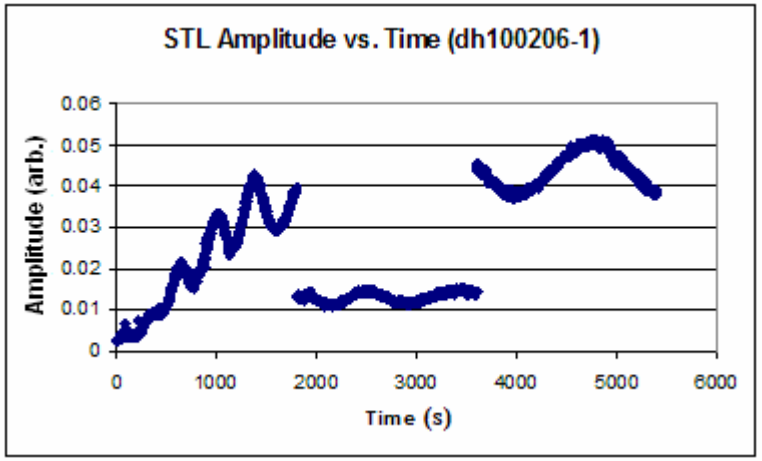

Figure 31. STL amplitude versus time with 1 W, varied chopping frequency of pump beam (37 Hz, 107 Hz, and 37 Hz) for 1 hour and 30 minutes.

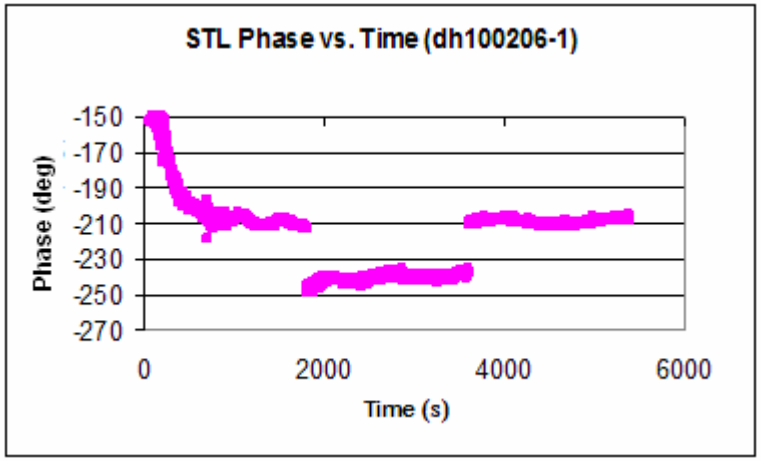

Figure 32. STL phase versus time with 1 W, varied chopping frequency of pump beam (37 Hz, 107 Hz, and 37 Hz) for 1 hour and 30 minutes.

Similar oscillation patterns were observed at the various pump beam power and chopping frequencies. Changing the laser power and chopping frequency simply changed the amplitude of STL signals. The power of the pump beam did not significantly affect the nature of the oscillation. Other variations in power and frequency show similar results (see Appendix III-4). In the beginning of each run, the plot showed an upward trend superimposed on the oscillation of the STL amplitude, but the reason for this has not yet been identified.

The experiments have shown that varying the pump beam power and the chopping frequency affects the strength of the STL signal; however, why oscillations have occurred has yet to be determined. Several experiments were performed to rule out instabilities in the chopper and lasers, so presumably the oscillations are due to one or more of the properties of Zeonex, but the details are not yet clear. We can at least conclude that surface relaxation between beam chops cannot be complete. There would be no time dependence at all in the signal if relaxation were complete. The lack of complete relaxation is likely related to some asymmetry in the arrangement of the polymer molecules, since oscillations were detected only in the presence of polarizers.

Factors affecting the time lag in the response of Zeonex to the pump beam are not varying much since the phase is not varying much. That is, the repeated flexing of the surface is probably not changing the thermal diffusivity or the visoelastic response. On the other hand, it may be changing the optical properties, such as absorptivity of the pump beam or reflectivity of the probe beam, giving rise to a change in the amplitude of the STL signal.

At this point, the experiments with Zeonex sample had to be stopped because it was destroyed while re-aligning the beams. A surface imperfection absorbed an unusually high amount of the pump beam, causing it to overheat. Unfortunately, the Zeonex could not be replaced soon enough to continue the experiment with it. Originally, the intent was to compare Zeonex with acrylic using multiple methods. However, because Zeonex was no longer available, it became somewhat more challenging to make a comparison between the two. Thus, this paper focuses on experiments that were done with the Zeonex until it was destroyed.

2.2. **Surface Thermal Lens (STL) measurements on acrylic (PMMA) using polarized light**

The experiment using Zeonex resulted in unexpected oscillations of the STL signal. Thus, in this next experiment, a different kind of polymer, acrylic, was used to investigate whether such oscillation would occur. As previously mentioned (see Table I), acrylic has different chemical and physical properties than Zeonex. In contrast with Zeonex, the STL signal of acrylic showed no significant changes by using crossed-polarizers on the probe. Figures 33 and 34 showed no significant difference in both amplitude and phase of the STL signal during the one-hour experiment.

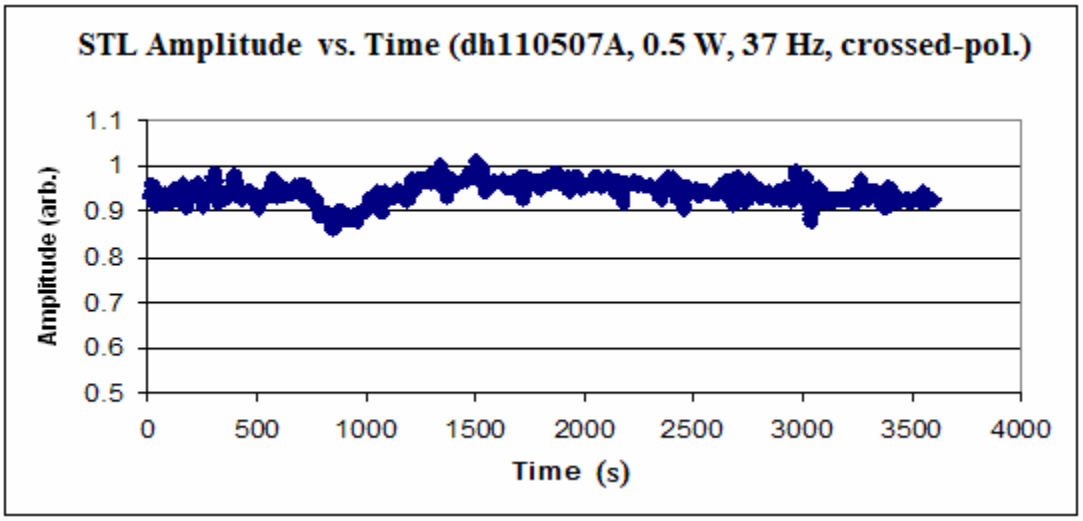

Figure 33. STL amplitude versus time with crossed-polarizers (acrylic, 0.5 W, 37 Hz, and 1 hr).

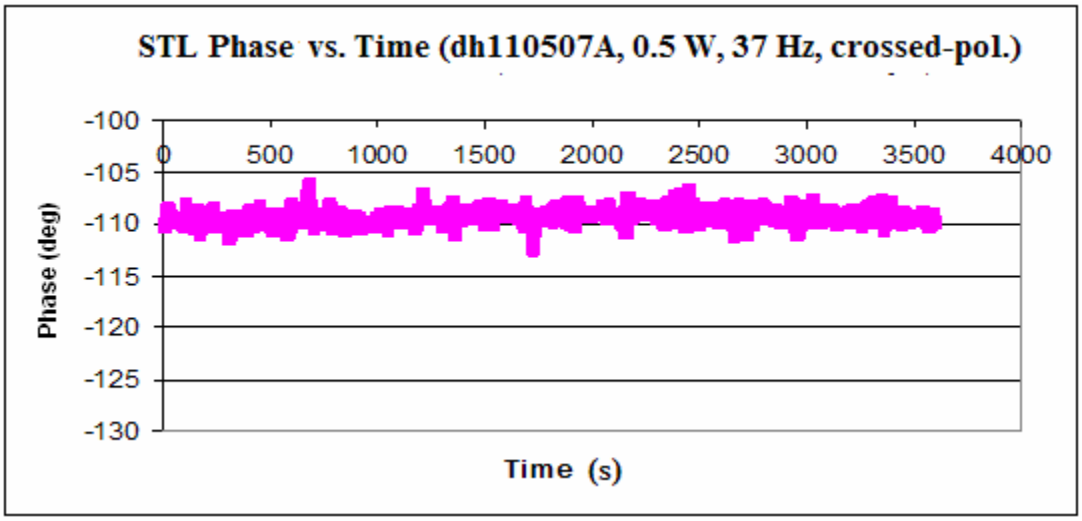

Figure 34. STL phase versus time with crossed-polarizers (acrylic, 0.5 W, 37 Hz, and 1 hr).

It was observed that using parallel-polarizers on the probe beam resulted in significant time dependence. Therefore, parallel-polarizers were used in most of the following studies.

Overall, the experiments compared the differences in using a probe beam with parallel-polarizers and a non-polarized probe beam using acrylic as a sample. As with Zeonex, the experiments were conducted with the expectation that the results would be different between a polarized and a non-polarized probe beam.

Figure 35 shows the STL amplitude when both polarizers were oriented horizontally and Figure 36 shows the STL amplitude when both polarizers were oriented vertically.

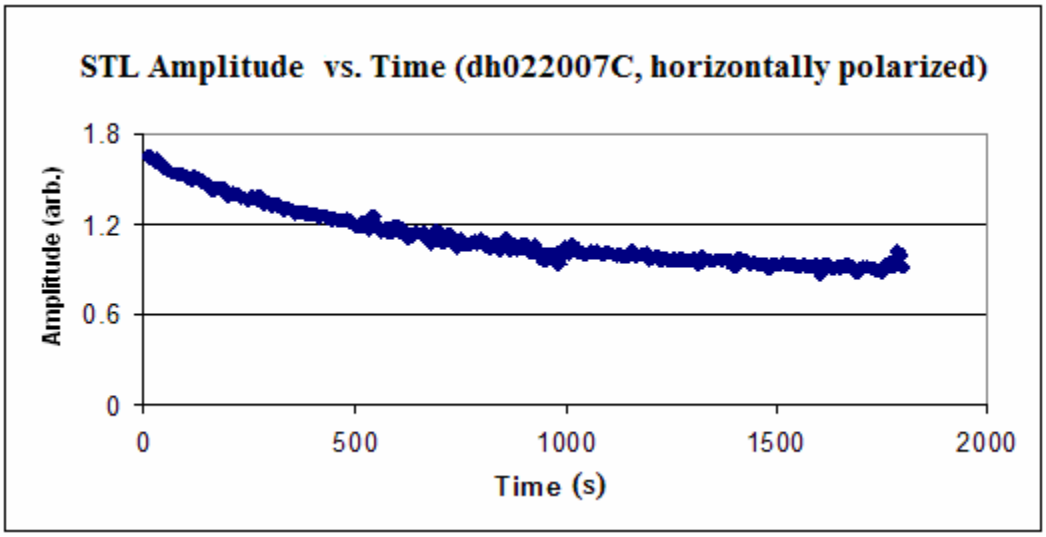

Figure 35. STL amplitude versus time; both polarizers are horizontally polarized (acrylic).

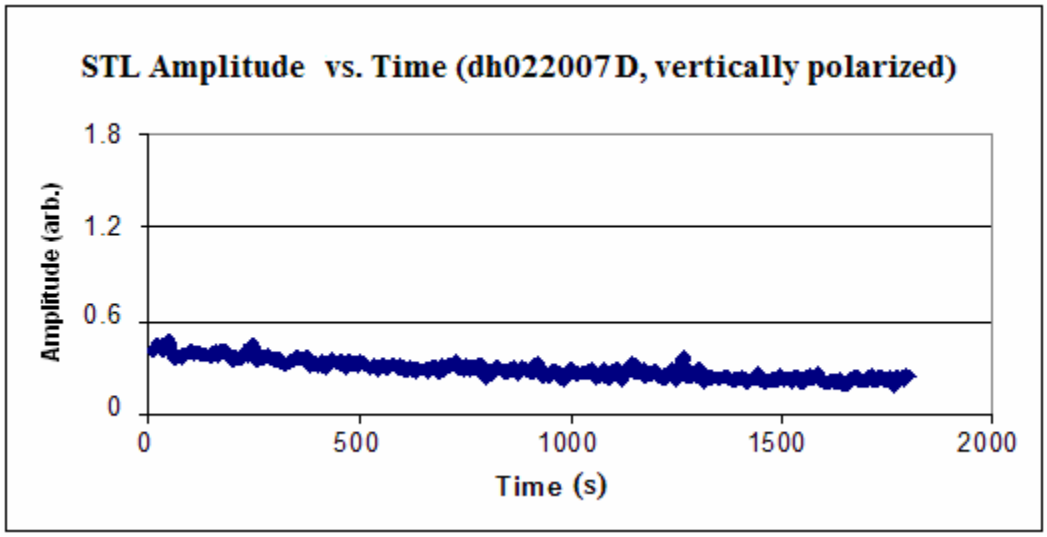

Figure 36. STL amplitude versus time; both polarizers are vertically polarized (acrylic).

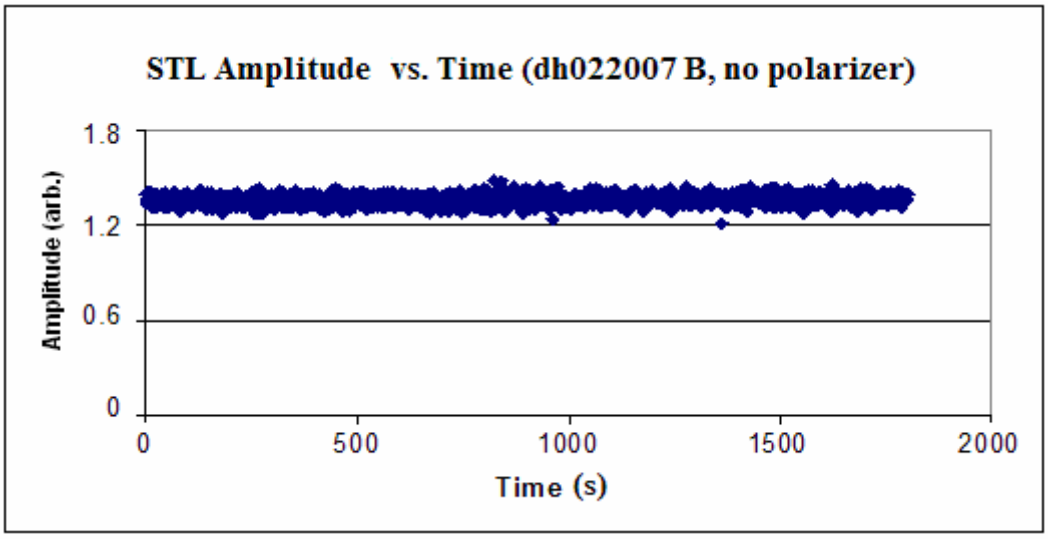

Figure 37. STL amplitude versus time with no polarizers (acrylic).

As seen in Figures 35 and 36, both horizontal and vertical polarizers show an exponential decay pattern in the STL amplitude, while the non-polarized probe beam shows no significant differences in the STL amplitude, as shown in Figure 37. This contrasts with the oscillations in the STL amplitude observed with Zeonex. In addition,

despite the fact that data for Zeonex and acrylic using a polarized probe beam has shown time dependence in the STL amplitude, no significant changes appear over time in STL phase (see, for instance, Figure 38).

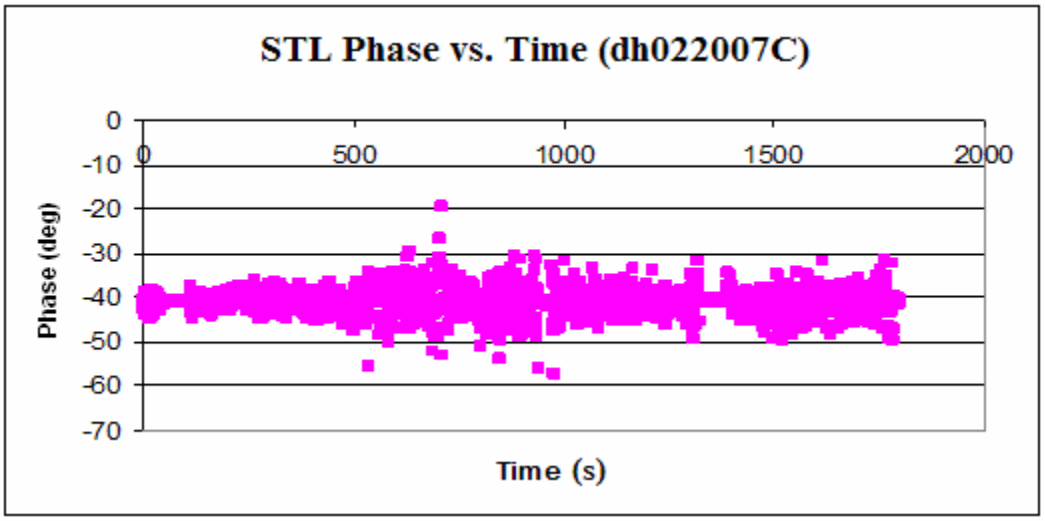

Figure 38. STL phase versus time with horizontal polarizers (acrylic, 0.5 W, 37 Hz, and 30 min).

Thus, as with the Zeonex sample, properties such as thermal diffusivity and voscoelastic response are unlikely to be varying in time, but optical properties may be.

In typical light experiments, one expects that summing the intensities of horizontally polarized and vertically polarized light will yield the intensity of unpolarized light. The situation here is much more complicated, since there are three elements affecting the polarization (two polarizers and the surface), so the intensity of the unpolarized signal was not simply the sum of the horizontally and vertically polarized signals. This is likely because the surface acts as a third polarizer with much more complicated properties. Further insight comes from the single polarizer experiment as

shown in Figures 39 and 40. In this experiment, just one polarizer was used, between the sample and the detector. That is, only the reflected beam was polarized.

.

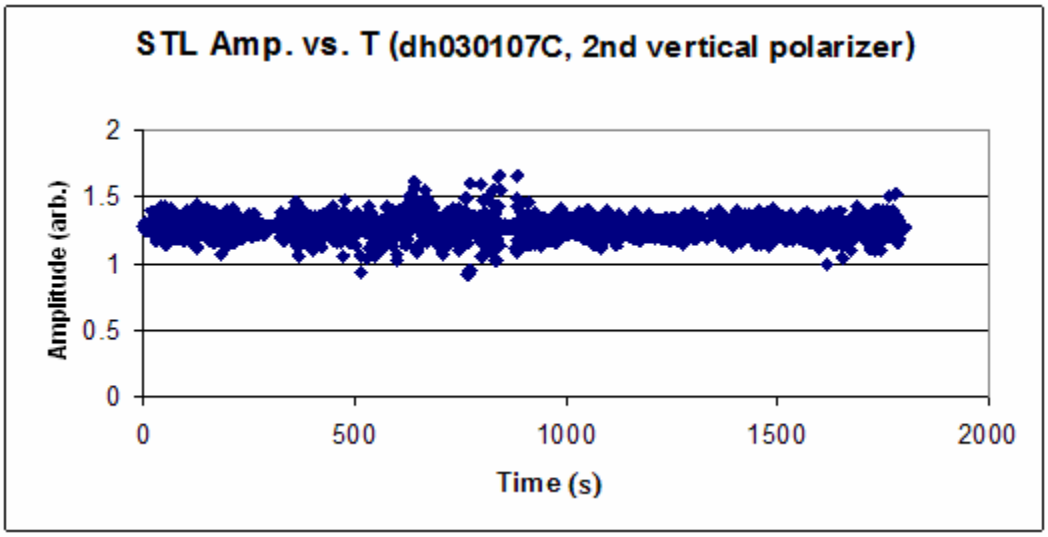

Figure 39. STL amplitude versus time, a single vertical polarizer (acrylic, 0.5 W, 37 Hz, and 30 min).

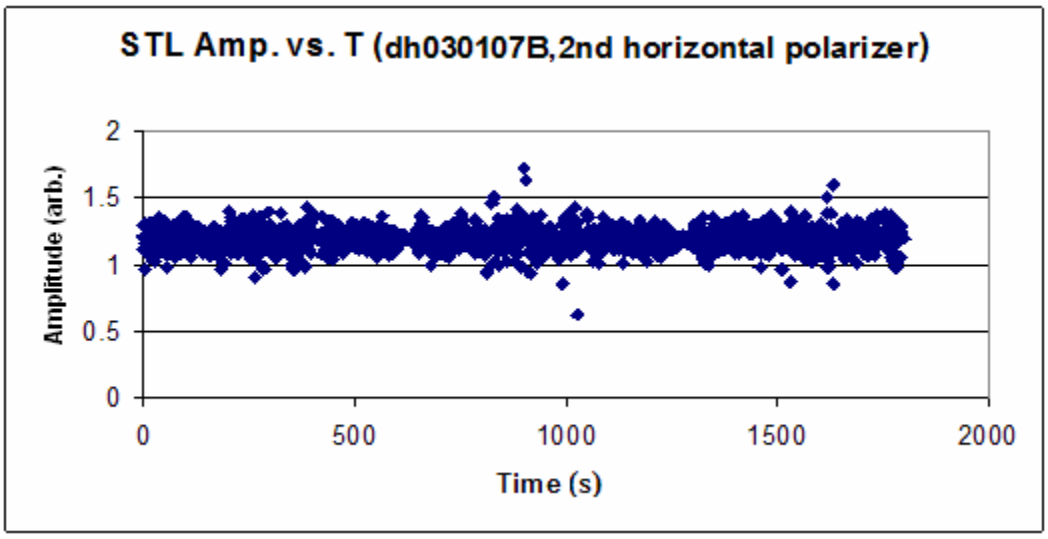

Figure 40. STL amplitude versus time, a single horizontal polarizer (acrylic, 0.5 W, 37 Hz, and 30 min).

Theoretically, if a single ideal polarizer is used, the resulting amplitude of unpolarized light should be equal to the sum of the amplitudes from the vertically and horizontally polarized probe beams. However, in this experiment, sometimes, the sum of amplitudes from the vertically and horizontally polarized probe beams was higher or lower than the amplitude gathered using unpolarized light. This apparent paradox is resolved in the next section.

Both Figures 39 and 40 show polarizing only the reflected beam does not result in a decay of the STL amplitude over time. This is in contrast to the situation when two polarizers were used, the result of which was time dependence.

It is clear that there is a more significant change in the diffraction pattern when polarized light is employed. Presumably, this is due to the reflectivity of the surface being at least weakly polarization dependent, and this polarization dependence is changing over time as the surface is repeatedly flexed. It may be then that the polarized light is revealing stress alignment of the polymer molecules. It would therefore appear to be the case that when a polarized probe beam is used, additional information about the configuration of polymer molecules on the surface can be gained.

3. Scanning across the diffraction pattern with acrylic

In the previous experiments I collected data from a single point in the STL diffraction pattern. In order to better understand the nature of the time dependence in STL signals using polarized light, the STL diffraction pattern was scanned to see how the pattern as a whole changes over time. The experiment helped us to understand two curious aspects: 1) sometimes it was difficult to obtain reproducible results; 2) it

appeared that summing the vertically polarized reflected beam with the horizontally polarized reflected beam did not yield the unpolarized beam.

In this experiment, only the acrylic sample was used. The STL signal was scanned by shifting the horizontal detector position as shown in Figure 41. This experiment involved horizontally scanning the detector with non-polarized light and then with polarized light continuously, where one polarizer was placed between the probe beam and the sample while another polarizer was placed between the sample and the detector. Then, the STL signal as a function of time for one hour was measured as shown in Figure 42. In addition, the STL signal was scanned again along the horizontal direction to measure any changes in the signal. The following Table IV represents the experimental procedure and description.

Table IV.
Experimental procedure and description of the horizontal detector scan.

Steps	Step label	Duration	Description
1	B/no pol (before)	20 minutes	Repeated scanning of detector horizontally with non-polarized light, before the one hour run
2	B/pol (before)	20 minutes	Repeated scanning of detector horizontally with polarized light before the one hour run
3	Figure 27, (dh043007A)	1 hour	STL measurement with polarized light @ 0.5 W and 37 Hz of pump beam
4	A/no pol (after)	20 minutes	Repeated scanning of detector horizontally with non-polarized light after the one hour run
5	A/pol (after)	20 minutes	Repeated scanning of detector horizontally with polarized light after the one hour run

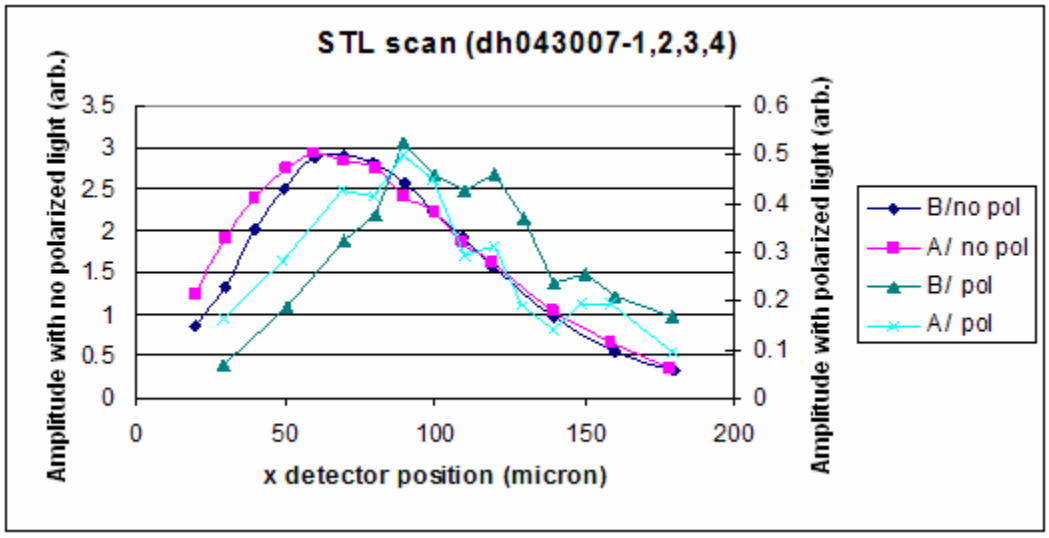

Figure 41. STL signal versus x (horizontal) detector position (acrylic, pump beam power 0.5 W and chopping frequency 37 Hz).

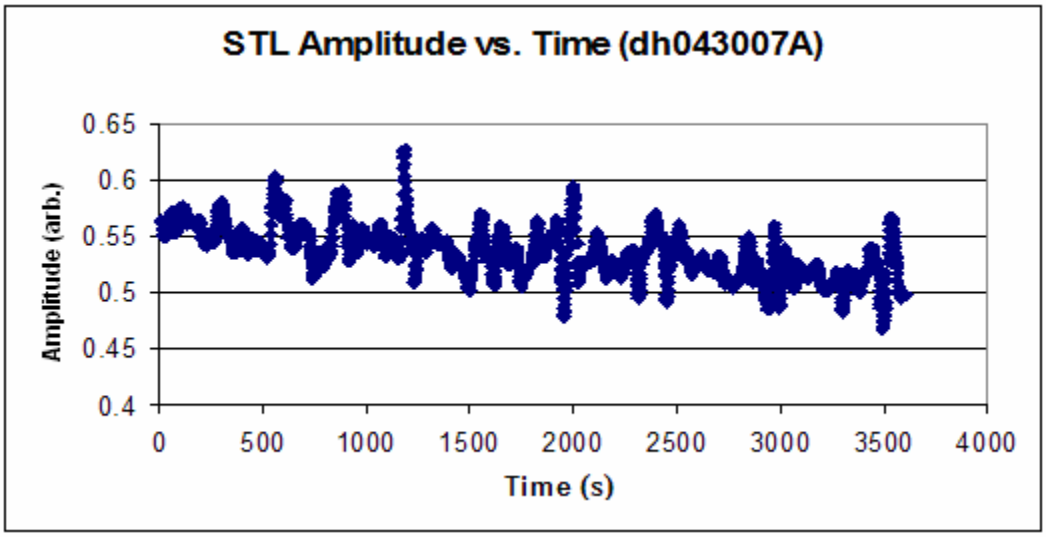

Figure 42. STL amplitude versus time (acrylic, pump beam power 0.5 W and chopping frequency 37 Hz for 1 hour).

As shown in Figure 41, the STL scans with non-polarized light at the beginning and the end of this experiment were almost identical. With polarized light, the STL signal scanned before and after had significant differences, although for both the peak point was similar with each other. The scan showed unpolarized light produced very little time dependence anywhere in the pattern but that polarized light produced varying amounts of time dependence, depending on the position in the scan. Figure 42, which was data produced during the one-hour run between scans (see Table IV), shows the STL amplitude versus time. The noise that is shown may have occurred due to the signal being weak or due to the presence of dust. However, this experiment has been run multiple times and this level of noise that is present does not affect our ability to record the diffraction pattern.

Further detailed analysis has shown that the presence of the polarizer likely shifts and expands the beam, making comparison between non-polarized and polarized

signals more challenging. Figures 43-45 show the difference between the scanning of polarized and non-polarized light on acrylic. Figure 43 shows data with non-polarized light. Figure 44 was found from a single vertical polarizer and Figure 45 was found from a horizontal polarizer.

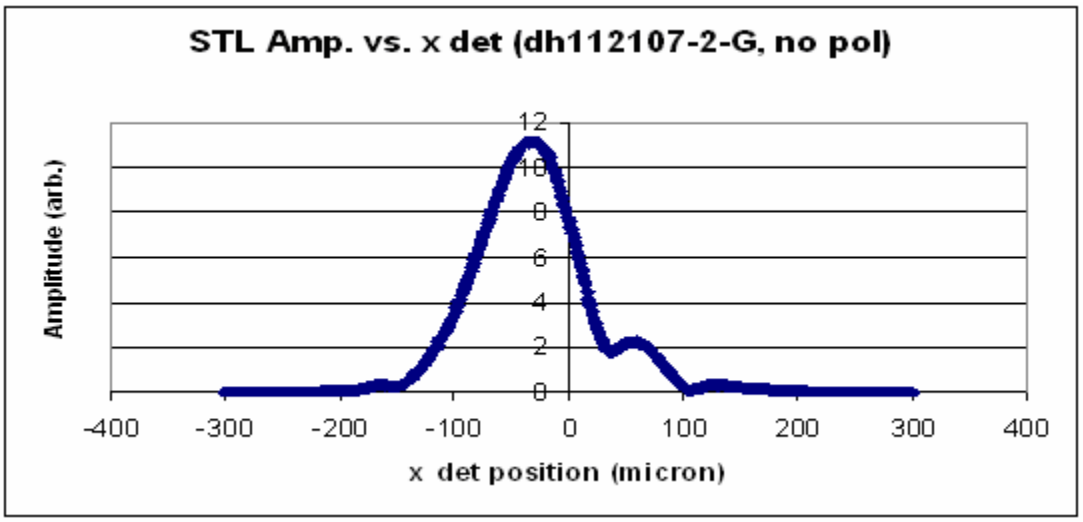

Figure 43. Scanning horizontal detector position with no polarizer (acrylic).

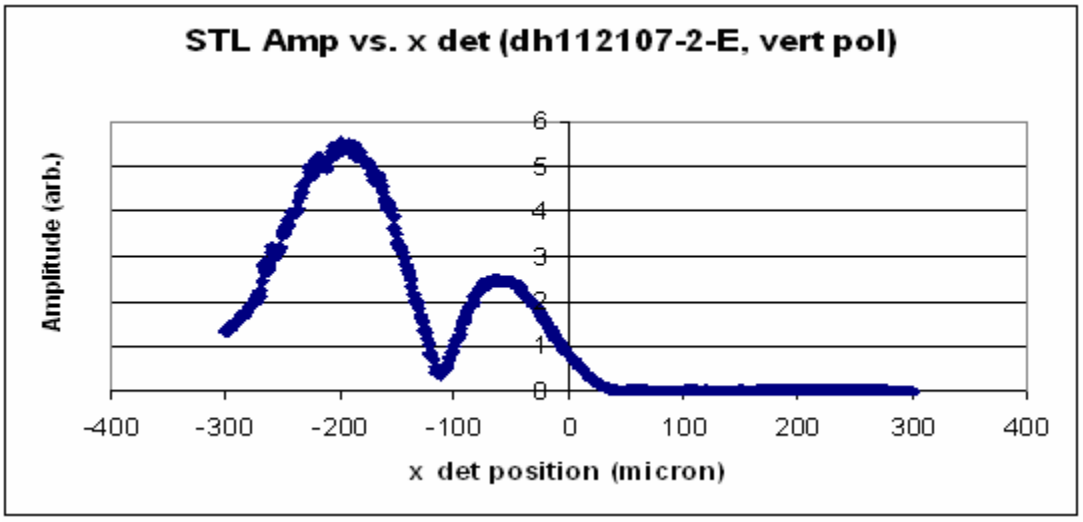

Figure 44. Scanning horizontal detector with vertical polarizer (acrylic).

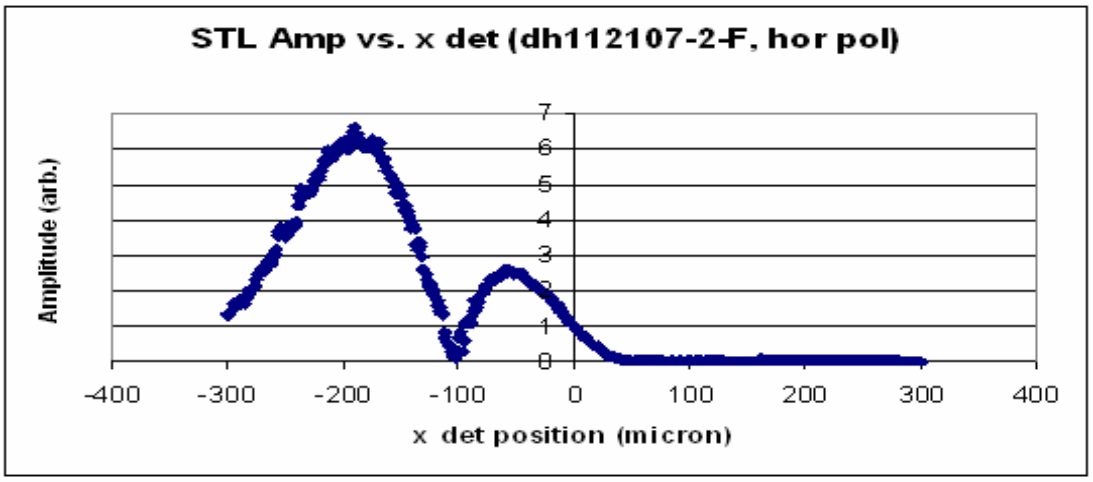

Figure 45. Scanning horizontal detector with horizontal polarizer (acrylic).

Figure 43 shows that the peak of the signal in non-polarized light is at -26 microns, while the peak of the signal in vertically (Figure 44) and horizontally (Figure 45) polarized light occurs at -188 microns. The width of a test laser beam was measured using the CCD profiler. The polarizer shifted the signal approximately 150 microns and expanded it by 35% (Appendix III-6). Thus, if we assume the polarizer transforms the probe beam in a similar way, the signal has to be compressed and the scanning distance also has to be shifted. That is why the previous discussion on the quantitative analysis of the amplitude of the signal using polarized light and non-polarized light produced apparently paradoxical results: the polarizer shifted the beam so that the detector was viewing a different part of the diffraction pattern.

Based on the diffraction scan, the detector position is important in trying to achieve even qualitative reproducibility of the results, since some portions of the polarized scans were time dependent and some were not. Furthermore, the polarization makes a difference since the vertically polarized light produced qualitatively different results from the horizontally polarized light.

DISCUSSION

Thermal diffusion and the specific heat also affect the STL signal. The more rapid the thermal diffusion is or the greater specific heat is, the smaller the temperature increase is from the pump beam and hence the smaller the STL signal is. In addition, the greater the rate of thermal expansion, the greater the STL signal. In the absence of probe beam polarizers, the results showed no significant time dependence in the signal. This suggests that the bump relaxes completely between pulses in Zeonex and acrylic. But further studies are needed to identify the other polymers.

If there is any time dependence in the signal, while using polarized light, then the structure of the sample must be changing. Repeated flexing is having a significant effect on the material in that it does not return to its original state after each pulse. For understanding these phenomena, some quantitative analysis of data was tried. However, insufficient evidence was found from which to draw a conclusion.

There is a more significant change in the diffraction pattern when polarized light is employed. Presumably this is due to the reflectivity of the surface being at least weakly polarization dependent, and this polarization dependence is changing over time as the surface is repeatedly flexed. It may be, then, that the polarized light is revealing stress alignment of the polymer molecules.

During the experiment some unexpected factors were found to affect the signal. Sometimes the detector position had to be shifted to get reproducible result. Furthermore, the presence of the polarizer expanded the probe beam, and small changes in its orientation shifted the peak position.

Chapter 5: CONCLUSION

In this study, by comparing different sample spot positions and different polymers, property variation was demonstrated both between polymer types and within a given polymer sample. In addition, the STL signal demonstrated time dependent behavior for both polymers explored. However, use of probe beam polarizers produced different STL signals for Zeonex as compared to acrylic.

Although the molecular structure of Zeonex and acrylic are different, the pattern of the STL signal was not significantly different when using non polarized light. While using polarized light, the pattern of the STL signals showed significant differences. With Zeonex the STL signal oscillated while in acrylic the STL signal decayed as a function of time. The oscillations in the STL signal of Zeonex showed significant changes under the crossed-polarizers conditions, and acrylic showed significant changes under the parallel-polarizers conditions.

Furthermore, in comparing data acquired by scanning across the full diffraction pattern of the acrylic STL signal significant differences were observed between polarizer and no-polarizer conditions. The diffraction patterns of signal were also time dependent in the polarized case. These results demonstrate the importance of observing the same portion of the diffraction pattern when making comparisons of different STL signals.

By comparing the results using polarized and non-polarized light, this research provides new insight into changes in the structure of polymers. However, there is still a lot more to be learned about how to interpret these signals. Further investigation is necessary to quantitatively interpret the signals obtained by the STL experiment. In

addition, further studies should also involve redesigning the experimental procedure such that it would always include a diffraction pattern scan to ensure that the same point on the pattern is being studied from one run to the next. The experiment could also be improved by using a new laser to apply higher power or by using an infrared laser since polymers absorb more in the infrared region. Furthermore, the experimental set-up could be enhanced by designing a mechanism for positioning the polarizer's in a more reproducible way. Future research should continue to refine the experiment and explore possibility of developing a theoretical and experimental study of the polarization effects in STL signals using polymer samples.

REFERENCES

1. A.D. Yalcinkaya , O. Ergeneman, and H. Urey, Sensors and Actuators A: Physical. **135**, 36 (2007).
2. W.Y. Shieh, W.H. Lee, S.L. Tung, B.S. Jeng, and C.H. Liu, IEEE Transactions on Intelligent Transportation Systems, **7**, 565-566 (2006).
3. H. Zhou, N. Sun, H. Shan, D. Ma, X. Tong, and L. Ren, Applied Surface Science. **253**, 9514 (2007).
4. Y. Ye, Y. Jiang, J. Yu, Z. Wu, and H. Zeng, Materials Science and Engineering: B. **132**, 280-282 (2006).
5. B.G. Sukhorukov, A.L. Rogach, M. Garstka, S. Springer, W.J. Parak, A.M. Javier, O. Kreft, A.G. Skirtach, A.S. Susha, Y. Ramaye, R. Palankar, and M. Winterhalter, SMALL 3 , 944-955 (2007).
6. L.B. Pavlovich, N.M. Alekseeva, V.P. Dolgopolov, and A.A. Popov, Metallurgist, **48** (5-6), 272-274 (2004).
7. D. Bäuerle, *Laser Processing and Chemistry*, 3rd ed. Springer, Heidelberg (2000).
8. A.H. Frazer, *High Temperature Resistant Polymers*, New York (1968).
9. M.I. Bessonov, *Polyimides—a Class of Thermally Stable Polymers*, NASA Technical memorandum, Washington D. C. (1986).
10. W.D. Callister, *Materials Science and Engineering*: An Introduction, Jr. Wiley, John & Sons, 7th Ed, New York (2006).
11. C. Wochnowski, M.A. Shams Eldin, and S. Metev, Polymer Degradation and Stability. 89, 252 (2005).

12. P.K. Kuo, M. Munidasa, Applied Optics, 29, 5326-5331 (1990)

13. C. Wochnowski, Y. Cheng, K. Meteva, K. Sugioka, K. Midorikawa, and S. Metev, Journal of Optics. A, **7**, 493-501 (2005).

14. R. Chow, J.R. Taylor, Z.L. Wu, R. Krupka, and T. Yang, "*High reflectors absorptance measurements by surface thermal lensing technique"*, in *Laser-induced Damage in Optical Materials: 1996,* eds. H.E. Bennett, A.H. Guenther, M.R. Kozlowski, B.E. Newman and M.J. Soileau, SPIE Proc. 2966, Bellingham (Washington, USA) (1997).

15. G.R. Strobl,, *The physics of polymer: concepts for understanding their structures and behavior*, Springer-Verlag Berlin Heidelberg, New York (1996).

16. A. Ravve, Principles *of Polymer Chemistry* 2nd Ed., Kluwer Academic/ Plenum Publishers, New York (2000).

17. P. Bahadur, N.V. Sastry, *Principles of Polymer Science*, CRC Press, New Delhi, India (2002).

18. G. W. C. Kaye and T. H. Laby, *Tables of Physical and Chemical Constants and Some Mathematical Functions*, 15th ed., 289, Longman, London (1986).

19. J. R. Fried, *Polymer science and technology*, Prentice Hall PTR, New Jersey (1995).

20. R.A. Pethrick and G.E. Zaikov, and Editors, *Handbook of Polymer Research*, Volume 20, Nova Science (2006).

21. Liu MZ (Liu, Mingzhu), Liang R (Liang, Rui), Zhan FL (Zhan, Falu), Liu Z (Liu, Zhen), and Niu AZ (Niu, Aizhen), Polymer Degradation and Stability, **92** (4), 630-634 (2007).

22. N.T. Dintcheva, N. Tzankova, and F. P. La Mantia, Polymer International, **56** (6), 729-737(2007).

23. M. Li, J.W. Kim, and T.L. Peeples, Separation Science and Technology, **38** (12-13), 2709-2724 (2003).

24. Z. Wang, J. Kang, H. Zhang, X. Liu, X. Lu, and Y. Ma, Acta Chimica Sinica, **65** (18), 2019-2024 (2007).

25. G.G. Niederauer, D.R. Lee, and S. Sankaran, Sports Medicine and Atthroscopy Review, **14** (3), 163-168 (2006).

26. F.J. Macedo, J.A. Ferreira, F.W.J. Van Hattum, and C.A. Bernardo, Journal of Materials Processing Technology, **93**, 151-155 (1999).

27. L.G. Aleksandrova, Polymer science Series C, **49** (2), 121-126 (2007).

28. E.V. Sivtsov, and N.A. Lavrov, Polymer Science Series C, **49** (3), 245-250 (2007).

29. H. Zhu, J. He, and B.B. Kim, IEEE Transaction on Components and Packaging Technologies, **30** (3): 390-396 (2007).

30. Q. Wei, Y. Liu, D. Hou, and F. Huang, Journal of Materials Processing Technology, **194** (1-3), 89-92 (2007).

31. J.T. Wiltshire, and G.G. Qiao, Australian Journal of Chemistry, **60** (10), 699-705 (2007).

32. S. Chaterji, I. Kwon, and K. Park, Progress in Polymer Science, **32** (8-9), 1083-1122 (2007),

33. J.M. Buescher, A. Margaritis, Critical Reviews in Biotechnology, **27**, (1), 1-19 (2007).

34. B.H. Stuart, *POLYMER ANALYSIS*; Analytical Techniques in the sciences, Wiley, West Sussex, England (2002) p.4-29.

35. F.W. Billmeyer, *Textbook of Polymer science*, 3rd Ed., Wiley, New York (1984).

36. G.W. Ehrenstein, P*olymeric Material: Structure- Properties- Applications*, Hanser, Munich (2001) p. 169, 262.

37. E. Baer, and A. Moet, *High Performance Polymers*, Carl Hanser Verlag, Munich, (1991).

38. A.E. Hamielec, J.E. MacGregor, and A. Penlidis, *'Copolymerization', in Comprehensive Polymer Science*, Vol. 3, Ledwith, A., Russo, S, and Sigwatt, P (Eds), Pergamon Press, Oxford, UK (1989) pp 17-32.

39. J.M.G. Cowie, *'Block and Graft Copolymerization', in Comprehensive Polymer Secience*, Vol. 3, A. Ledwith, S. Russo, and P. Sigwatt, (Eds), Pergamon Press, Oxford, UK (1989) pp 33-42.

40. W.J. MacKnight, and F.E. Karasz, '*Polymer Blends' in Comprehensive Polymer Science*, Vol. 7, S.L. Aggarwal and S. Russo, (Eds), Pergamon Press, Oxford, UK, (1989), pp 111-130.

41. D.J. Walsh, '*Polymer blends', in Comprehensive Polymer Science*, Vol. 2, Booth, C. (Eds), and Price, C, Pergamon Press, Oxford, UK (1989), pp 135-154.

42. V. Perce, and D. Tomazos, *'Molecular Engineering of Liquid Crystalline Polymer, in Comprehensive Polymer Science*, 1st Suppl., Aggarwal, S. L. and Russo, S. (Eds), Pergamon Press, Oxford, UK (1992), pp 135-154.

43. P. Chandrasekhar, Conducting *Polymer, Fundamental and Applications: A Practical Approach*, Kluwer Academic, Bosto (1999).

44. R.W. Dyson, *Engineering Polymers, Blackie*, Glasgow, UK (1990).

45. M.P. Stevens, *Polymer chemistry; An introduction*, Oxford University Press, Oxford, UK (1999).

46. R. J. Young, and P. A. Loveell, *An introduction to Polymers*, 2nd Ed, Chapman and Hall, London (1991).

47. G. Odian, *Principles of Polymerization*, 4th Ed., Wiley-Interscience, Hoboken, NJ (2004), Ch. 6.

48. "ZEONEX 2005 Brochure", Zeon Corporation, Tokyo, Japan (2000).

49. Data from product literature, Zeon Corporation, Tokyo, Japan 100-8323.

50. J. Shin, J. Park, C. Liu, J. HE, and S. K, Pure Applied Chemistry, **77**, (5), 801–814 (2005).

51. Y. Konishi, T. Sawaguchi, K. Kubomura, K. Minami, SPIE, Volume 5872, pp. 18-25 (2005).

52. Data from *Specifications of Optical Grade Plastics*, G-S Plastic Optics, Rochester, NY 14603-1091.

53. G. W. C. Kaye and T. H. Laby, *Tables of Physical and Chemical Constants and Some Mathematical Functions*, 15th ed. ,Longman, London (1986), p. 289.

54. I.M.Lifshitz. *Some Problems of the Statistical Theory of Biopolymers*. *Zh. Eksp. Teor. Fiz.*, 1968, v.55, p.2408.

55. T. Kawakatsu, *Statistical Physics of Polymers*; An introduction, Springer-Verlag Berlin Heidelberg, New York (2004).

56. M. Rubinstein, R.H. Colby, *Polymer Physics*, Oxford, New York (2003).

57. Section J25, American Physical Society (APS) 2007 annual meeting, Colorado, March (2007).

58. Section A24, American Physical Society (APS) 2007 annual meeting, Colorado, March (2007).

59. Section H17, American Physical Society (APS) 2007 annual meeting, Colorado, March (2007).

60. Section A25, American Physical Society (APS) 2007 annual meeting, Colorado, March (2007).

61. Section J25, American Physical Society (APS) 2007 annual meeting, Colorado, March (2007).

62. Section P25, American Physical Society (APS) 2007 annual meeting, Colorado, March (2007).

63. Section A 25 and B25, American Physical Society (APS) 2007 annual meeting, Colorado, March (2007).

64. Section Y14, American Physical Society (APS) 2007 annual meeting, Colorado, March (2007).

65. K. Oura, V. G. Lifshits, A. A. Saranin, A. V. Zotov, M. Katayama, *Surface Science : An introduction*, Springer-Verlag Berlin Heidelberg, New York (2003).

66. J. M. Walls, R. Smith, *Surface Science Techniques*, Pergramon, New York, 1994

67. Q.F. Wei, Surface characterization of plasma-treated polypropylene fibers, *Material Characteristics.* **52** (3) (2004), pp. 231–235.

68. J.F.Moulder, W.F.Stickle, P.E.Sobol, and K.D.Bomben, *Handbook of X-ray Photoelectron Spectroscopy*, published by Perkin-Elmer Corp., Eden Prairie, MN, USA (1992).

69. A. Rosencwaig, *Photoacoustics & photoacoustic spectroscopy*, John Wiley & Sons, NY (1980).

70. J. C. Murphy and L. C. Aamodt, eds., *Photoacoustic and Photothermal Phenomena II*, Vol. 62 of the Springer Optical Science Series, Springer, Berlin (1990).

71. A. Mandelis, ed., *Priciples and Perspectives of Photothermal and Photoacoustic Phenomena*, Vol. 1 Progress in Photothermal and Photoacoustic Science and Technology Series, Elsevier, New York (1992).

72. E.T. Ogawa, C. Hu, and P.S. Ho, Journal of Applied Physics, **86**(11), 6018 (1999).

73. J. E. de Albuquerque, W. L. B. Melo, and R. M. Faria, Rev. Sci. Instrum. **74**(1), 306 (2003).

74. M.A. Olmstead, S.E. Kohn and N.M. Amer: Bull. American Physical Society. **27**, 227 (1982).

75. J. Opsal, A. Rosencwaig and D. L. Willenburg, Applied Optics, 22, 3169 (1983).

76. Y. Chen, M.S. thesis, Eastern Michigan University (2000).

77. S. Bandi, M.S. thesis, Eastern Michigan University (2002).

78. D.P. Almond and P.M. Patel, *Photothermal Science and Techniques*, p64, Chapman & Hall (1996).

79. H. Vargas, L.C.M. Miranda, Rev. of Sci. Inst., **74**(1), 794 (2003).

80. O. Pessoa, Jr., C.L. Cesar, N.A. Patel, H. Vargas, C.C. Ghizoni, and L.C.M. Miranda, J. Appl. Phys. 59, 1316 (1986).

81. A. M. Mansanares, M.L. Baesso, E.C. da Silva, F.C.G. Gandra, H. Vargas, and L.C.M. Miranda, Physics Review B, **40**, 7912 (1989).

82. M.L. Baesso, A. M. Mansanares, E.C. da Silva, H. Vargas, and L.C.M. Miranda, Physics Review B. **40**, 1880 (1989).

83. D.C. Fork and S.K. Herbert, *Photochemistry and Photobiology*. 57, 207 (1993).

84. W.J. Silva, L.M. Priolli, A.C.N. Magalhaes, A.C. Pereira, H. Vargas, A.M. Mansanares, N. Cella, L.C.M. Miranda, and Alvarado-Gil, Plant Sci. 104, 177 (1995).

85. Y. Han, J.S. Rosenshein, Z.L. Wu, W. Ye, M. Thomsen, and Q. Zhao, Optical Engineering, 40(2), 303 (2001).

86. A. Sánchez-Lavega, A. Salazar, A. Ocariz, L. Pottier, E. Villar, and E. Macho, Applied Physics A, 65, 15 (1997).

87. A. Lachaine and P. Poulet, Appl. Physics Letter, 45, 953 (1984).

88. A.Torres-Filho, L.F. Perondi, and L.C.M. Miranda, Journal of Applied Polymer Science, 35, 103 (1988).

89. C. Hu, E.T. Ogawa, and P.S. Ho, Journal of Applied Physics.. 86(11), 6028 (1999).

90. L. D. Favro, P. K. Kuo, and R. L. Thomas, ‘‘Thermal wave propagation and scattering in semiconductors,’’ in *Photoacoustic and Photothermal Phenomena in Semiconductors*, A. Mandelis, Ed., pp. 69–96, North-Holland, New York ~1987.

91. L. D. Favro and X. Han, ‘‘Thermal wave materials characterization and thermal wave imaging,’’ in *Proc. ASNT Advanced School on Sensors for Process Monitoring and Quality Control* ~in press.

92. Z. L. Wu, M. Thomsen, P. K. Kuo, Y. Lu, C. Stolz and Ma. Kozlowski, Optical Engineering, 36 (1), 251 (1997).

93. J. E. de Albuquerque, W. L. B. Melo, and R. M. Faria, Review Science Instruments, 74(1), 306 (2003).

94. E.S. Bialkowski, *Photothermal Spectroscopy Methods for Chemical Analysis*: Chemical Analysis v. 134, Wiley, New York (1996).

95. D. Fournier, A.C. Boccara, N. Amer and Gerloch, Applied Physcis Letter. 37, 519 (1980).

96. M. A. Olmstead, N. M. Amer, S. Kohn, D Fournier, and A. C. Boccara, Applied Physics A 32, 141 (1983).

97. E. Welsch, H. G. Walther, K. Freidrich and P. Echardt, Journal of Applied Physcis. 67, 6575 (1990).

98. Z.L. Wu, J. Jauregui, E. Matthias, Proc. SPIE 1624, 13 (1992).

99. A.C. Tam, Review Modern Physics, 58, 381 (1986).

100. A. Sánchez-Lavega, A. Salazar, A. Ocariz, L. Pottier, E. Villar, and E. Macho, Applied Physics A, 65, 15 (1997).

101. A. Rosencwaig, J. Opsal, W. L. Smith, and D. L. Willenborg, Applied Physcos Letter. 46, 1013 (1985).

102. D. Guidotti and H. M. van Driel, Applied Physcis Letter, 47, 1336 (1985).

103. C. Christofides, I. A. Vitkin, and A Mandelis, Journal of Applied Physics, 67, 2815 (1990).

104. A. Seas and C. Christofides, Applied Physcis Letter, 66. 3348 (1995).

105. Z. L. Wu, M. Reichling, H. Groenbeck, Z. X. Fan, D. Schaefer, and E.Matthias, ‘‘Photothermal measurement of thermal conductivity of optical coatings,’’ *Proc. SPIE* 1624, 331–345 (1992).

106. René Krupka and Z. L. Wu, Proc. SPIE 2864, 286 (1996) Denver Colorado.

107. Z. L. Wu, P. K. Kuo, Y.S. Lu, S. T. Gu, R. Krupka, Thin Solid Films, 290-291, 271 (1996).

108. P. K. Kuo and M. Munidasa, Applied Optics, **29** (36), 5326 (1990).

109. Y. Lu, P. K. Kuo, L. D. Favro, R. L. Thomas, Z. L. Wu, and S. T. Gu, Progress in National Science, **6**, S-202 (1996).

110. H. Haiyang, F. Zhengxiu and L. Ye, Laser Physics, **10** (2), 633 (2000).

111. Z. L. Wu, Critical Rev. Opt. Sci. and Tech., **CR69,** 326 Proc. SPIE, California, (1997).

112. H. Saito, M. Irikura, M. Haraguchi, and M. Fukui, Applied Optics, **31**, 2047 (1992).

113. Z. L. Wu, P. K. Kuo, Y. S. Lu, and S. T. Gu, Proc. SPIE **2714**, 294 (1996).

114. P. K. Kuo, Y. X. Du, X. J. Shui and S. Y. Zhang, Progress in National Science, **6**, s-198 (1996).

115. B. Hussain, M.S. thesis, Eastern Michigan University (2005).

116. L. Escoubas, P. Roche and M. Commandre, Optical Engineering, 36 (4), 1196 (1997).

117. D. G. Legrand and J. T. Bendler, eds. *Handbook of Polycarbonate Science and Technology,* Marcel Dekker, New York (2000), p. 112.

118. G. W. Ehrenstein, *Polymeric Materials: Structure- Properties- Applications*, Hanser, Munich (2001), p.169, 262.

119. A. Harata, and N. Yamaguchi, Analytical Science, 16, 743-749 (2000).

120. B. Li, H. Blaschke, D. Ristau, Applied Optics, 45 (23),5827-5831 (2006).

121. B. Li, S. Xing, Y. Zhang, S. Martin, E. Welsch, Optics Communication, 244, 367-376 (2005).

122. E Welsch, M. Reichling, Journal Modern Optics, 40, 1455-1475 (1993).

123. M. Commandre, P. Roche, Applied Optics, 35, 5021-5043 (1996).

124. Section X25, American Physical Society (APS) 2007 annual meeting, presented by Marshall Thomsen, Colorado, March (2007).

Appendix I

Appendix I-1. History of modern polymer industries

Table I.
History of modern polymer industries and applications (from 1927 to 1971).

Year	Polymer	Application
1927	polymeric compound	Plumbing (PVC) pipe, Euttery tile, and bottles.
1930	Poly-styrene (Styrofoam)	Videocassettes, cups, packaging, and thermally insulated containers
1938	Nylon	Ropes and clothes.
1941	Poly-ethylene	Packaging film and toys.
1970	Ekonol	Electronic devices and aircraft engines
1971	Kevlar	Bullet proof vests, fire proof garments for firefighting and auto racing.

Appendix I-2. Application of the Thermoplastics

Table II.
Applications of the thermoplastics [140]

Thermoplastics	Applications
Poly-ethylene (PE)	Packaging, containers, tubing and household goods
Poly-propylene (PP)	Packaging, containers, furniture, pipes
Poly-vinyl-chloride (PVC)	Cable, insulation, pipes, toys
Poly-styrene (PS)	Food containers, appliance housing
Poly-methyl-meth-acrylate (PMMA or acrylic)	Transparent sheets and moldings, aero-plane windows, street lamps, display signs, optical lenses
Poly-amide (PA) or Nylons	Textiles, brushes, surgical applications, bearings, gears
Poly-tetra-fluoro-ethylene (PTFE) or Teflon	Non-stick surfaces, insulation tape, engineering applications
Poly-acrylo-nitrile (PAN)	Wool type applications
Cellulose acetate or cellophane	Textile fibers, molded products, film
Poly-ethylene-terephthalate (PET)	Textile fibers, film, magnetic tapes
Poly-butylenes-terephthalate (PBT)	Electrical, electronic and automotive engineering
Cyclo-olefin-polymer (COP, Zeonex)	Optical applications for lenses and prisms, liquid crystal display components

Appendix I-3

Table III.
Applications of the Thermoset

Thermoset	Applications
Phenol-formoa-aldehyde resins	Electrical moldings, appliance handles, laminates
Epoxy resins	Adhesives, protective coatings, laminates, building and construction, electrical and electronic components
Amino resins	Kitchenware, flooring, particleboard, plywood
Polyester resins	Automotive engineering, construction, boat building
Polyurethanes	Furniture, tyro treads, clothing, floor

Appendix I-4

Table IV.
Applications of the Elastomer.

Elastomer	Applications
Poly-cis-isoprene (or natural rubbers)	Gaskets, shoe soles, condoms
Silicone	Medical implants, sealants, flexible moulds, electrical insulation
Poly-chloroprene	Cables, hoses, seals, gaskets

Appendix I-5

Table V.
Applications of High-Performance Polymers

High-performance polymers	Applications
Poly-carbonate (PC)	Compact discs, glazing, computer housing, aeronautical engineering applications
Poly-phenylene-oxide (PPO)	Electrical and automotive engineering
Poly-sulfones	Electrical and electronic applications, medical equipment
Poly-ether-imide (PEI)	Automotive and aerospace applications
Poly-phenylene-sulfide (PPS)	Electrical and electronic applications, computer components
Poly-m-phenylene-terephthalamide or Nomex	Nomex fibers were introduced on to the market because of their superior heat resistance.
Poly-p-phenylene-terephthalamide or Kevlar	Kevlar fibers have been used for application including protective clothing, ropes, composites, sporting goods and aeronautical engineering components.
Poly-ether-ether-ketone (PEEK) or Victrex	Composites and the aerospace industry.

Appendix I-6

Table VI.
Applications of Copolymers

Copolymer	Applications
Styrene-acrylo-nitrile (SAN)	Automotive, medical and household applications
Styrene-butadiene-rubber (SBR)	Tires, shoe soles, flooring, hoses
Acrylonitrile-butadiene (NBR)	Seals, hoses, shoe soles

Appendix II-1

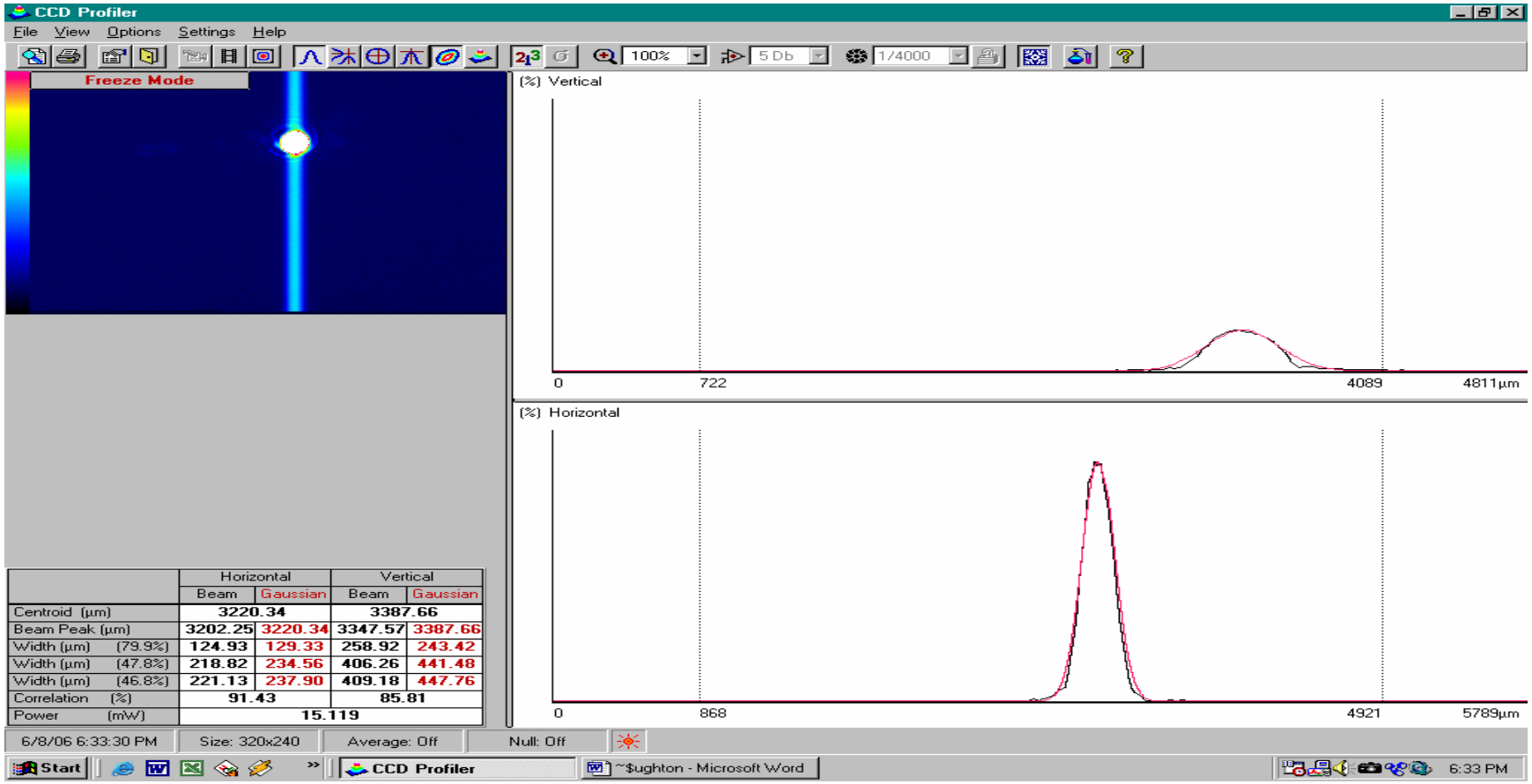

Figure II- 1. Size of focused probe beam on a sample (measured by CCD profiler).

Appendix II-2

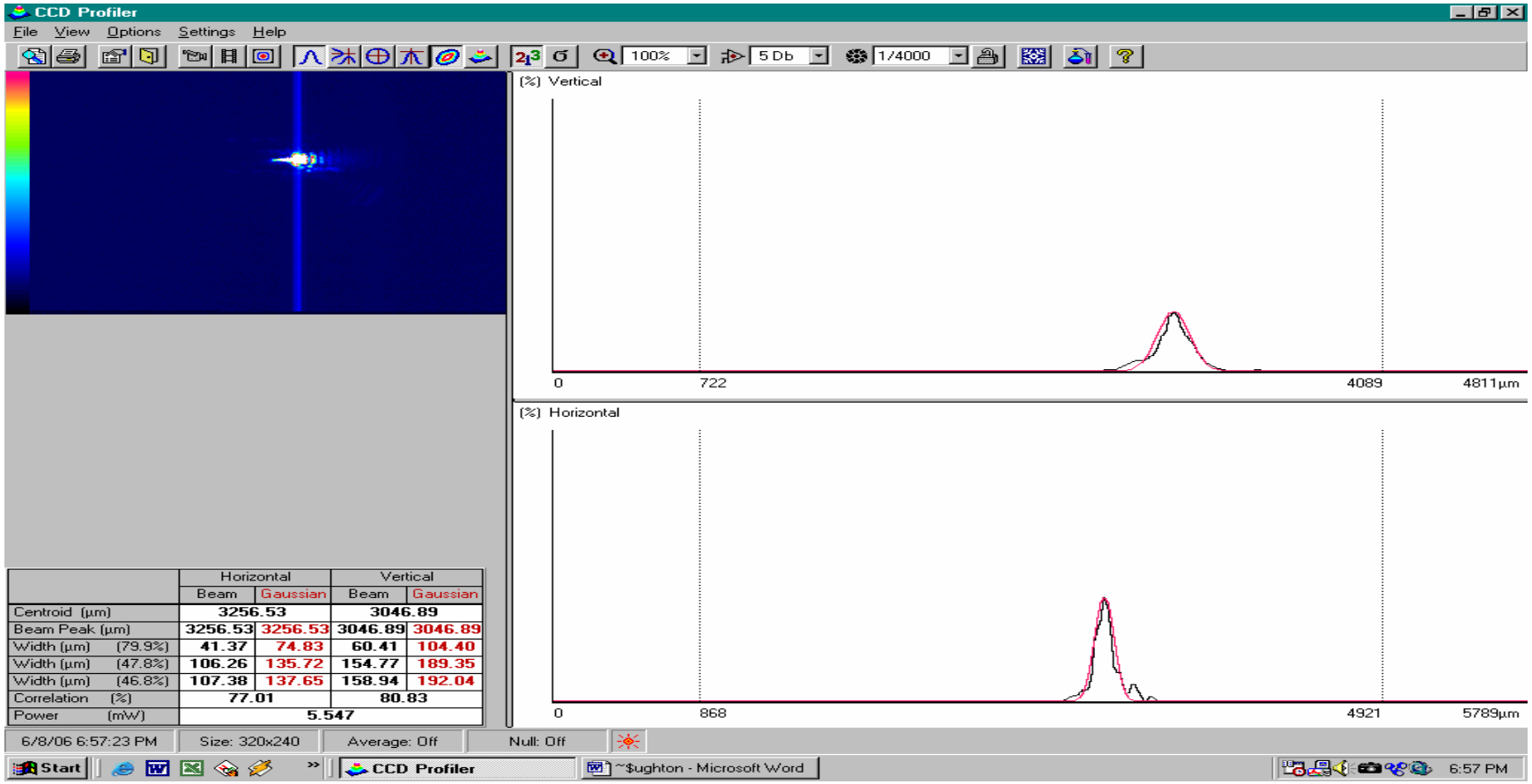

Figure II- 2. Size of focused pump beam on a sample (measured by CCD profiler).

Appendix III -1. STL signal versus time with variable pump beam power in crossed-polarizers (Zeonex)

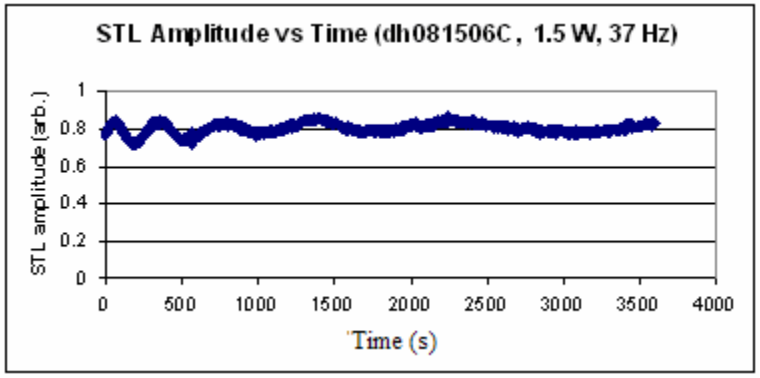

Figure 1-1 STL amplitude versus time with polarized light. Pump beam power was 1.5 W and chopping frequency was 37 Hz.

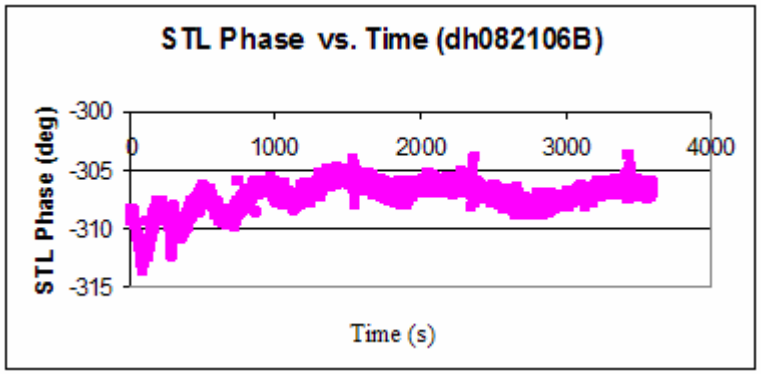

Figure 1-2 STL phase versus time with polarized light. Pump beam power was 1.5 W and chopping frequency 37 Hz for 1hour.

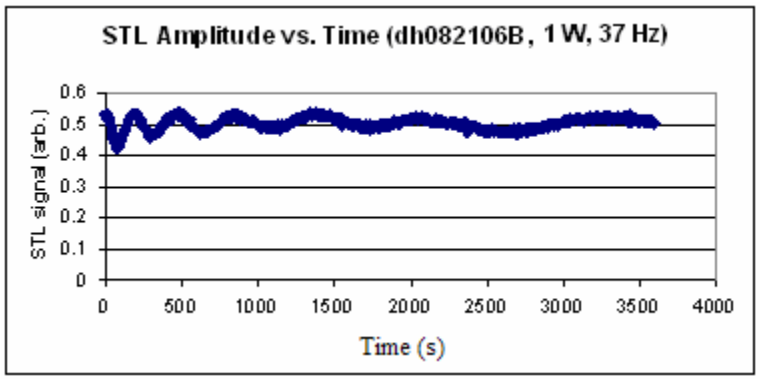

Figure 1-3 STL amplitude versus time with polarized light. Pump beam power was 1 W and chopping frequency 37 Hz for 1hour.

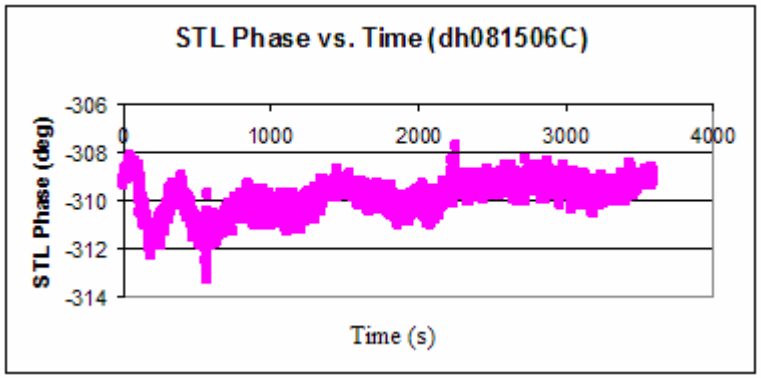

Figure 1-4 STL phase versus time with polarized light. Pump beam power was 1 W and chopping frequency 37 Hz for 1hour.

Appendix III -2. <u>The STL amplitude oscillation period versus time relationship using crossed-polarizers (Zeonex)</u>

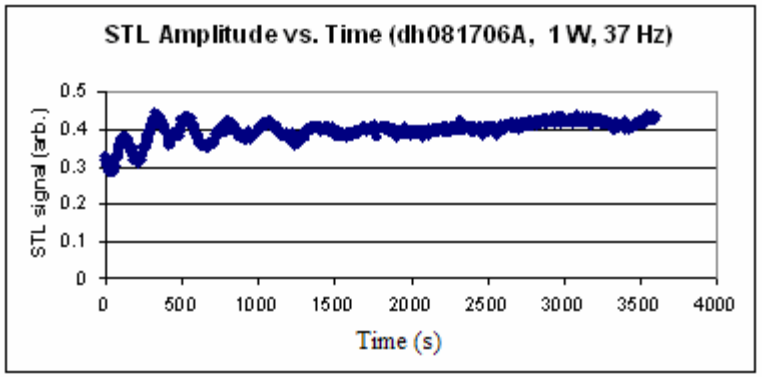

Figure 2-1 STL amplitude versus time with polarized light. Pump beam power was 1 W and chopping frequency 37 Hz for 1hour.

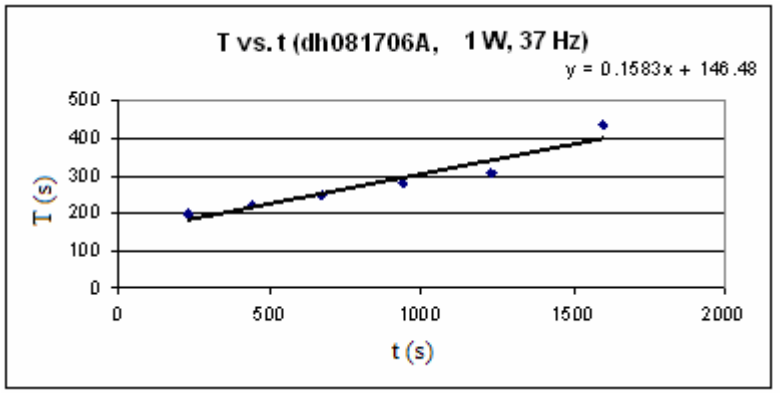

Figure 2-2 Period versus time from amplitude versus time in dh081706A.

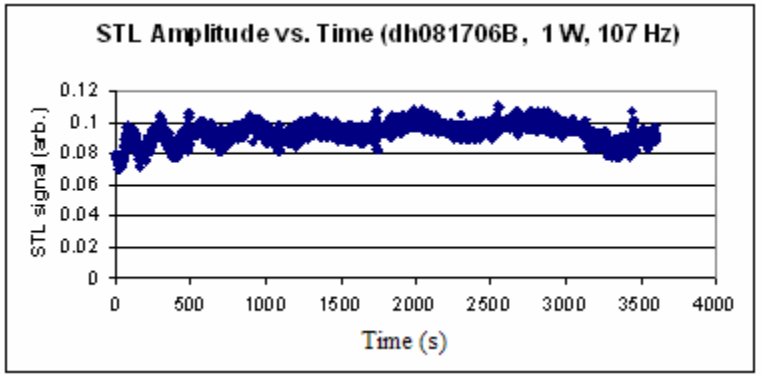

Figure 2-3 STL amplitude versus time with polarized light. Pump beam power was 1 W and chopping frequency 107 Hz for 1 hour.

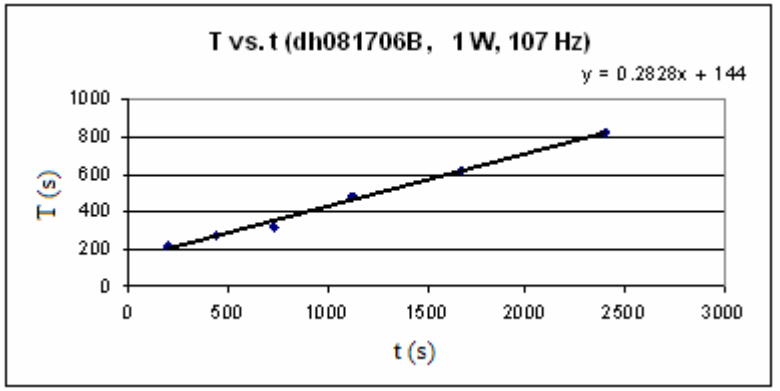

Figure 2-4 Periods versus time from amplitude versus time in dh081706B.

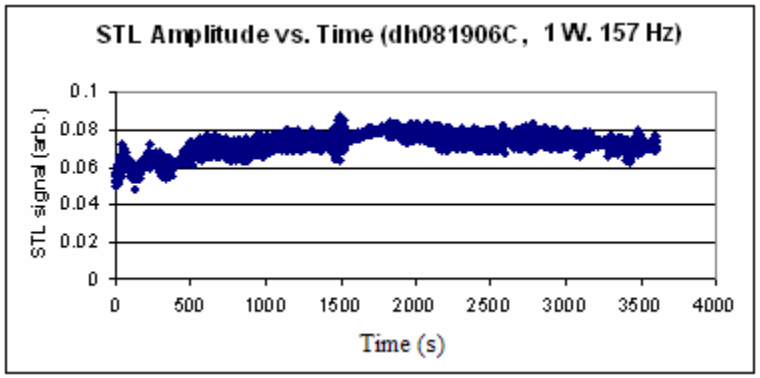

Figure 2-5 STL amplitude versus time with polarized light. Pump beam power was 1 W and chopping frequency 157 Hz for 1 hour.

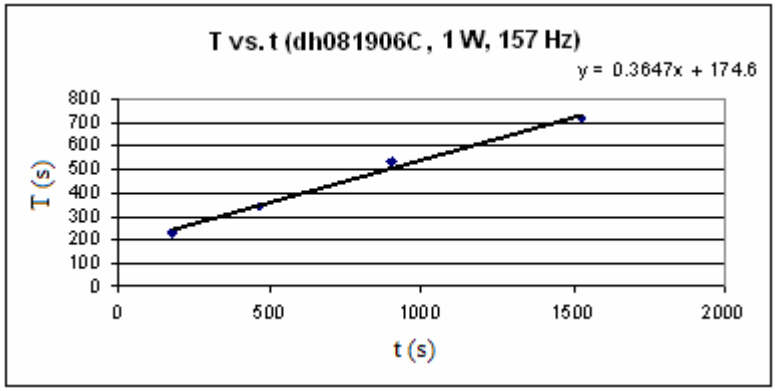

Figure 2-6 Periods versus time from amplitude versus time in dh081906C.

Appendix III -3. <u>The period versus time relationship as a function of pump beam power (Zeonex)</u>

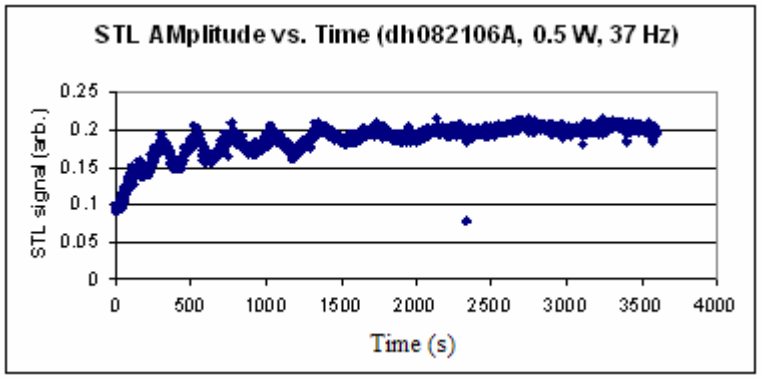

Figure 3-1 STL amplitude versus time with polarized light. Pump beam power was 0.5 W and chopping frequency 37 Hz for 1 hour.

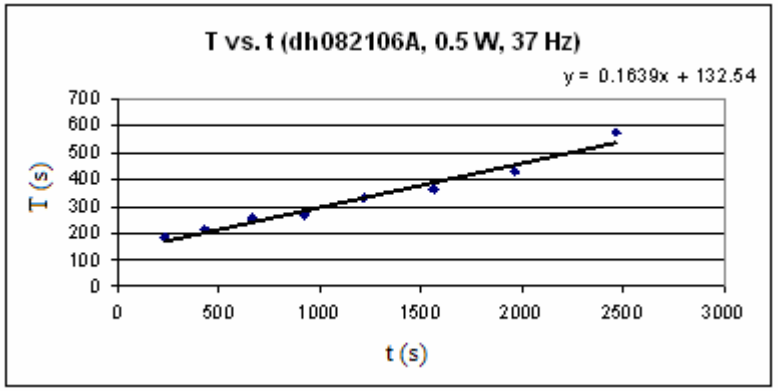

Figure 3-2 Periods versus time from amplitude versus time in dh082106A.

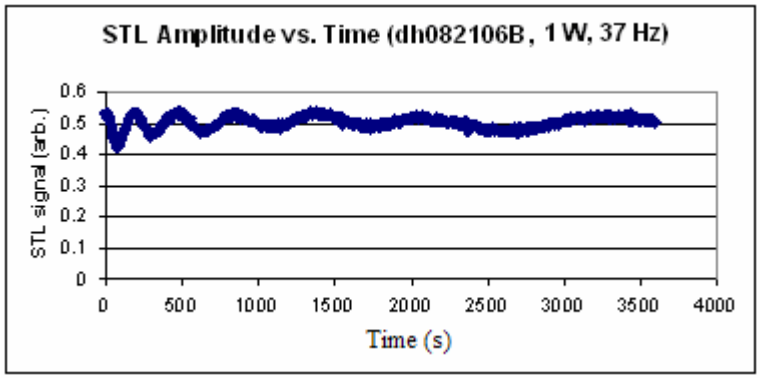

Figure 3-3 STL amplitude versus time with polarized light. Pump beam power was 1 W and chopping frequency 37 Hz for 1 hour.

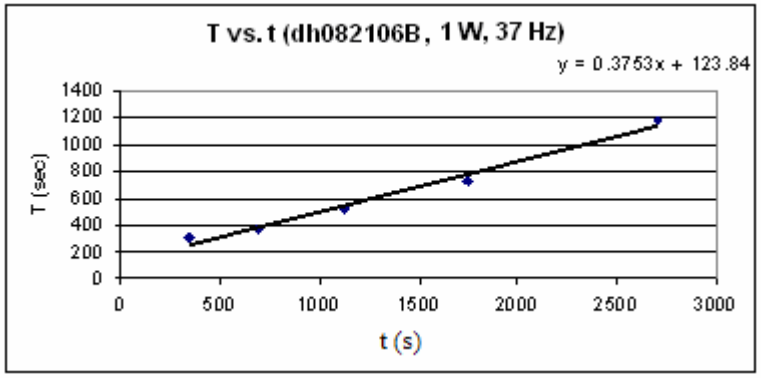

Figure 3-4 Periods versus time from amplitude versus time in dh082106B.

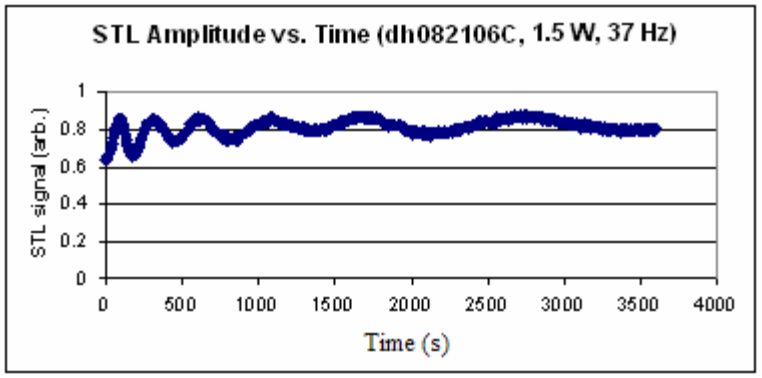

Figure 3-5 STL amplitude versus time with polarized light. Pump beam power was 1.5 W and chopping frequency 37 Hz for 1 hour.

.

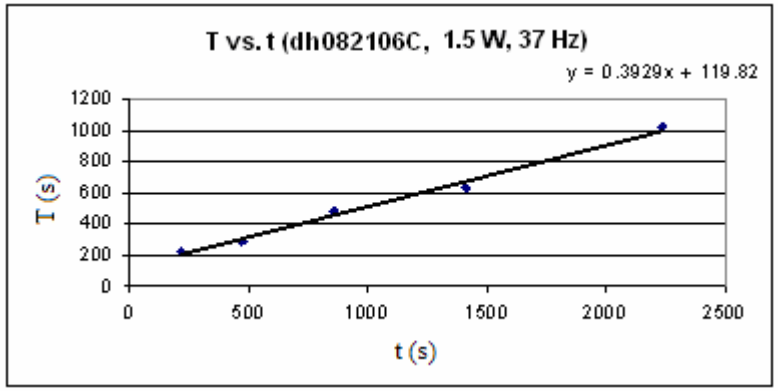

Figure 3-6 Periods versus time from amplitude versus time in dh082106C.

Appendix III -4. STL signal versus time with power and chopping frequency varied during the run.

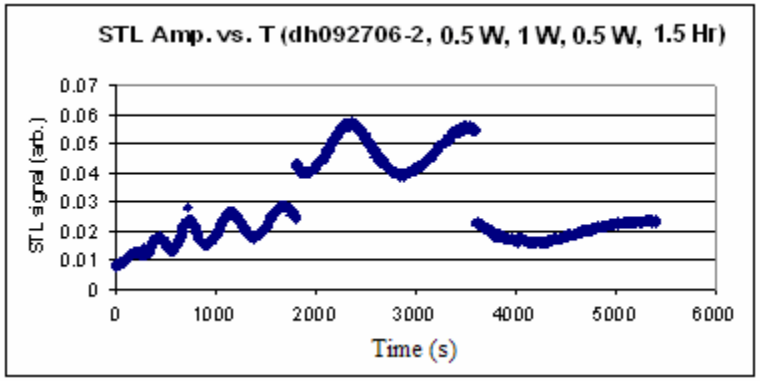

Figure 4-1 STL amplitude versus time with 37 Hz. Varied pump beam power , with 0.5 W, 1 W, then 0.5 W continuously for 1 hour and 30 minutes.

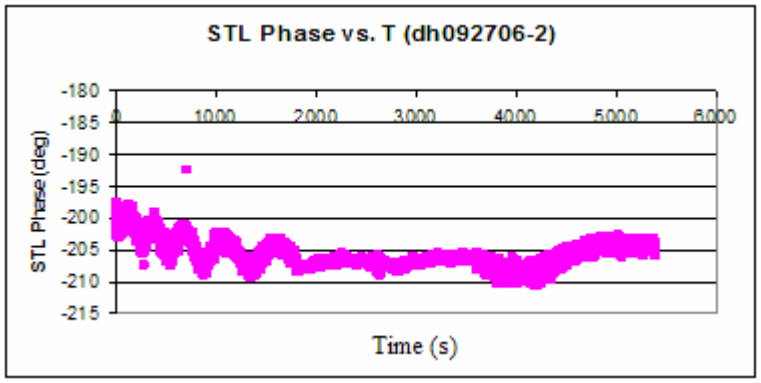

Figure 4-2 STL phase versus time with 37 Hz. Varied pump beam power , with 0.5 W, 1 W, then 0.5 W continuously for 1 hour and 30 minutes.

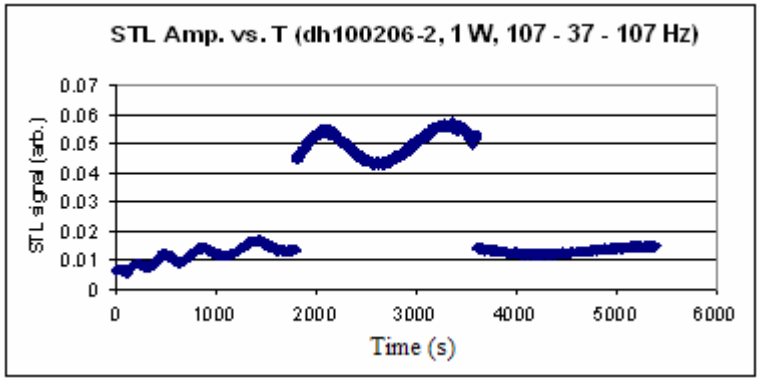

Figure 4-3 STL phase versus time with 1 W. Varied chopping frequency, with 107 Hz, 37 Hz, then 107 Hz continuously for 1 hour and 30 minutes.

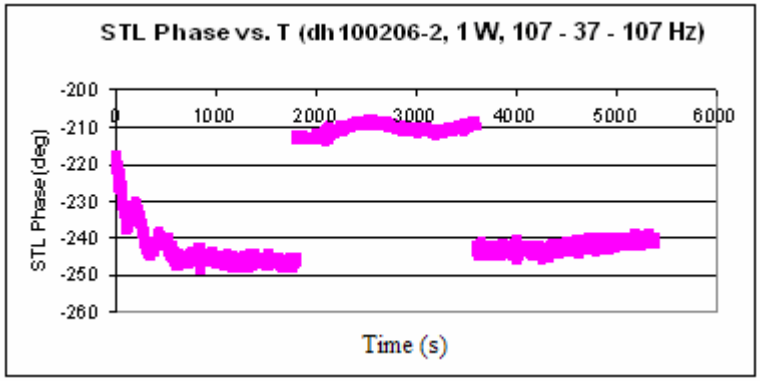

Figure 4-4 STL phase versus time with 1w. Varied chopping frequency with 107 Hz, 37 Hz, then 107 Hz continuously for 1 hour and 30 minutes.

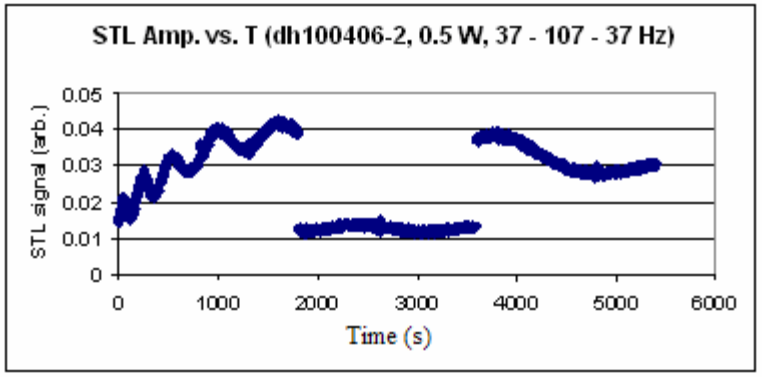

Figure 4-5 STL phase versus time with 0.5 W. Varied chopping frequency, with 37 Hz, 107 Hz, then 37 Hz continuously for 1 hour and 30 minutes.

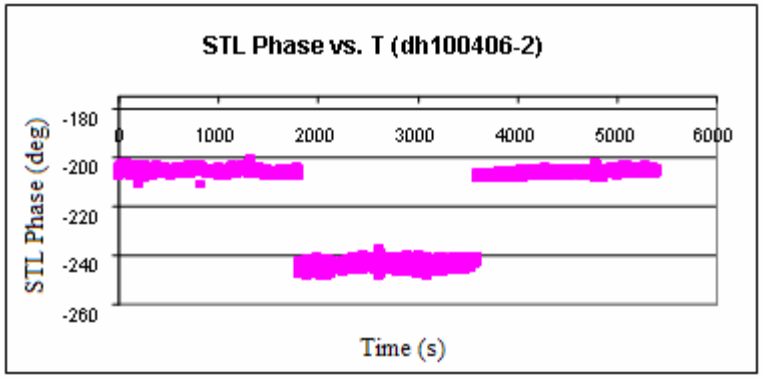

Figure 4-6 STL phase versus time with 0.5 W. Varied chopping frequency, with 37 Hz, 107 Hz, then 37 Hz continuously for 1 hour and 30 minutes.

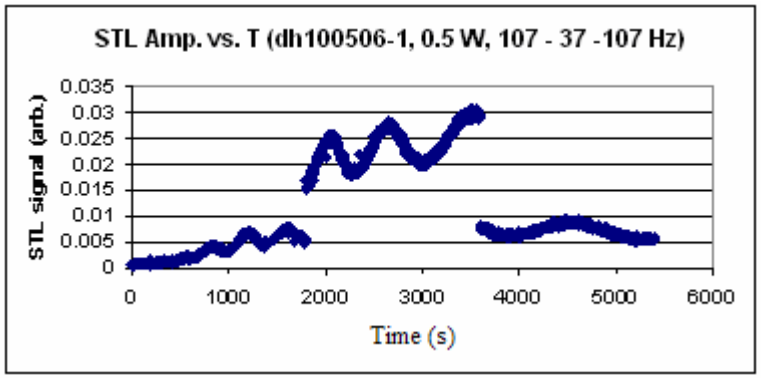

Figure 4-7 STL phase versus time with 0.5 W. Varied chopping frequency, with 107 Hz, 37 Hz, then 107 Hz continuously for 1 hour and 30 minutes.

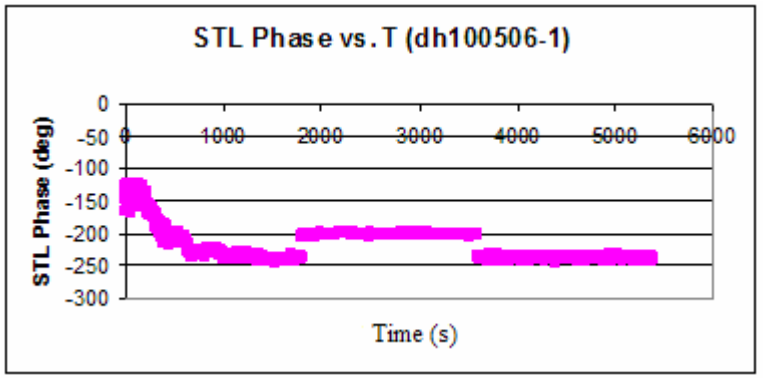

Figure 4-8 STL phase versus time with 0.5 W. Varied chopping frequency, with 107 Hz, 37 Hz, then 107 Hz continuously for 1 hour and 30 minutes.

Appendix III -5. Scan of diffraction pattern in the vertical direction (acrylic)

Table VII.
Experimental procedure and description of the experiment in vertical detector scan

Steps	Step label	Duration	Description
1	B/no pol (before)	20 minutes	Repeated scanning of detector vertically with non-polarized light, before the one hour run
2	B/pol (before)	20 minutes	Repeated scanning of detector vertically with polarized light before the one hour run
3	Figure 22, (dh043007A)	1 hour	STL measurement with polarized light @ 0.5 W and 37 Hz of pump beam
4	A/no pol (after)	20 minutes	Repeated scanning of detector vertically with non-polarized light after the one hour run
5	A/pol (after)	20 minutes	Repeated scanning of detector vertically with polarized light after the one hour run

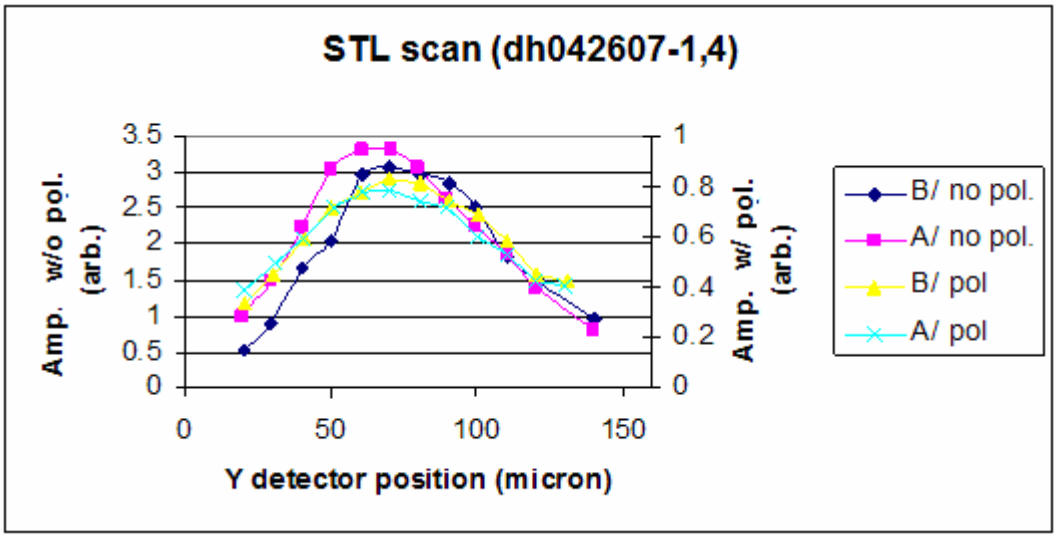

Figure 5-1. STL signal versus y (vertical) detector position. Power of pump beam was 0.5 W and chopping frequency of pump beam was 37 Hz.

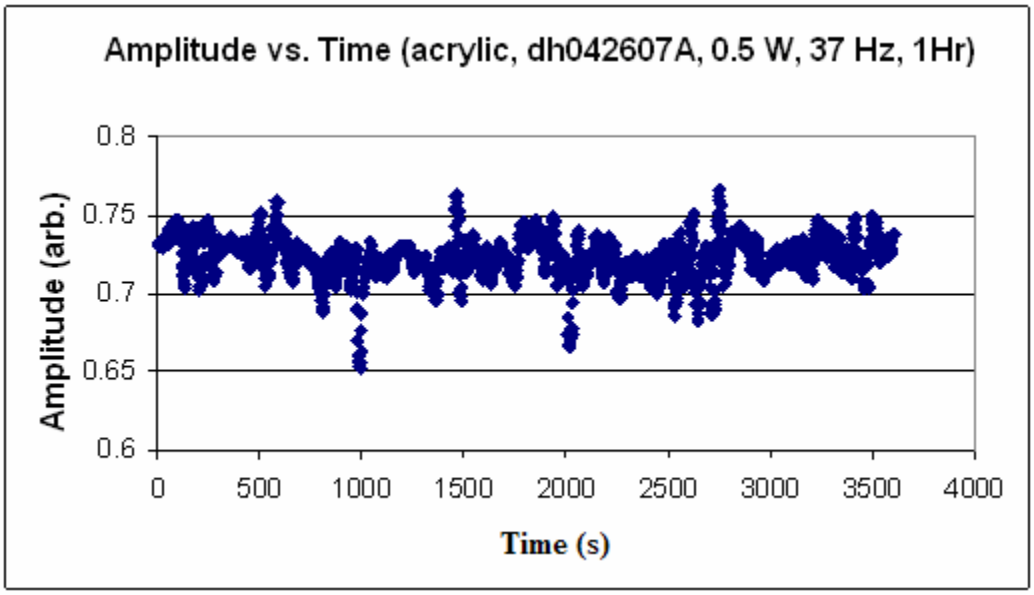

Figure 5-2. STL amplitude versus time. Power of pump beam was 0.5 W and chopping frequency of pump beam was 37 Hz.

Appendix III -6-1. Scanning horizontal detector position without a polarizer and with a single polarizer (acrylic)

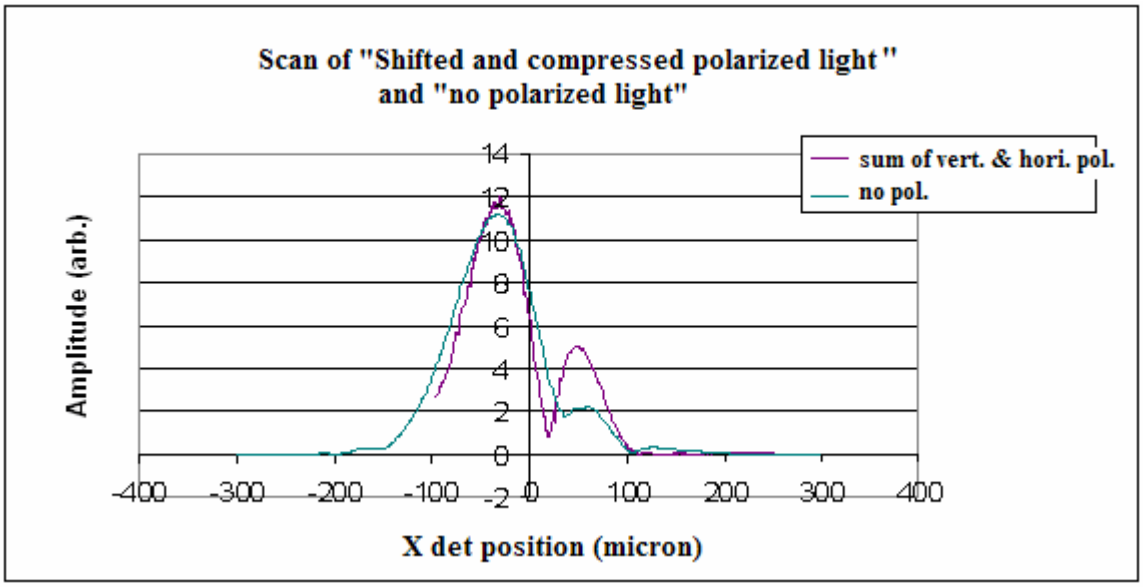

Figure 6-1. A comparison of STL signals with and without single polarizers is shown. Data for vertical and horizontal polarizer has been summed and then shifted and compressed to correct for the influence of the polarizer on the probe beam profile.

Appendix III -6-2. Measured width of a test laser beam by CCD profiler

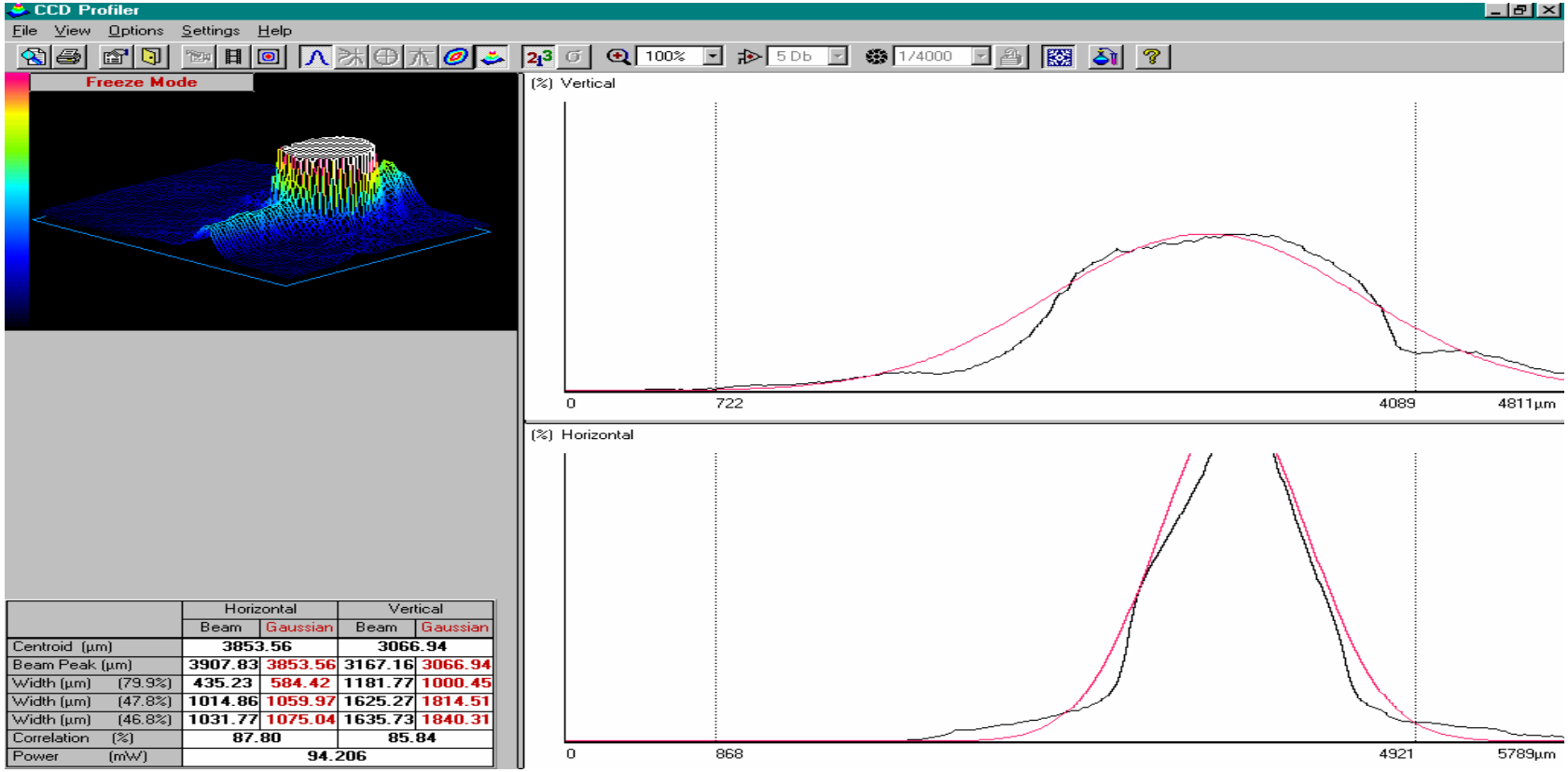

	Horizontal		Vertical	
	Beam	Gaussian	Beam	Gaussian
Centroid (µm)	3853.56		3066.94	
Beam Peak (µm)	3907.83	3853.56	3167.16	3066.94
Width (µm) (79.9%)	435.23	584.42	1181.77	1000.45
Width (µm) (47.8%)	1014.86	1059.97	1625.27	1814.51
Width (µm) (46.8%)	1031.77	1075.04	1635.73	1840.31
Correlation (%)	87.80		85.84	
Power (mW)	94.206			

Figure 6-2. Measured width of the light with non polarized light.

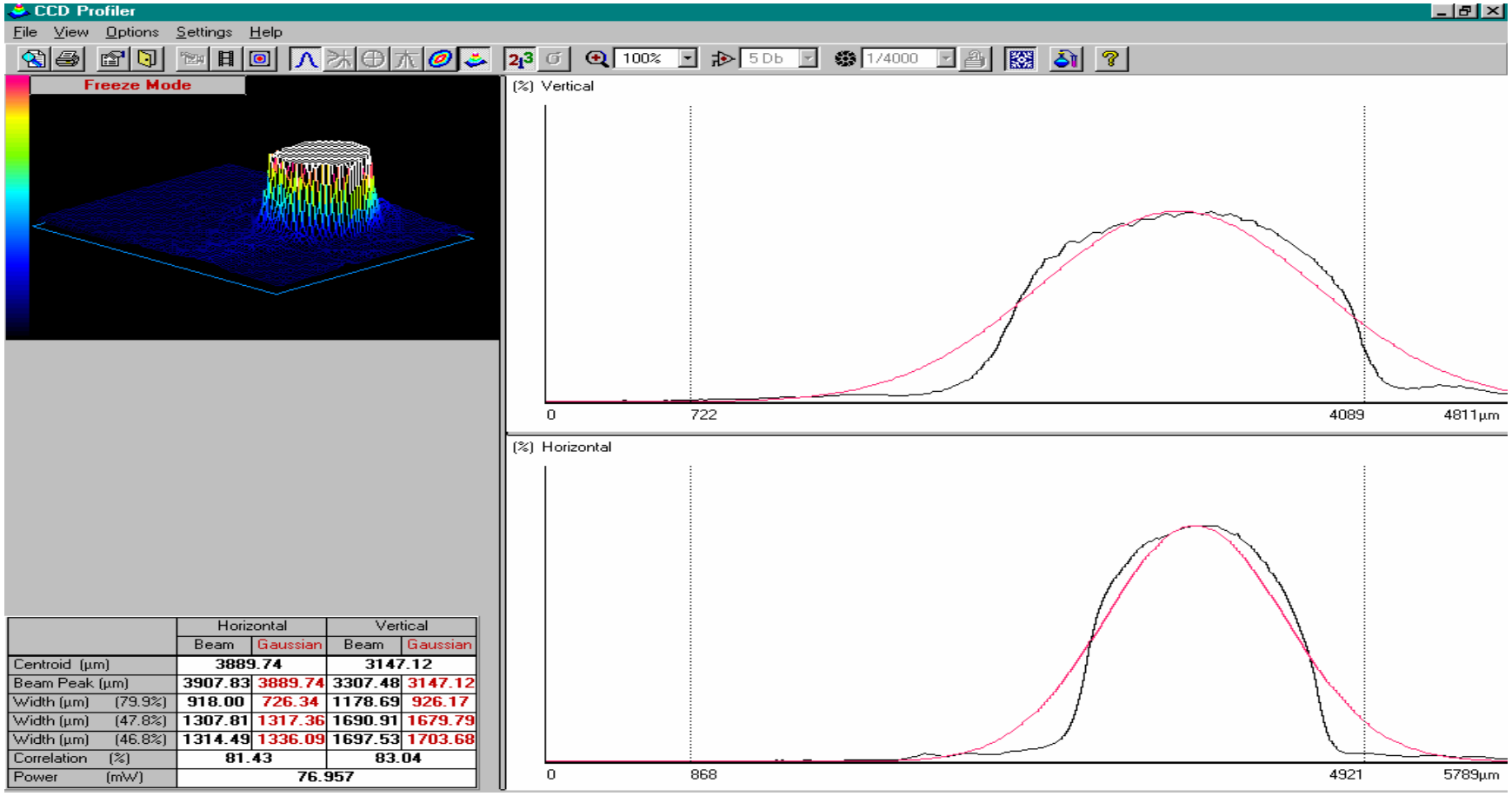

Figure 6-3. Measured width of the light with vertically polarized light

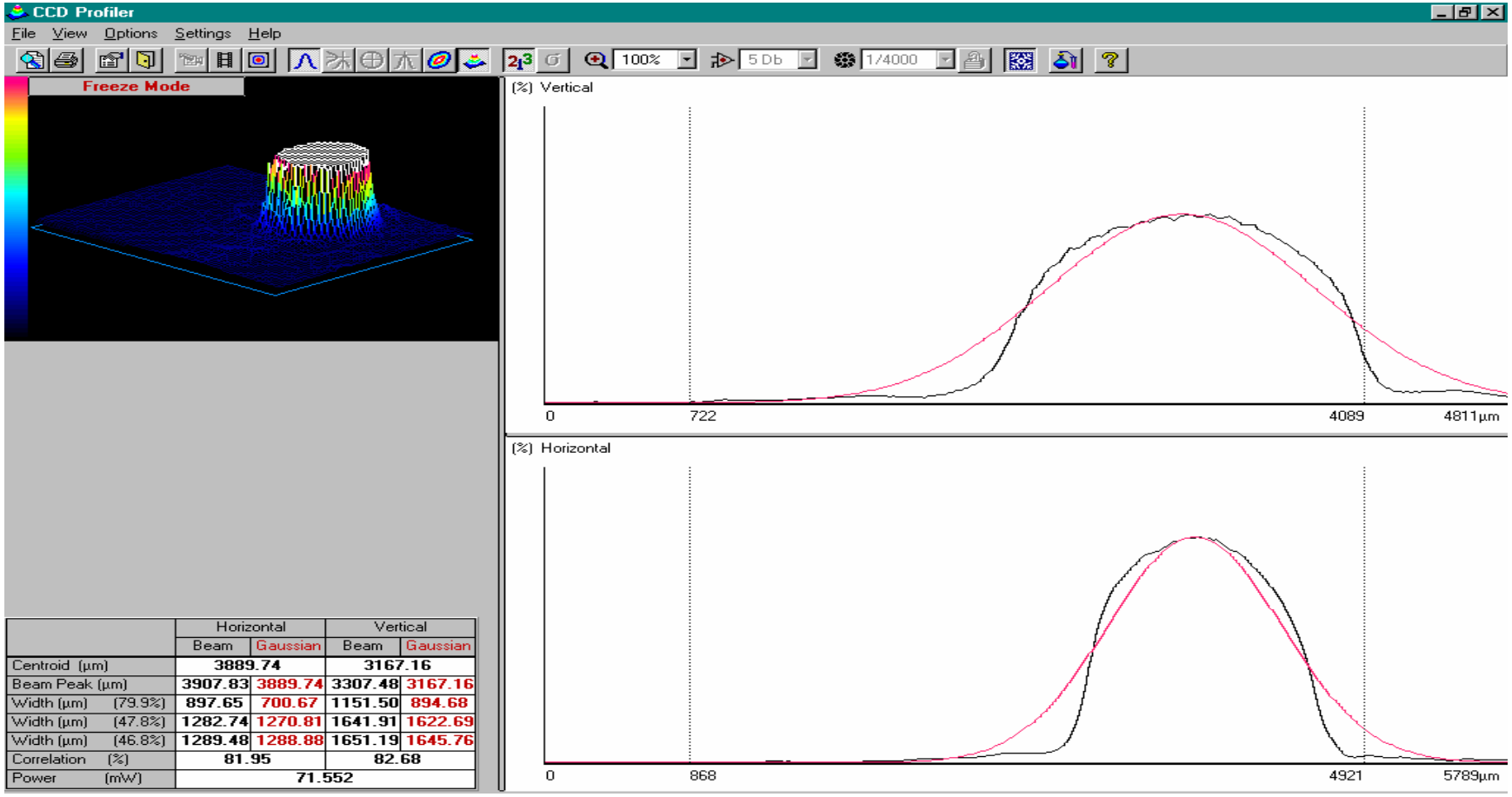

Figure 6-4. Measured width of the light with horizontally polarized light.